UNIVERSITAT POLITÈCNICA DE VALÈNCIA

Contribution to the simulation of new standard testing cycles by means of a 0D/1D tool

DOCTORAL THESIS

Presented by:

Ms. Sushma Artham

Supervised by:

Dr. Jaime Martin Diaz

In the:

DEPARTAMENTO DE MAQUINAS Y MOTORES TERMICOS of the UNIVERSITAT POLITECNICA DE VALENCIA

In fulfilment of the requirements for the degree of:

Doctor of Philosophy

Valencia, October 2023

INDEX

Resumen

El objetivo principal de esta tesis es establecer una metodología para predecir el consumo de combustible y las emisiones de un motor de encendido por compresión en condiciones transitorias. Además, su objetivo es explorar cómo las diferentes configuraciones del motor y los factores ambientales impactan el comportamiento del motor utilizando un enfoque de modelado 0D/1D. Además, el estudio pretende extender esta metodología a los motores duales, analizando específicamente las características de combustión de metano-diésel e hidrógeno-diésel. Para lograrlo, la herramienta de modelado 0D/1D se ajustó y validó meticulosamente utilizando un motor diésel de cuatro cilindros. Esta alineación entre la simulación y datos experimentales se centró especialmente en factores cruciales como la presión, la liberación de calor, las temperaturas en los fluidos del motor y el par. Se realizó un análisis exhaustivo del Balance Energético Global (GEB) utilizando VEMOD (Virtual Engine Model). Este análisis proporcionó información detallada sobre el consumo del motor y su reacción en diversas condiciones de funcionamiento, particularmente durante el Ciclo de ensayo mundial armonizado de vehículos ligeros (WLTC). La comparación de términos energéticos entre diferentes condiciones ambientales y de motor destacó aspectos como la fricción, la transferencia de calor y la acumulación de calor. Además, el análisis GEB permitió explorar cómo se distribuía la energía con diferentes temperaturas y altitudes ambientes. El estudio también evaluó las emisiones de NOx, revelando patrones influenciados por factores como las tasas de recirculación de gases de escape (EGR) y la temperatura de admisión. En el ámbito de los motores de combustible dual, se elaboró y validó un modelo de combustión utilizando la herramienta de simulación 0D/1D. La atención inicial se centró en la combustión de metano-Diesel, validada con datos experimentales. Posteriormente, el alcance de este modelo se amplió para simular la combustión de hidrógeno-Diesel. Esta tesis ha introducido con éxito una metodología que utiliza VEMOD para predecir el consumo y las emisiones del motor en distintos escenarios. El análisis exhaustivo arrojó luz sobre cómo funcionan los mecanismos de distribución de energía y cómo diferentes factores influyen en el comportamiento del motor. La aplicación de esta metodología a motores de encendido por compresión ha demostrado su versatilidad y capacidad de predicción, lo que la convierte en una herramienta valiosa para investigar escenarios futuros, también con combustiones duales.

Resum

L’objectiu principal d’aquesta tesi és establir una metodologia per predir el consum de combustible i les emissions d’un motor d’encesa per compressió en condicions transitòries. A més, pretén explorar com diferents configuracions de motors i factors ambientals afecten el comportament del motor mitjançant un enfocament de modelització 0D/1D. A més, l'estudi s'esforça a estendre aquesta metodologia als motors de doble combustible (duals), analitzant específicament les característiques de combustió de metà-dièsel i hidrogen-dièsel. Per aconseguir-ho, l’eina de modelització 0D/1D es va ajustar minuciosament i es va validar mitjançant un motor dièsel de quatre cilindres. Aquesta alineació entre dades de simulació i món real es va centrar especialment en factors crucials com la pressió, l’alliberament de calor, les temperatures dels fluids del motor i el parell. Es va realitzar una anàlisi completa del Balanç Global d’Energia (GEB) mitjançant VEMOD (Virtual Engine Model). Aquesta anàlisi va proporcionar una visió profunda sobre el consum del motor i la seua reacció en diverses condicions de funcionament, especialment durant el Cicle mundial d'assaig de vehicles lleugers harmonitzats (WLTC). La comparació de termes energètics entre diferents condicions ambientals i del motor van posar de manifest aspectes com la fricció, la transferència de calor i l’acumulació de calor. A més, l’anàlisi GEB va explorar com es va distribuir l’energia amb diferents temperatures i altituds ambientals. L’estudi també va valorar les emissions de NOx, revelant patrons influenciats per factors com la recirculació de gasos d’escapament (EGR) i la temperatura d’admissió. En l'àmbit dels motors duals, es va elaborar i validar un model de combustió mitjançant l'eina de simulació 0D/1D. El focus inicial es va centrar en la combustió metà-Diesel, validada amb dades experimentals. Posteriorment, l’abast d’aquest model es va ampliar per simular la combustió hidrogen-Diesel. Aquesta tesi ha introduït amb èxit una metodologia que utilitza VEMOD per predir el consum i les emissions del motor en diferents escenaris. L’anàlisi completa va donar llum a com funcionen els mecanismes de distribució d’energia i com diferents factors influeixen en el comportament del motor. L’aplicació d’aquesta metodologia als motors d'encesa per compressió va demostrar la seva versatilitat i capacitats de predicció, convertint-la en una valuosa eina per investigar els futurs escenaris, fins i tot amb combustions duals.

Summary

The main aim of this thesis is to establish a methodology for predicting fuel consumption and emissions of a compression ignition engine in transient conditions. Additionally, it aims to explore how different engine setups and environmental factors impact the engine's performance using a 0D/1D modelling approach. Moreover, the study strives to extend this methodology to dual fuel engines, specifically analysing methane-Diesel and hydrogen-Diesel combustion characteristics. The 0D/1D modelling tool was meticulously fine-tuned and validated using a four-cylinder Diesel engine to achieve this. This alignment between simulation and experimental data focused on crucial factors such as pressure, heat release, engine fluid temperatures and torque. A comprehensive Global Energy Balance (GEB) analysis was conducted using VEMOD (Virtual Engine Model). This analysis provided insights into the engine consumption and performance under diverse operating conditions, particularly during the Worldwide Harmonized Light Vehicles Test Cycle (WLTC). The comparison of energy terms across different engine and boundary conditions highlighted aspects such as friction, heat rejection, and heat accumulation. Additionally, the GEB analysis allowed exploration of how energy was split across varying ambient temperatures and altitudes. The study also assessed NOx emissions, revealing patterns influenced by factors such as Exhaust Gas Recirculation (EGR) rates and intake temperature. A combustion model was developed and validated using the 0D/1D simulation tool in the scope of dual fuel engines. The initial focus was on methane-Diesel combustion, validated against experimental data. Subsequently, this model scope was expanded to simulate hydrogen-Diesel combustion. This thesis has successfully introduced a methodology based on VEMOD to predict engine consumption and emissions across varying scenarios. The comprehensive analysis illuminated how energy distribution mechanisms operate and how factors influence engine performances. The application of this methodology to compression ignition engines demonstrated its versatility and prediction capabilities, making it a valuable tool for investigating future combustion scenarios, including dual fuel operation.

Acknowledgement

I extend my heartfelt thanks to the entire team at the CMT for providing a conducive research environment and access to essential resources. Your collaborative spirit and dedication have enriched my academic experience. I would like to acknowledge the UPV for providing access to resources, libraries, and research facilities essential to my thesis.

This research has been partially funded by the European Union's Horizon 2020 Framework Programme for research, technological development and demonstration under grant agreement 723976 ("DiePeR") and by the Spanish government under the grant agreement TRA2017-89894-R ("MECOEM") and I was supported by FPI grant with reference PRE2018-084411.

I am grateful to my thesis advisor, Jaime Martín Díaz, for his guidance. His mentorship has been invaluable throughout this research journey.

Heartfelt thanks to my colleagues who have played a significant role in this journey, offering their expertise, sharing ideas, and fostering a collaborative academic environment.

My time in Valencia was made memorable by my dear friends. Their encouragement and laughter have made the challenges more manageable and the successes more joyful during the ups and downs of this academic endeavor.

Special thanks to those friends who stood by me during challenging times, believed in me, providing motivation and a shoulder to lean on when I felt low. Your friendship has been a source of strength and inspiration.

I am profoundly grateful to my family, and I owe them a debt of gratitude for their unwavering and unconditional support. Their belief in my capabilities has been my constant source of strength. In a society where societal pressures often steer one's life choices, my family stood by my side, allowing me the freedom to pursue my dreams. Their faith in my abilities, their encouragement, and their unconditional love have been the driving force behind my accomplishments. This thesis stands as a testament to their faith in me, and I dedicate it to them with all my heart.

This thesis is a reminder that with the right support system and an unwavering commitment to one's dreams, even the most challenging of goals can be achieved. I am deeply grateful for the privilege of pursuing knowledge and contributing to my field.

Thank you, from the bottom of my heart to my family, to my friends, and to myself for the journey we've undertaken together.

Sushma

Nomenclature

$S_{L,0}$	Speed of the laminar flame
ϕ	In-cylinder equivalence ratio
ϕ_m	Equivalence ratio at maximum speed
B_m	Maximum laminar speed
B_ϕ	Laminar speed roll-off value
$\dot{m}_f H_v$	Chemical energy stored in the fuel with its heating value
N_b	Brake power
$\dot{Q}_{cool}$	Heat transfer to the engine coolant
H_{exh}	Net flow of the sensible enthalpy
$\dot{Q}_{oil}$	Heat dissipated to the engine oil
$\dot{Q}_{WCAC}$	Heat rejection in the intercooler
$\dot{Q}_{mat}$	Heat accumulated within the engine structure
$\dot{Q}_{HPEGR}$	Heat rejection in the high pressure EGR
$\dot{Q}_{LPEGR}$	Heat rejection in the low pressure EGR
$\dot{Q}_{pipes}$	Heat rejection in the pipes
$\dot{Q}_{turbo-amb}$	Heat rejection in the turbocharger
N_a	Auxiliary power
H_{bb}	Enthalpy flow of blow-by losses

Acronyms

ACS	Ambient Cold Start
BMEP	Brake Mean Effective Pressure
CI	Compression Ignition
DI	Direct Injection
ECU	Engine Control Unit
EGR	Exhaust Gas Recirculation
GEB	Global Energy Balance
HPEGR	High-Pressure Exhaust Gas Recirculation
HSDI	High-Speed Direct Injection
ICE	Internal Combustion Engines
IMEP	Indicated Mean Effective Pressure
LPEGR	Low-Pressure Exhaust Gas Recirculation
LTCS	Low-Temperature Cold Start
NEDC	New European Driving Cycle
1D	One-Dimensional
VEMOD	Virtual Engine Model
WLTC	World harmonised Light-vehicles Test Cycle
WLTP	World harmonised Light-vehicles Test Procedure
0D	Zero-Dimensional

CHAPTER 1

Introduction

Internal combustion engines (ICE) convert the chemical energy stored in fuel into mechanical energy. They are widely used in various applications such as automobiles, freight transport, aircraft, boats, stationary applications, etc. Internal combustion engines have been a crucial part of modern society for over a century. They have revolutionised the economy and the way we travel and interact with the world around us. These engines have continued to evolve over the years, with advances in technology and materials that have resulted in their improvement; thus, they continue to be one of the most important and widely used inventions. One type of IC engine is the compression-ignition (CI) engine. Diesel-powered vehicles use these engines and are essential to the internal combustion engine family [12].

CI engines have been the preferred choice for many years due to their reliability and fuel efficiency, making them ideal for commercial use in trucks, buses, and other heavy-duty applications. For decades, they also have been an excellent solution for light vehicles. They have been widely used in the transportation industry to achieve high efficiency and low emissions thanks to their higher thermal efficiency. In addition, these engines are typically more durable, making them a cost-effective option for many applications. However, modern CI engines now face challenges such as improved thermal efficiency and meeting real driving emissions standards. In recent years, significant efforts have been made to enhance combustion, reduce emissions, and improve the overall performance of CI engines [40-41]. However, new improvements are needed to enable the development of strategies that further reduce emissions and enhance fuel efficiency.

When analysing the performance of CI engines, two types of tests are commonly used: stationary tests and transient tests. Stationary tests involve running the engine at a constant load and speed. In contrast, transient tests simulate real-world driving conditions and replicate the different driving scenarios, such as acceleration, deceleration, braking, and uphill or downhill driving, to provide a more accurate and realistic representation of the vehicle performance. On the other hand, stationary tests measure the engine outputs at a specific operating point and do not account for the various driving conditions that a vehicle may experience. Transient tests are preferred over stationary tests because they provide a more realistic vehicle performance evaluation.

Transient tests are an essential tool for evaluating the performance and emissions of CI engines. One of the most widely used transient tests in the past for light vehicles was the New European Driving Cycle (NEDC). The NEDC evaluated a vehicle's fuel consumption and emissions under different driving conditions. However, the NEDC was abandoned for being outdated and not representative of real-world driving conditions. The Worldwide Harmonized Light Vehicle Test Procedure (WLTP) was developed to address these

limitations. The WLTP is a global standard for measuring vehicle fuel consumption and emissions and includes a series of driving cycles replicating real-world driving conditions. It considers different vehicle options and technologies and provides a more accurate representation of a vehicle's emissions, including nitrogen oxides (NOx), carbon monoxide (CO), particulate matter (PM) and unburned hydrocarbons [1-2].

When evaluating the performance and emissions of CI engines in transient operation, it is crucial to consider the effect of temperature conditions. During prolonged transient operation under warmed conditions, the engine can reach high peak temperatures that can cause thermal stress on engine components such as the turbocharger and exhaust system, leading to premature wear and reduced engine life. Moreover, high temperature and engine calibration to prevent engine damage can result in an increased production of pollutants emissions. Similarly, during cold-start conditions, it takes longer to reach optimal operating temperature, resulting in increased emissions of hydrocarbons (HC), carbon monoxide (CO), and particulate matter (PM). This may cause the engine to fail to meet regulatory emission standards, resulting in suboptimal vehicle performance. Moreover, the engine may experience higher fuel consumption due to increased friction between engine components, reducing fuel efficiency. Therefore, engine manufacturers must account for these factors during development to ensure they meet regulatory standards, and their engines deliver optimal performance and emissions. The World Harmonized Light Vehicle Test Procedure highlights the importance of considering a wide range of operating conditions, including ambient, warmed, and cold-start conditions.

In addition to considering temperature conditions during transient operation, it is also essential to account for high altitude conditions when evaluating the performance and emissions of CI engines, which can significantly affect engine performance and emissions. At high altitudes, the reduced air pressure leads to a lower oxygen supply to the engine, resulting in reduced power output and increased fuel consumption. It also affects the combustion process, leading to incomplete combustion, increased hydrocarbons (HC) and carbon monoxide (CO) emissions, and reduced efficiency. The turbocharger, designed to boost the engine's power output by compressing inlet air, can experience reduced performance due to the reduced air pressure at high altitudes. Similarly, the reduced air pressure can also affect the EGR system, which recirculates some of the exhaust gas back into the engine to reduce emissions. WLTP also emphasises the importance of high-altitude conditions. It includes simulating driving conditions at elevations up to 2000 meters above sea level [3-10].

The assessment and understanding of various technologies for transient operation have become crucial for tackling the issues of emissions formation and consumption in CI engines. To evaluate the advantages of engine strategies, experimental and simulation techniques have become more and more relevant. A valuable methodology for this purpose is the Global Energy Balance (GEB) [37], which can identify the pathways of chemical energy degradation and helps to understand the mechanisms affecting engine consumption. GEB methodology is a powerful tool for evaluating the performance and efficiency of combustion engines, in general, and compression ignition engines, in particular. The GEB provides a detailed breakdown of the chemical energy released during combustion and how

it is converted into mechanical work, heat rejection, and exhaust gas energy. By analysing the GEB, it is possible to identify the sources of energy loses and the mechanisms that affect engine efficiency, making it a valuable tool for developing engine strategies that optimise energy conversion and reduce energy loss. One of the main outcomes of the detailed GEB methodology is that it provides a comprehensive analysis of the engine's energy balance, accounting for specific conversion between energy inputs and outputs. This allows for a more accurate assessment of the engine's performance and efficiency than traditional methods, which only focus on a few key variables such as indicated and brake parameters and fuel consumption [11-15].

Despite the usefulness of GEB methodology for evaluating the performance and efficiency of CI engines, there is still a lack of research available in the literature on the application of GEB under transient conditions. Most existing literature focuses on GEB analysis under steady-state conditions, which is not representative of real-world engine operating conditions. The sudden changes in load and speed during transient operation affect the energy conversion pathways and result in different energy losses repartition. Hence, there is a need for more experimental and simulation studies on GEB under transient conditions to provide a better understanding of the mechanisms that affect engine efficiency and emissions during transient operation. This work includes the analysis of energy balance in transient operation with different ambient conditions [16].

Transient operation is characterised by quick changes in the operating conditions, which can be particularly demanding in terms of engine response and control and requires specific simulation analysis to improve and accelerate engine development. Simulation is an essential tool for engine development, especially in the context of transient operations. It allows predicting the engine performances under different operating conditions, such as changes in load or speed, which are challenging to analyse in experiments. Additionally, simulations can provide insight into complex phenomena that are difficult or impossible to observe directly, such as the interaction between different engine sub-systems and the effects of various engine layouts.

Simulating the engine performance under different conditions makes it possible to evaluate its performance and optimise the energy balance, including aspects such as fuel efficiency and emissions. Furthermore, simulations can guide further engine improvement, reducing the time and cost required for experimental work. In this framework, the use of zero/one dimensional (0D/1D) tools to simulate the complete engine response (system modelling) has shown to be useful [38]. These models can capture the interactions between different sub-systems while being computationally efficient. However, the accuracy of these models is limited by the quality of the input data and the assumptions made in the modelling process.

To overcome this limitation of modelling, it is common to combine simulation with experimental data. It can be used to validate simulations, allowing for more accurate predictions while simultaneously reducing the need for further experimentation. For example, simulations may predict that a particular design change will improve fuel efficiency, but experiments may reveal unexpected interactions between sub-systems that

affect the overall performance. Combining both information makes it possible to better understand the engine's performance and make wiser decisions. Combining experimental and simulation information is helpful to perform a complete analysis and improves the accuracy of simulations. It can also reduce the time and cost required for further experimental work. [17-19]

There is a lack of comprehensive analysis on the energy balance in engine research, as currently available works do not provide deep analysis from either experimental or modelled perspectives. This work also aims to bridge this gap by presenting a new methodology combining experimental and simulated information to analyse the energy balance. The experimental fluid temperatures are used to validate the model's performance, while certain experimental settings, such as instantaneous fuel and air mass flows are targeted for engine control during simulations. The methodology adopted involves using VEMOD (Virtual Engine Model) [39]. VEMOD is a home developed tool, developed at CMT and is similar to the well-known tool GT-suite. This 0D/1D modelling tool has been calibrated under stationary conditions and will be validated during the WLTC (Worldwide harmonised Light-duty Test Cycle) by comparing key variables, such as brake torque or turbine outlet temperature, that describe the engine's thermal performance. The VEMOD is a stand-alone tool aimed at simulating new standard testing cycles. This computational tool was developed as a response to limiting requirements of new standards closer to real-world driving conditions. VEMOD can predict engine performance and emissions along with the thermal and fluid dynamic conditions in the different fluid circuits, including gas and liquids (coolant and oil). The core of VEMOD is the combustion model, a 1D model based on the concept of Apparent Combustion Time (ACT), which provides VEMOD with the capacity to predict heat release rate and emissions by calculating local conditions in the Diesel flame. VEMOD will be used to model the different energy terms to complete the energy balance of the system. A combustion diagnosis tool called CALMEC [43, 44], developed at CMT-Motores Térmicos, was also used in the current work to calculate the heat release and to calibrate the in-cylinder heat transfer in VEMOD based on the experimental measurements in stationary conditions.

After working on the development of a methodology to predict the performance and emissions of a DI Diesel engine in transient conditions, the work is focused on expanding the performance of the 0D/1D modelling tool to explore the potential of innovative dual fuel combustion modes aimed at the decarbonisation of the transport sector, thus boosting its ability for future cleaner combustion powerplants.

Recently, fuels other than Diesel have emerged as an alternative to compression ignition engines. A significant technological evolution is required to obtain the best engine potential in consumption and emissions. There is a promising path based on using gaseous fuels alone or gaseous fuels along with Diesel fuel. The latest, called dual fuel operation, is another approach to reducing emissions and improving engine efficiency. Dual fuel engines operate using two different fuels at the same time. They are commonly used in various transportation applications, such as trucks, buses, and locomotives. One of the fuels is typically a conventional liquid fuel, such as Diesel or gasoline, while the other is a gas fuel with low carbon content, such as natural gas or propane. Dual fuel engines offer several

advantages, including lower emissions, increased engine efficiency and fuel flexibility [20-21]. The major challenge with dual fuel engines is the need to carefully control the fuel ratio to optimise engine performance and minimise emissions, which requires advanced control systems and sensors. Despite these challenges, dual fuel engines are becoming increasingly attractive in transportation as the demand for cleaner, more efficient engines continues to rise. Simulation models can be used to predict the performance of dual fuel engines, while experimental data can be used to validate the simulation results. This approach can lead to a better understanding of the underlying physical processes in dual fuel engines, which can help to optimise their performance. [20-24]

Methane, a key component of natural gas, is one of the fuels that can be used in dual fuel engines. Its advantages over traditional fuels include lower carbon content, a high-octane rating, and lower pollutant emissions such as carbon monoxide, nitrogen oxides, and particulate matter, making it an attractive option for reducing greenhouse gas emissions. In a dual fuel engine, methane is typically injected into the intake air stream and mixed with liquid fuel, such as Diesel or gasoline. The methane is ignited by the combustion of the liquid fuel, leading to a more complete combustion of both fuels. In literature, the use of methane as the gaseous fuel has been shown to reduce Diesel consumption by up to 30% while also reducing emissions of nitrogen oxides by up to 70%, particulate matter by up to 50%, and carbon monoxide by up to 90% approximately [42]. Overall, utilising methane in dual fuel engines offers several advantages, including improved fuel flexibility, higher efficiency, and reduced emissions. This technology may become increasingly important in the heavy-duty vehicle industry [29] as the search for sustainable and cleaner energy sources continues. [24-30]

The scope of this thesis has been extended from the scope of conventional Diesel engines to analyse the characteristics of methane-Diesel combustion by commissioning a combustion model. Specifically, a laminar flame speed model for methane will be developed. Unfortunately, the combustion model available does not include pre-defined constants for the laminar flame speed model for methane. As a result, there is a need to develop a new model. To develop a new laminar flame speed model, approaches from Heywood and Gülder will be used. These approaches will enable to create a model that accurately predicts the speed at which flames propagate in a laminar flow of methane. Once the laminar flame speed model is developed, it will be incorporated into the combustion model. Simulation results will be compared with experimental data to validate the model, ensuring the model accuracy in predicting engine performance [31, 32].

The potential of the previously created dual fuel combustion model will be extended to predict the combustion characteristics of hydrogen-Diesel dual fuel engines, a promising technology that can significantly reduce greenhouse gas emissions, as hydrogen is a clean-burning fuel with no carbon emissions. However, hydrogen has low energy density and high combustion temperature, which limits its use as a main fuel in internal combustion engines. Therefore, dual fuel engines can be an effective solution for utilising hydrogen as a gaseous fuel to improve engine efficiency and reduce emissions by combining the high energy density of Diesel with the clean-burning properties of hydrogen. The model considers the differences in combustion properties between Diesel and hydrogen, such as the ignition

delay, flame speed, and heat release rate. By carefully controlling the fuel ratio and injection timing, the dual fuel operation can optimise the combustion process to achieve high efficiency and low emissions. Furthermore, hydrogen as a secondary fuel can provide additional benefits, such as improved engine durability and reduced particulate matter emissions [34, 35].

In this framework, a dual fuel combustion model has the potential to predict the combustion characteristics of hydrogen-Diesel dual fuel engines and optimise their performances [33-37]. In the current work, the dual fuel combustion model will be adapted to simulate and assess the properties of hydrogen-Diesel combustion. New correlations for laminar flame speed are required based on empirical measurements found in the literature. Numerical simulations are based on an experimental campaign using the methane-Diesel but operating with hydrogen. The challenge lies in accurately determining laminar flame speed in extremely lean conditions, leading to the development of two new correlations for different ranges of equivalence ratio.

Once the combustion model is commissioned for Diesel and dual fuel operation and the complete system model is validated to operate in transient (only for Diesel), a thorough analysis of the energy split will be presented, utilising the tool to compute different terms that are difficult or impossible to obtain experimentally, such as the heat rejection to different engine parts and mechanical losses split. This work will compare energy balance between ambient, cold, and warmed conditions. A cumulative approach was used to plot the energy terms along the WLTC for a 1.6 L CI engine. This involved accumulating and averaging the energy terms from the start until a certain point to provide a smoother and less noisy evolution. The study also investigated the effect of engine altitude on the GEB during transient operation. Two altitudes (0 and 1000 meters) were considered. The analysis involved examining the instantaneous evolution of the energy terms, discussing the observed trends, and comparing the cumulated energy terms at the end of WLTC to summarise the main effects. The study also includes the analysis of in-cylinder and combustion parameters and NOx emissions, covering different engine architectures and ambient conditions. Due to time and experimental data availability, this study focused only on Diesel operation.

Objectives

The main objective of the thesis is to contribute to the development of a methodology that allows predicting the consumption and, with lower accuracy, the emissions of a compression ignition engine operating under transient conditions and considering the effect of different engine architectures (high/low-pressure EGR, cooling, lubrication…) and ambient conditions (hot/cold or normal), using a 0D/1D modelling tool. It also aims to expand the potential to dual fuel engines by adapting the 0D/1D tool and evaluating its ability for future combustion. The specific objectives are as follows:

1. **Commissioning a 0D/1D modelling tool for CI engines to operate in transient** considering low temperature/pressure conditions to approach real-time operation. Tool upgrade will focus on accurately calculating the thermodynamic conditions in the combustion chamber, considering the particularities of cold conditions and transient operation.
2. **Commissioning a dual fuel combustion model** to simulate and investigate the characteristics of methane-Diesel combustion and extrapolate its potential for predicting hydrogen-Diesel combustion characteristics.
3. **Performing an extensive analysis of the engine energy repartition during transient** operation to assess the effect of different variables on the Global Energy Balance (GEB) and engine performances, focusing on various altitudes and thermal conditions such as ambient, cold, and warmed.

CHAPTER 2

Publication 1

"0D Laminar Flame Speed Model for Methane Lean Mixture in Dual Fuel Combustion"
De Robbio, R., Mancaruso, E., Vaglieco, B.M. STEMS-CNR Naples, Italy
Artham, S., Martín, J. CMT- Motores Térmicos Valencia, Spain

Publication 2

Experimental Validation of Laminar Flame Speed Model for CH4/Diesel Dual Fuel Engine applied to H2/Diesel Combustion / De Robbio, R.; Mancaruso, E.; Vaglieco, B. M.; Artham, S.. - (2022), pp. 321-335. (Intervento presentato al convegno : Proceeding of THIESEL 2022 Conference on Thermo- and Fluid Dynamics of Clean Propulsion Powerplants. nel Settembre 2022) [10.4995/Thiesel.2022.632801].

Publication 3

Olmeda P, Martin J, Arnau FJ, Artham S. Analysis of the energy balance during World harmonized Light vehicles Test Cycle in warmed and cold conditions using a Virtual Engine. International Journal of Engine Research 2019; DOI:10.1177/1468087419878593.

Publication 4

Payri F, Martín J, José Arnau F, Artham S. Analysis of temperature and altitude effects on the Global Energy Balance during WLTC. International Journal of Engine Research. 2022;23(11):1831-1849. doi:10.1177/14680874211034292

All the above-mentioned papers are attached in the appendix.

CHAPTER 3

General discussion of the results

Throughout this thesis, investigations and simulations have been conducted, considering a wide range of engine operating conditions and fuel types. The results presented in this general discussion represent the culmination of an in-depth analysis and interpretation of the findings obtained from both experiments and simulations.

In the subsequent sections, each specific objective will be examined in detail, focusing on highlighting the key findings, implications, and potential applications of the research. Additionally, the challenges encountered during this study will be addressed, providing a comprehensive overview of the contributions made to the field of compression ignition engines operating under transient conditions. Furthermore, the limitations of the research will be discussed, and potential paths for future research and advancements in this area will be suggested.

This work aims to improve the understanding of engine operation under transient conditions using a 0D/1D modelling tool and contribute to developing cleaner, more efficient, and sustainable propulsion technologies for the transport field. By presenting the aggregate results, this research aspires to contribute to the knowledge base in this domain and foster progress towards a greener and more sustainable future.

Objective 1: Commissioning a 0D/1D modelling tool for CI engines

This section focuses on commissioning combustion sub-models for the 0D/1D modelling tool (VEMOD) to enable real-time operation and accurate calculation of thermodynamic conditions in the combustion chamber during transient engine operation, particularly under low temperature and pressure conditions. Stationary and transient tests were conducted in the experimental setup to achieve this. The relevant parameters required for analysis, such as engine speed, torque, air and fuel mass flows, oil and coolant temperatures, temperature and pressure at intake and exhaust lines, coolant mass flows and in-cylinder pressures in the four cylinders, were measured.

The next step involves calibrating the combustion and emission sub-models, in-cylinder heat transfer, and mechanical losses using the data obtained from the stationary points. The calibration procedure utilised a combination of motoring and combustion tests under stationary conditions, as detailed in Table 1.

Engine speed in rpm	Load in %
1000	Motoring
2000	Motoring
3000	Motoring
4000	Motoring
850	idle
1000	21, 44, 66, 88
1250	13, 26, 50, 76, 100
1500	11, 25*, 50, 75*, 100
2500	25, 50, 75, 100
3500	25*, 50, 75, 100

Table 1. Stationary tests performed (*Both conventional and cold ambient conditions at –7ºC).

The motoring tests were utilised to adjust engine uncertainties and convective heat transfer tuning. Warmed and cold combustion tests covering the complete engine map were conducted to further calibrate the remaining sub-models. The calibration process encompassed the following key aspects:

1. An in-house developed methodology was employed, combining experimental and simulated in-cylinder cycles [45]. This approach accurately calibrated the real compression ratio, deformations model, and in-cylinder heat transfer model, enhancing overall simulation accuracy.

2. The injector model was fine-tuned using a comprehensive experimental matrix in an injector test rig. This calibration was aimed to accurately predicting the injection rate, the starting point for the combustion prediction.

3. After calibrating the heat transfer model, the combustion model was calibrated. This involved determining fitting constants for ignition delay, premixed and diffusion combustion sub-models. The calibration criterion sought to minimise differences between experimental and simulated heat release, ensuring precise prediction of combustion characteristics.

4. Calibration of the friction model focused on achieving an accurate prediction of brake efficiency. Stationary operating points across the complete engine map, under cold and warmed conditions, were utilised for this calibration.

Continuing with the results, the model's performance was thoroughly assessed, and the key findings are presented. The top two plots of Figure 1 illustrate the experimental and modelled heat release at an engine speed of 2500 rev/min under varying loads (25% and 100%). The plotted dotted lines represent the modelled values obtained from the calibrated combustion model in VEMOD, while the solid lines represent the corresponding experimental values collected from all four cylinders. As can be seen, the model accurately

predicts the heat release evolution, and the observed discrepancy closely agrees with the inherent differences between cylinders.

The bottom of Figure 1 also presents the heat release at engine speeds of 1250 and 3500 rev/min, both operating at a 50% load, with the bottom two plots. Once again, a good overall agreement is observed between the modelled and experimental results. Notably, the modelled heat release is slightly slower than the experimental values at high speeds and loads. This difference in performance can be attributed to the primary focus of the calibration on the low to mid ranges, which play a critical role in simulating the WLTC. The agreement between the experimental and modelled heat release confirms the effectiveness of VEMOD in simulating compression ignition engines. It is worth mentioning that a study of Olmeda et al. [40] included detailed pressure and heat release evolutions at various speeds and loads. However, it has been omitted from this discussion for conciseness.

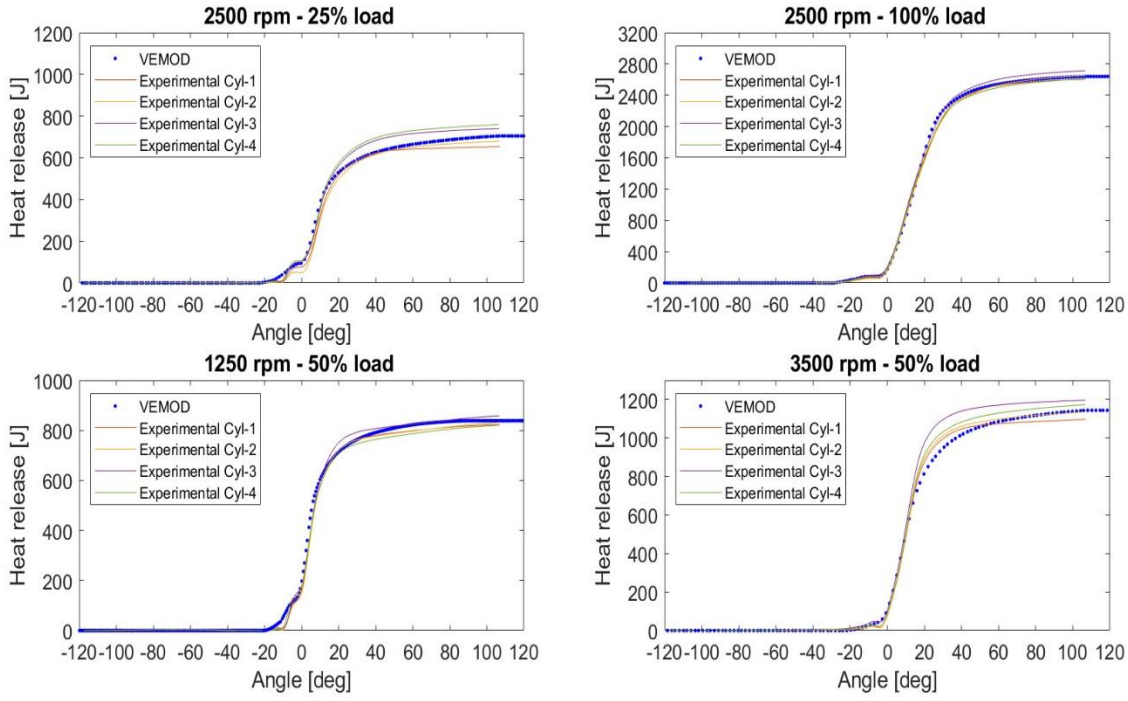

Figure 1. Heat release at different loads (top) and speeds(bottom) in steady-state conditions.

Figures 2–3 provide an overview of the experimental and modelled indicated mean effective pressure (IMEP) and turbine inlet temperature for all selected tests in steady-state, covering various engine speeds and loads, as shown in Table 1. The mean relative error for IMEP is approximately 2%, while it is around 1.5% for turbine inlet temperature. For the sake of brevity, other variables that will be later shown in transient operation have been omitted. However, it is important to note that their overall performance is similar to the variables already displayed. Specifically, the Brake torque mean error is approximately 4.5%, the

turbine outlet temperature shows a mean relative error of 2.5%, the coolant temperature exhibits 0.5%, and the oil temperature has a mean relative error of 1.5%.

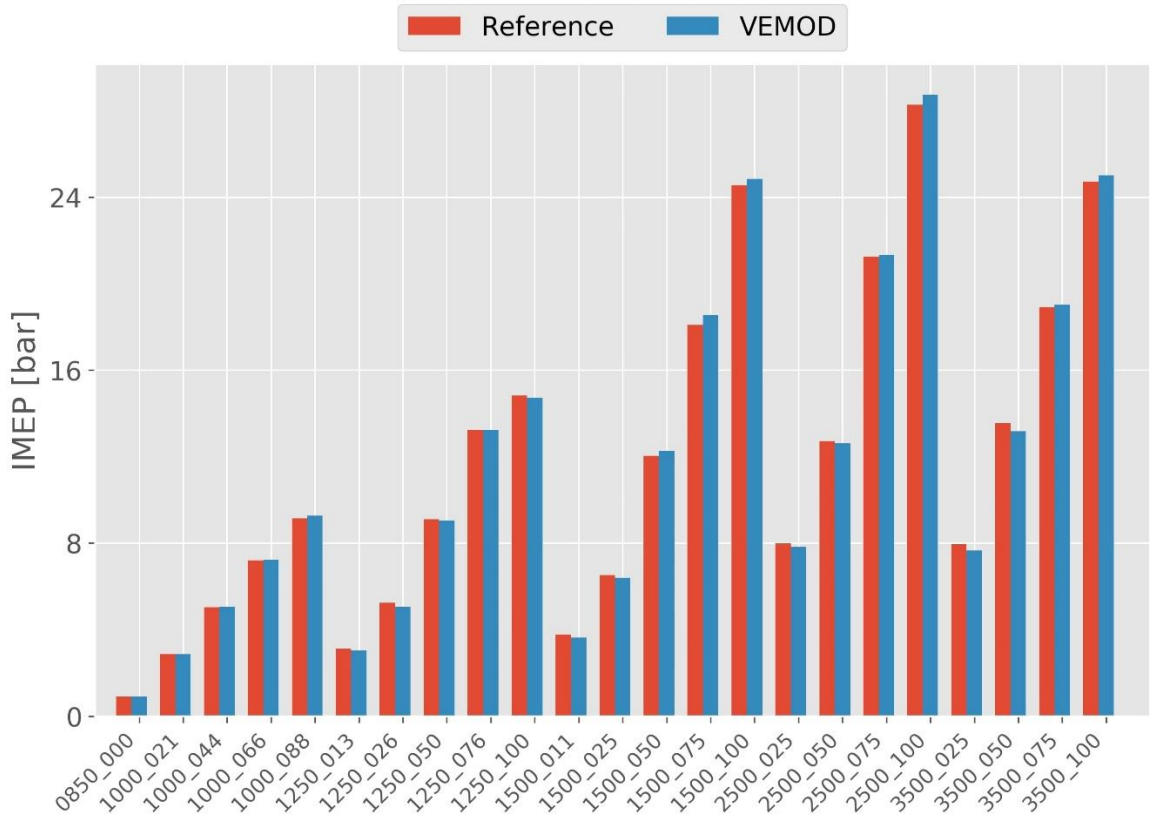

Figure 2. IMEP at different speeds and loads in steady-state conditions.

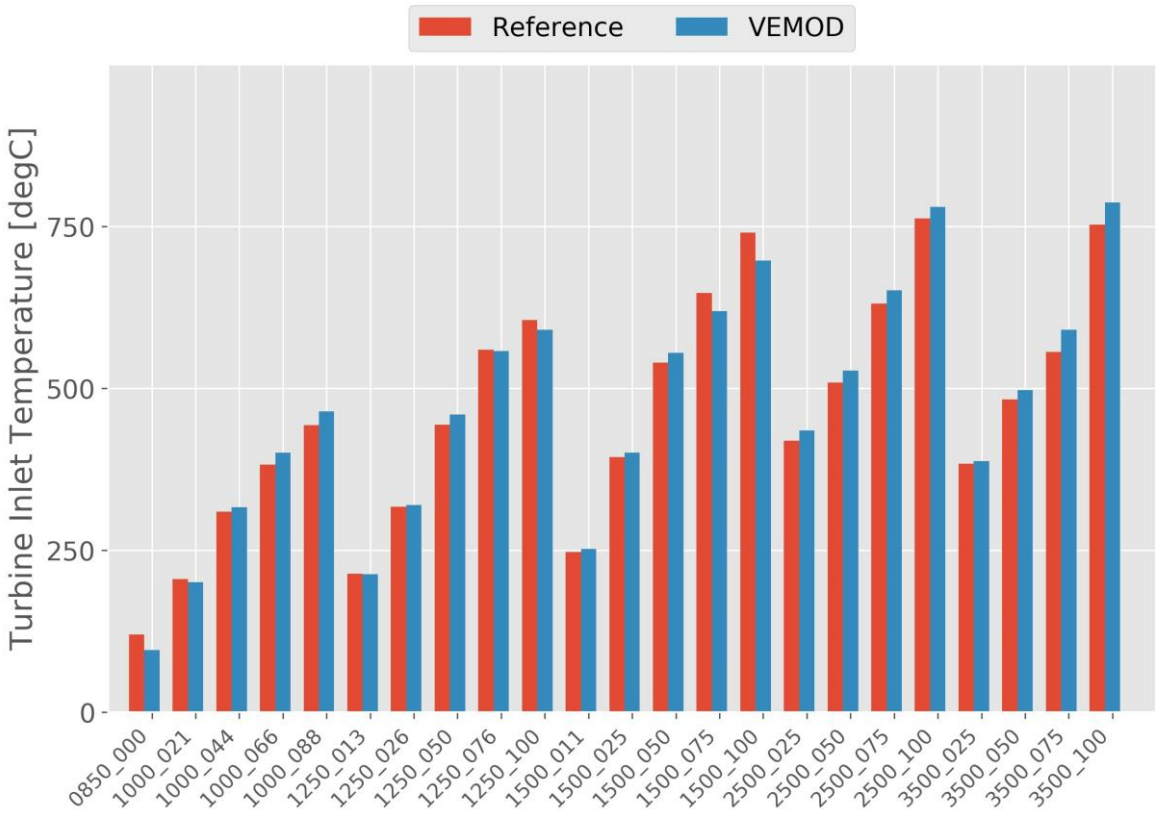

Figure 3. Turbine inlet temperature at different speeds and loads in steady-state conditions.

These results indicate that the modelling tool (VEMOD) performs well in predicting key parameters under steady-state conditions. The relatively low mean relative errors for IMEP, turbine inlet temperature, and other variables suggest that the tools predictions closely agree with the experimental data. The calibration process significantly improved the tool predictive capabilities and played a critical role in ensuring the accuracy and reliability of the VEMOD and ensured the sub-models accurately represented the performance of the real-world engine under steady-state operating conditions. Such predictions are crucial for ensuring the tool's accuracy in transient operation, which will be discussed in subsequent sections.

To validate VEMOD's performance under various transient conditions, the simulated WLTC was compared with experimental results at different engine temperatures. Table 2 summarises the different starting temperatures of the WLTCs.

Test conditions	Room temperature	Initial block temperature	Initial Coolant temperature	Initial Oil temperature
Ambient Cold Start (ACS)	20°C	20°C	20°C	20°C
Low-Temperature Cold Start (LCTS)	-7°C	-7°C	-7°C	-7°C
Warmed start	20°C	≈ 80°C	≈ 80°C	≈ 85°C

Table 2: Initial temperatures in the WLTC tests performed.

The validation at Low-Temperature Cold Start (at -7◦C) is presented in this section. The model has been validated considering several variables, the most relevant being torque, coolant temperature, and oil temperature.

Figure 4 displays the experimental and modelled torque and cumulated brake energy throughout a complete WLTC, starting at -7°C. The model effectively tracks the torque evolution, especially during rapid load changes. The torque prediction shows a mean error of 10 Nm (with a mean relative error of about 7%), with approximately 90% of the points having an error below 11 Nm. Although some differences are observed during the instantaneous evolution, the cumulative effect by the end of the complete cycle is merely 4%.

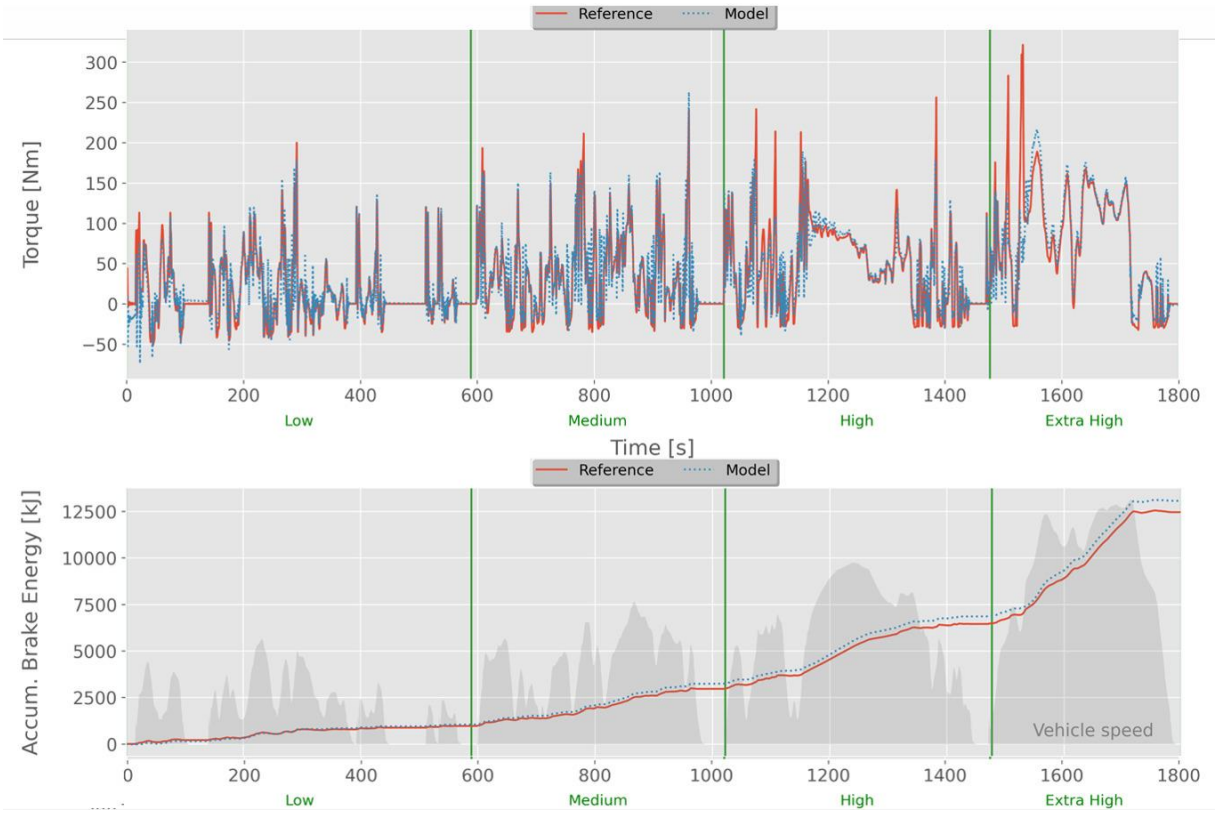

Figure 4. Brake torque and brake energy in transient at LTCS conditions 0 m.

Figures 5 and 6 illustrate the coolant and oil temperature, critical parameters for assessing the engine's thermal performance in low-temperature scenarios during the transient conditions. The mean error for coolant temperature is calculated at 3°C, with a relative error of 1%. Likewise, the mean error for oil temperature is approximately 4°C, with a relative error of around 1.5%. Notably, about 90% of the points show a relative error below 6°C for both coolant and oil temperatures, indicating a reliable model prediction.

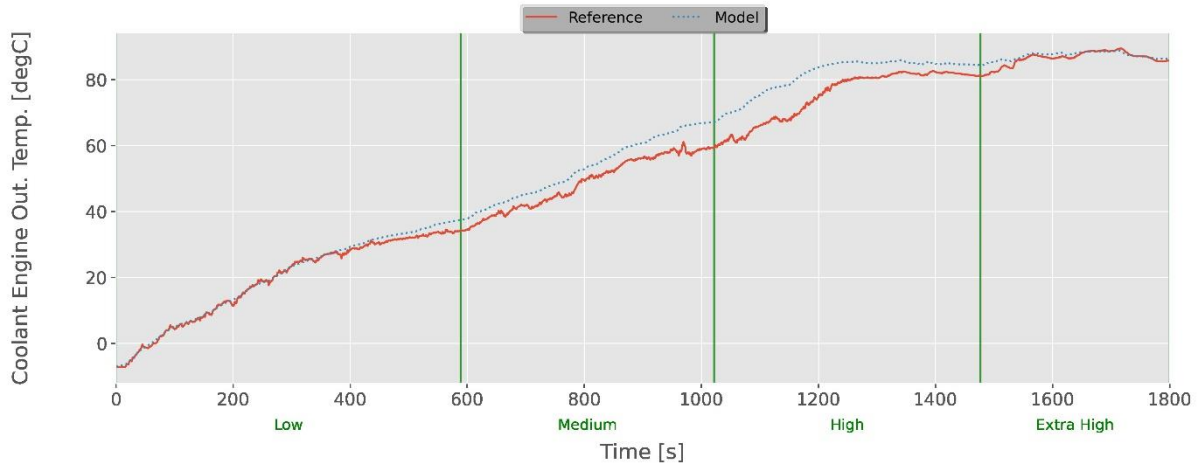

Figure 5. Coolant temperature in transient at LTCS conditions 0 m.

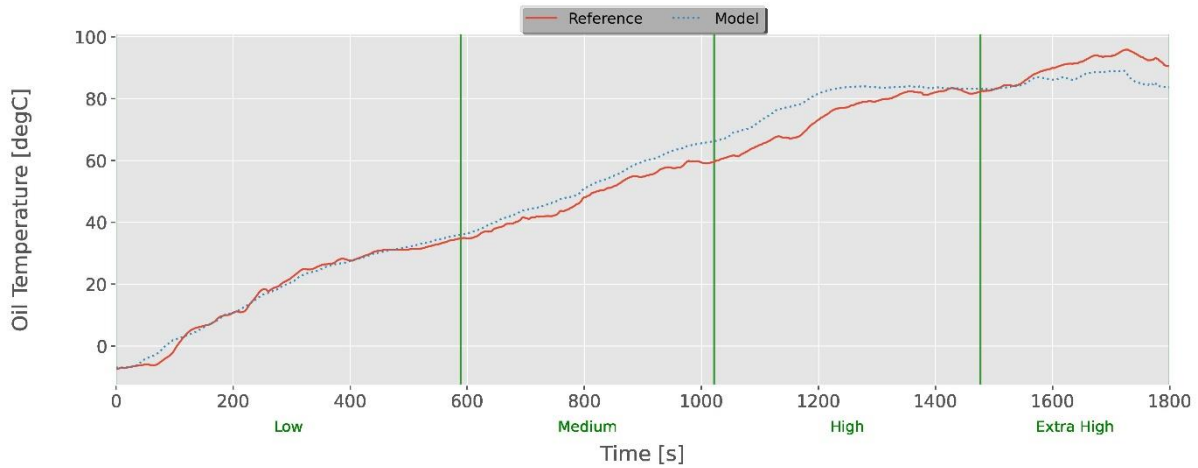

Figure 6. Oil temperature in transient at LTCS conditions 0 m.

The dependable performance of the coolant and oil temperatures ensures accurate heat rejection prediction, a crucial aspect of the energy balance in low-temperature conditions. For the sake of brevity, results at ambient cold start conditions [40] have been omitted, but they agree closely with those depicted for low-temperature cold start.

These results emphasise the model's capability to precisely predict key parameters during transient operation, particularly under challenging low-temperature conditions. The

agreement between the model's predictions and real-world data confirms the effectiveness of VEMOD in simulating engine performance, making it a valuable tool for optimising engine performance and achieving energy efficiency across various operating conditions.

The successful commissioning of the 0D/1D modelling tool demonstrated in this section validates VEMODs capability to accurately simulate Diesel compression ignition engines under transient conditions. Furthermore, the tool ability to predict engine performance during the WLTC cycle allows its practical application in engine optimisation.

Objective 2: Commissioning a dual fuel combustion model

After completing the commissioning of the 0D/1D modelling tool, the thesis focuses on extending the potential to the promising dual fuel combustion. This objective focuses on assessing engine performance in a dual fuel mode. It was fulfilled in two steps. First, with methane as the primary fuel and Diesel as the pilot fuel, and second, with hydrogen as the primary fuel.

This first step of the objective focuses on developing and implementing a dual fuel combustion model to replicate experimental results and explore the characteristics of methane-Diesel combustion.

The research was conducted employing a single-cylinder, four-stroke Diesel engine with a displacement of 522 cm^3. Utilising the engine simulation tool, GT-Suite, the engine was modelled following the specifications from the engine test bench. As depicted in Figure 7, the model features two injectors: one is situated at the intake port for methane injection, and the other is a direct injection injector for Diesel fuel for combustion initiation.

To ensure a good calibration, stationary tests were performed at four operating points. The engine model was updated with intake and exhaust conditions, initial pressures and temperatures at various locations, methane fuel mass flow rate, the start of injection (SOI), and injected Diesel fuel mass, which were obtained from experimental results obtained from the dual fuel methane-Diesel engine test data, covering a range of operating points as outlined in Table 3. The "VL-out" orifice connection diameter was adjusted to regulate the air mass flow according to the experimental value. After the initial calibration, the focus shifted towards refining the combustion model.

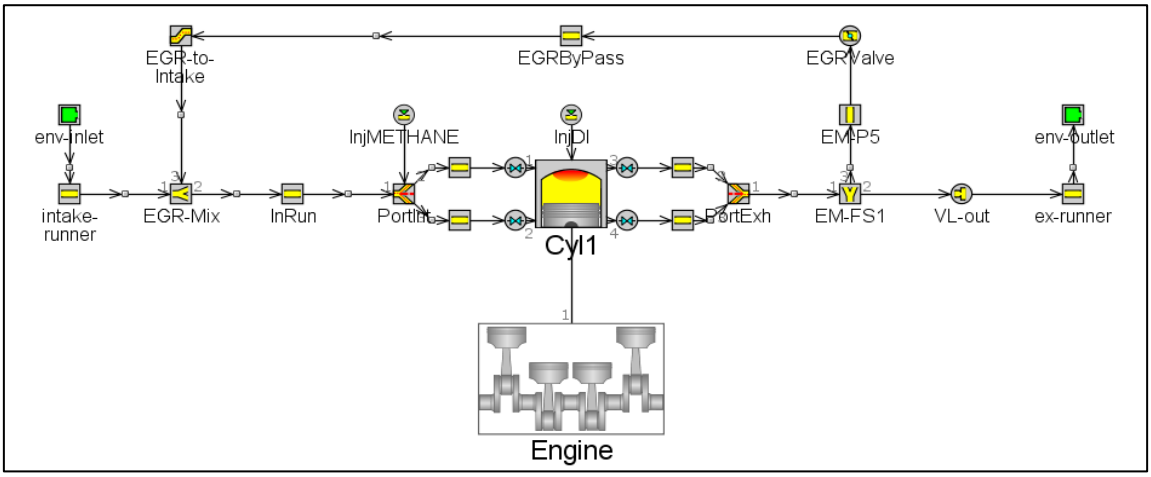

Figure 7. Compression ignition single cylinder Diesel engine in dual fuel mode.

A new laminar flame model was built and integrated into the setup for the methane-Diesel dual fuel model. The focus of this work is defining the $S_{L,0}$ term:

$$S_{L,0} = B_m + B_\phi(\phi - \phi_m)^2$$

$S_{L,0}$ represents the speed of the laminar flame in standard conditions (T_{ref}= 298 K and P_{ref} = 1.03 kPa), B_ϕ represents laminar speed roll-off value, ϕ represents in-cylinder equivalence ratio, ϕ_m is the equivalence ratio at maximum speed and B_m is the maximum laminar speed. A matrix for B_m, containing Gülder laminar flame speed values [46, 47] as a function of the equivalence ratio, was added in the 0D/1D tool.

Case	#1	#2	#3	#4
Engine Speed [rpm]	1500	1500	2000	2000
BMEP [bar]	2	5	2	5
Diesel mass injected [mg/cycle]	1.42	1.64	1.43	1.66
Methane mass [mg/cycle]	7.579	11.191	7.554	10.148
Rail pressure [bar]	615	867	700	891
Pressure inlet [bar]	1.5	1.7	1.5	1.7
Temperature inlet [°C]	44	46	50	51
Air mass [mg/cycle]	750.9	802.4	679.3	741.2
Methane/air equivalence ratio	0.174	0.240	0.192	0.236
Methane Premixed ratio [%]	86.1	88.8	86.0	87.6
Hydrogen mass [mg/cycle]	2.457	4.331	2.305	3.904
Hydrogen/air equivalence ratio	0.117	0.189	0.120	0.183
Hydrogen Premixed ratio [%]	82.8	88.0	81.8	86.7

Table 3. Dual fuel engine operating conditions.

Initially, the engine calibration was done under motoring conditions to determine the mass flow rate entering the system accurately. It's worth noting that the engine experiences mass loss, or "blow by," of the premixed air and methane charge in the cylinder's crevices region. This phenomenon was addressed through parameter calibration based on the findings in [42], tailored to the different cases.

Once the engine calibration of the mass flow rate and the respective simulation results matched with experimental data, the focus shifted towards calibrating the combustion. The 0D/1D tool consists of two models, “DIPulse” and “SITurb” for combustion calibration. “DIPulse” combustion model is tailored to predict the combustion rate in direct-injection diesel engines, accommodating both single and multi-pulse injection events. It offers the advantage of faster computational runtime while maintaining (or even overcoming) the predictive precision observed compared to other predictive models. It's worth noting that achieving accurate results with the “DIPulse” model relies on having a good injection profile and utilising four specific attributes (Entrainment, Ignition delay, Premixed and diffusion combustion) outlined in the “DIPulse” template for calibration. The “SITurb” model is designed to forecast the combustion rate in homogeneous charge, spark-ignition engines. This prediction considers various factors such as the cylinder's geometry, spark plug positions and timing, air circulation within the cylinder, and the properties of the fuel used. To calibrate this model effectively, it's crucial to focus on utilising key attributes such as laminar and turbulent flame velocities. The calibration was initially done with the 1500 rpm - 2 bar case, the available low-speed and low-load test. It was done using some design of experiments and optimisation techniques. The same values were used for the rest of the cases to test their reliability. All the cases have been calibrated to achieve the experimental values of air and methane masses, equivalence ratio, and accounting for blow-by effects.

The results comparing the experimental and numerical pressure curves and apparent Rate of Heat Release (RoHR) are shown in Figures 8-11.

Examining Figures 8-11 (b), an acceptable overall agreement in combustion characteristics can be found. The start of combustion, maximum intensity, and process duration agree across all cases. The 1500 rpm - 5 bar case displays some deviations, possibly due to some experimental noise. Heat release rates show different combustion stages. Initially, heat transfers to cylinder walls due to high compression temperature, while fuel vaporisation causes heat subtraction, which is seen as a negative RoHR. Low-temperature reactions activate, leading to positive apparent RoHR. This pattern is clear, especially in low-speed cases, illustrating good model performance. Overall timing and key combustion phases are well captured, even though the model slightly underestimates apparent RoHR during compression and overestimates it in the expansion's final part. This discrepancy likely stems from heat transfer calculation uncertainties rather than the combustion model's performance. In most cases, there is a close match between experimental and modelled pressure and apparent ROHR, except for the 1500 rpm - 5 bar case, which shows slight differences.

The calibration seems appropriate in Figures 8-11 (a), as compression curves agree well in each case, except for 1500 rpm - 5 bar. Even in the slightly worse 1500 rpm - 5 bar case, where combustion initiates a bit earlier than expected, the subsequent expansion performance closely mirrors the experimental pattern. The consistency witnessed in the expansion stages emphasizes the accuracy of the flame propagation model. This observation holds for most cases, supporting the model's reliability. In general, it can be observed that the laminar flame model effectively describes dual fuel combustion.

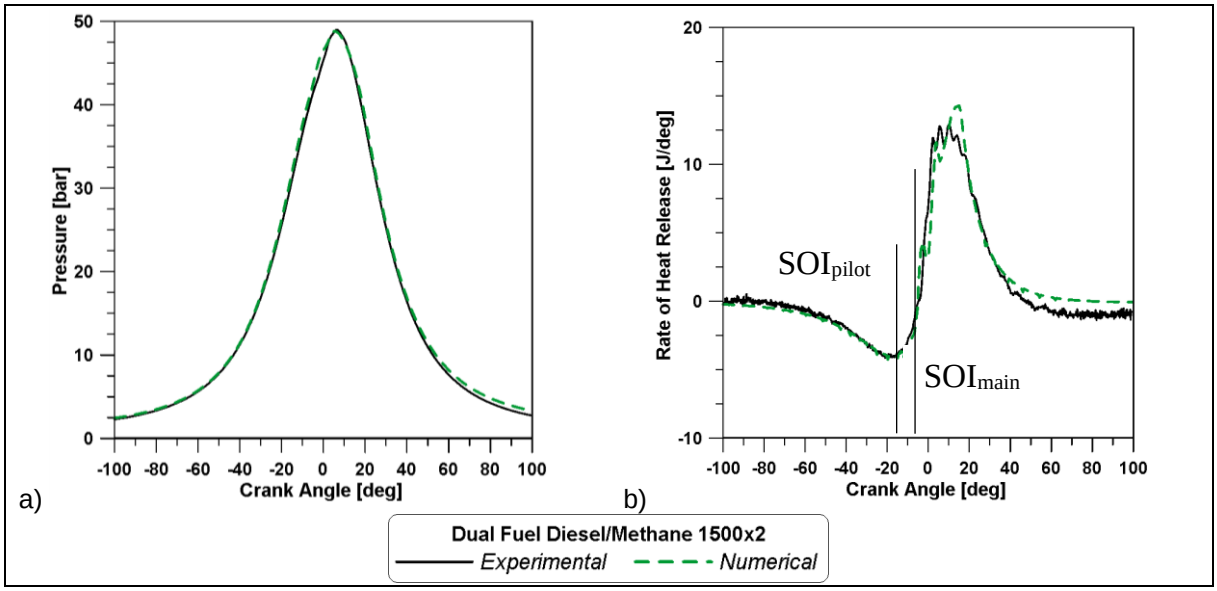

Figure 8. 1500 rpm - 2 bar - In-cylinder pressures (a) and apparent RoHR (b) for the Diesel-methane combustion.

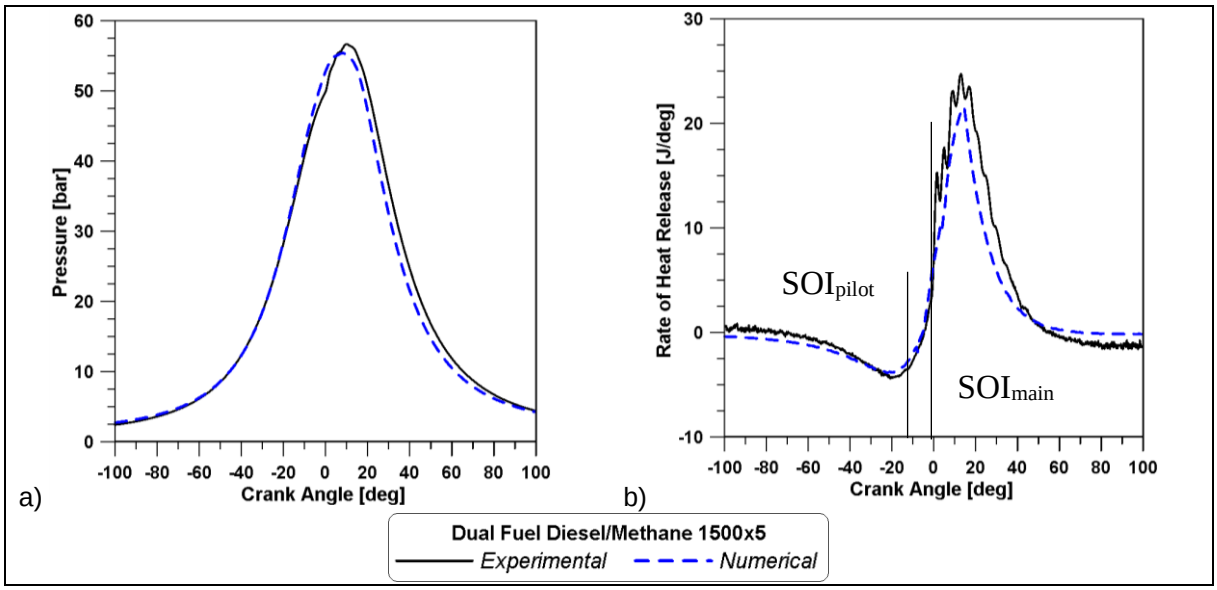

Figure 9. 1500 rpm - 5 bar - In-cylinder pressures (a) and apparent RoHR (b) for the Diesel-methane combustion.

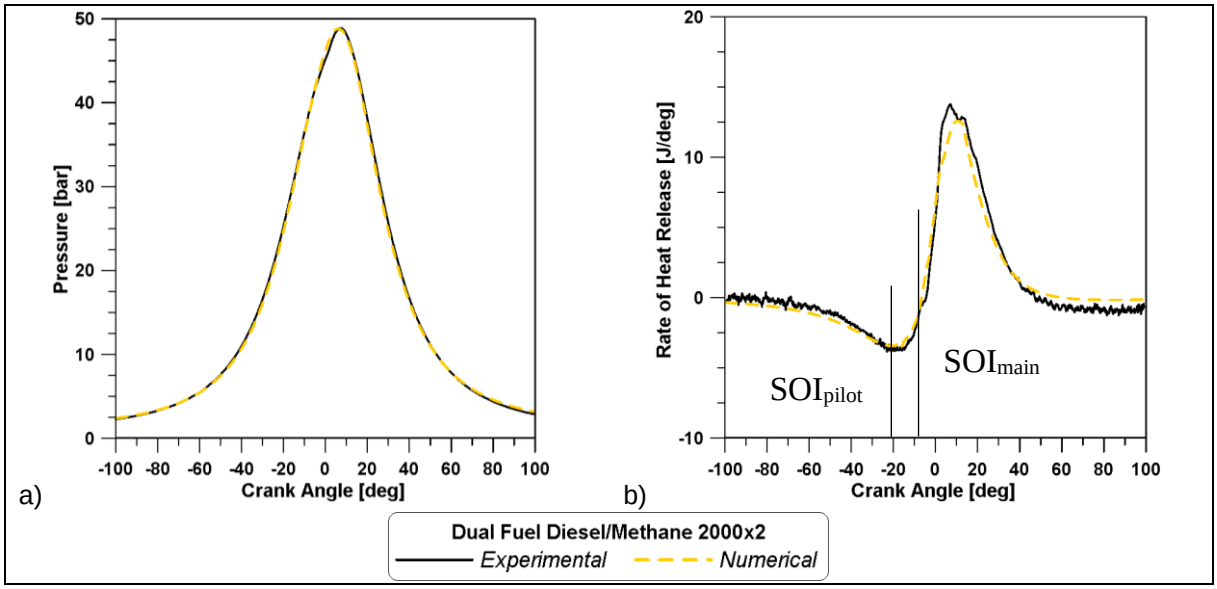

Figure 10. 2000 rpm - 2 bar - In-cylinder pressures (a) and apparent RoHR (b) for the Diesel-methane combustion.

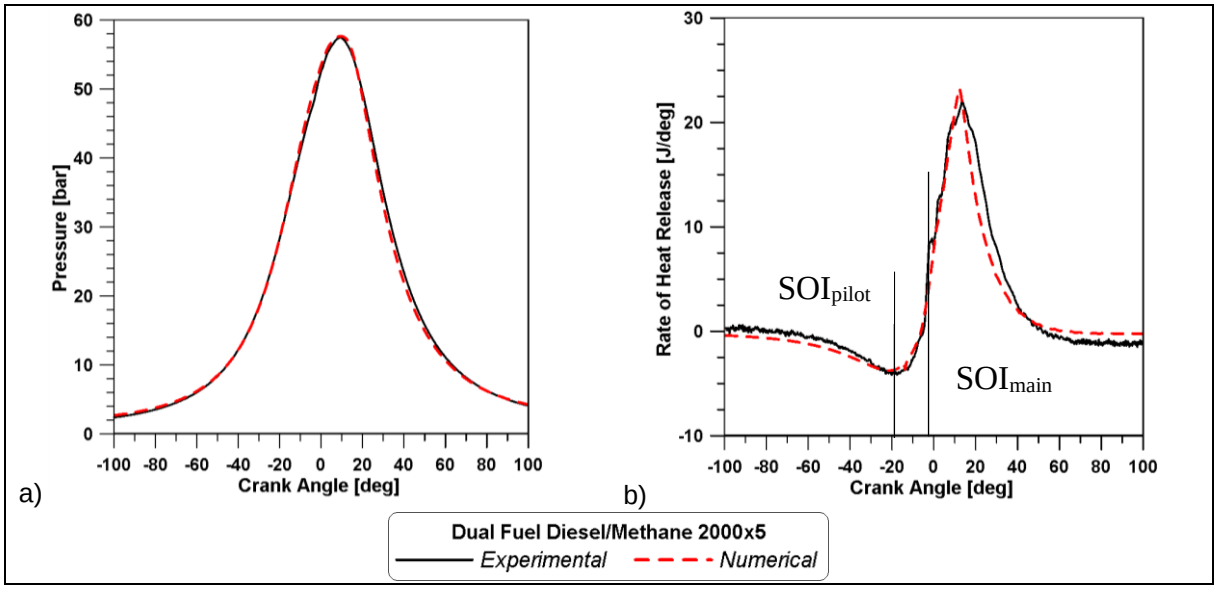

Figure 11. 2000 rpm - 5 bar - In-cylinder pressures (a) and apparent RoHR (b) for the Diesel-methane combustion.

The second step of the objective involves applying the methodology developed for dual fuel combustion modelling to predict the combustion characteristics of hydrogen-Diesel mixtures. The aim is to explore the potential of the established model in simulating hydrogen-Diesel combustion, offering insights into its feasibility.

For hydrogen, a similar methodology to that applied for methane was employed. However, it's worth noting that the correlations in the literature pertain to conditions different from the standard ones. Also, special care must be taken when estimating the laminar flame velocity, especially for low equivalence ratios, which tend to be lower in hydrogen simulations. To address this challenge, the development of a new correlation becomes necessary. The reason for resorting to the values proposed by Marinov et al. [48] lies in the inability to find an exponential correlation that adequately approximates the Taylor curve across the entire range of air-to-gaseous fuel ratios.

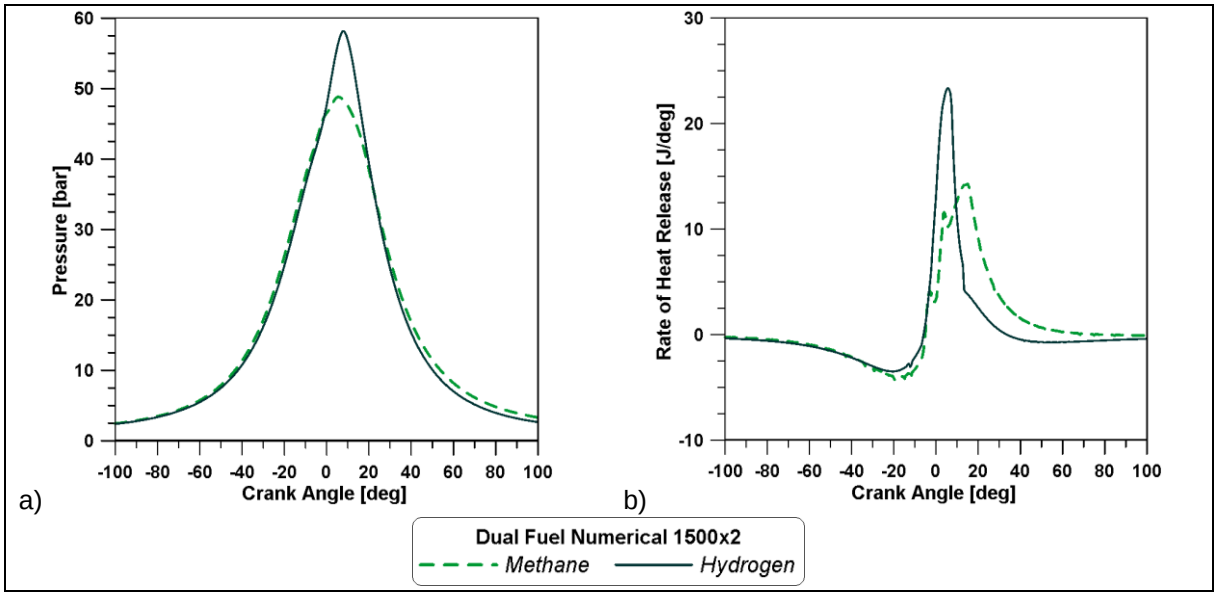

Figure 12. 1500 rpm - 2 bar - In-cylinder pressures (a) and apparent RoHR (b) for the Dual fuel numerical cases.

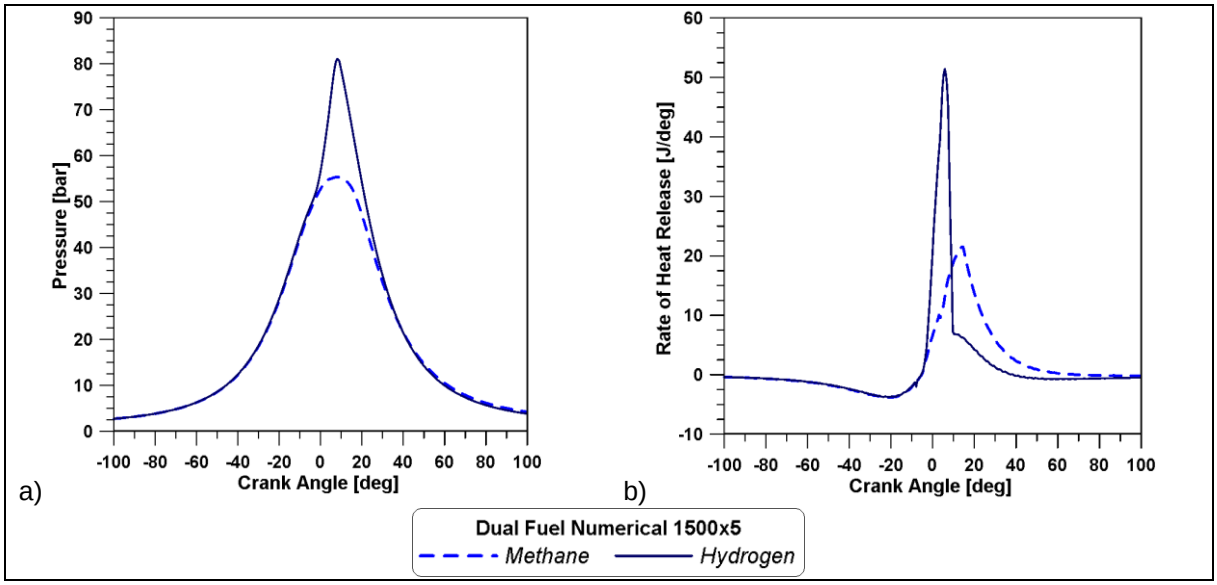

Figure 13. 1500 rpm - 5 bar - In-cylinder pressures (a) and apparent RoHR (b) for the Dual fuel numerical cases.

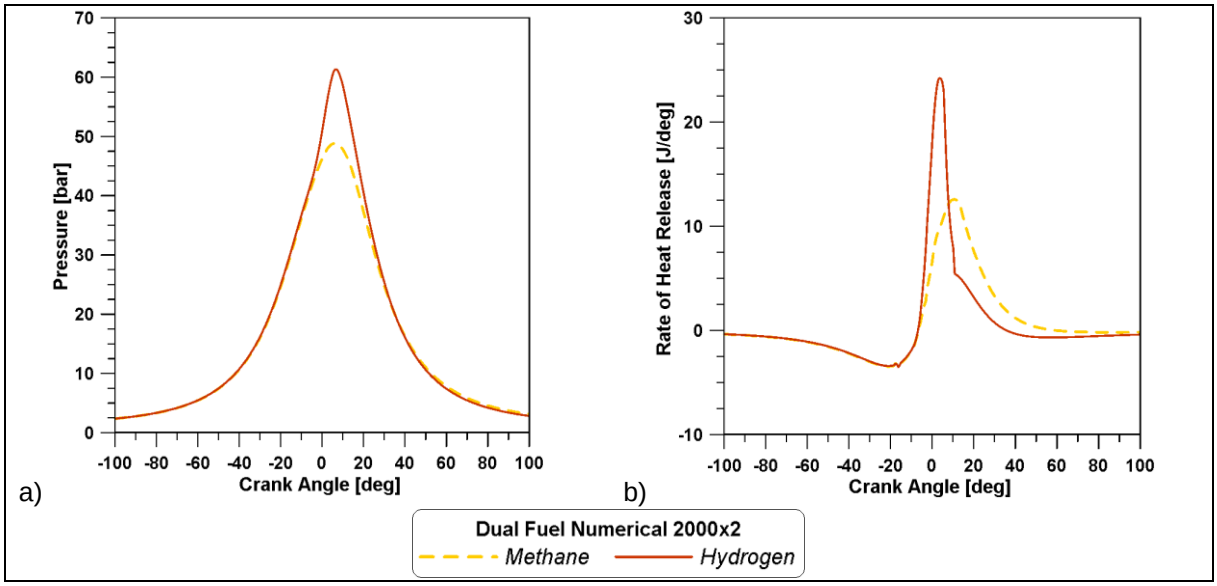

Figure 14. 2000 rpm - 2 bar - In-cylinder pressures (a) and RoHR (b) for the Dual fuel numerical cases.

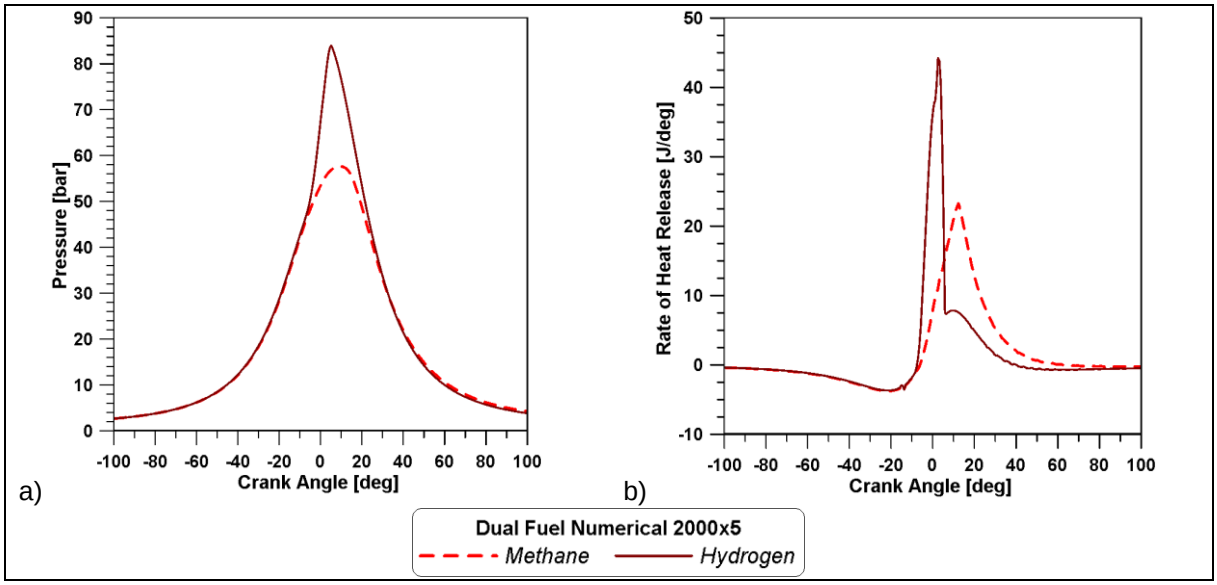

Figure 15. 2000 rpm - 5 bar - In-cylinder pressures (a) and RoHR (b) for the Dual fuel numerical cases.

The results presented in Figures 12-15 include the numerical outcomes and predictions for scenarios where hydrogen is used instead of methane. The main parameters are detailed in Table 3. In Figures 12-15 (a), it's evident that employing hydrogen leads to a notable increase in peak pressure across all instances. This effect can be attributed to hydrogen higher flame velocity, which results in an accelerated pressure rise right after the pilot ignition.

The apparent Rate of Heat Release (RoHR) is illustrated in Figures 12-15 (b). In contrast to the scenarios involving methane, hydrogen's high reactivity and rapid combustion trigger a substantial oxidation process immediately after the diesel pilot ignition. In each case, there is a noticeable deviation between the experimental and numerical slopes of the RoHR, with a more pronounced increase observed when hydrogen is in the mix. The quick consumption of gaseous hydrogen accelerates the entire process, leading to a single, more intense peak and a reduced duration of gaseous combustion. Due to the faster hydrogen combustion, the premixed phase in all cases is shorter than that observed with methane.

Objective 3: Extensive analysis of the engine energy repartition during Transient

This section is dedicated to the third objective of the thesis, which involves a comprehensive analysis of energy repartition in compression ignition engines operating under transient conditions. With the calibrated model, a detailed analysis was conducted on key parameters affecting engine performance during transient operations. These parameters include combustion characteristics, heat transfer, mechanical losses, and overall energy efficiency under varying altitudes and thermal conditions. The findings provide valuable insights into the engine's response to changes in operating conditions, offering opportunities for optimising engine performance in transient conditions.

The Global Energy Balance (GEB) analysis is based on the fundamental principle of the first law of thermodynamics, which requires an energy balance between the energy input into the engine, primarily from chemical power in the form of fuel, and the energy output from the engine. The energy flows entering the engine include the sensible enthalpy of air, fuel and the chemical energy stored in the fuel with its heating value ($\dot{m}_f H_v$). On the other hand, the energy flows exiting the engine comprise the brake power (N_b), the heat transfer to the engine coolant ($\dot{Q}_{cool}$), the net flow of the sensible enthalpy carried by the gases (H_{exh}), the heat dissipated to the engine oil ($\dot{Q}_{oil}$), the heat accumulated within the engine structure ($\dot{Q}_{mat}$), the heat rejection in the intercooler ($\dot{Q}_{WCAC}$), the heat rejection in the EGR heat exchangers ($\dot{Q}_{HPEGR}$ and $\dot{Q}_{LPEGR}$). Additionally, the heat emanating from the external walls of the engine to the ambient environment is accounted for through heat rejection in the pipes ($\dot{Q}_{pipes}$) and the turbocharger ($\dot{Q}_{turbo-amb}$). $\dot{Q}_{turbo-amb}$ is the heat rejected from turbocharger to ambient. It is determined in VEMOD using a lumped conductance model in which the ambient is a node used as boundary conditions. $\dot{Q}_{pipes}$ is the heat rejection to the ambient in the pipes. It is obtained with the help of simple lumped model, considering gas inside the pipes and ambient air as boundary conditions. The auxiliary power (N_a) and enthalpy flow of blow-by losses (H_{bb}) were considered as well. As the instantaneous terms fluctuate rapidly (making it challenging to identify relevant trends during transient operation), the energy balance will be analysed considering relative cumulated terms.

To facilitate a detailed analysis of energy distribution, the first law of thermodynamics was expressed as follows:

$$\dot{m}_f H_v = N_b + N_a + H_{exh} + \dot{Q}_{cool} + \dot{Q}_{oil} + \dot{Q}_{mat} + \dot{Q}_{WCAC} + \dot{Q}_{HPEGR} + \dot{Q}_{LPEGR} + \dot{Q}_{pipes} + H_{bb} + \dot{Q}_{turbo-amb} \quad (1)$$

Before delving into the analysis, a preliminary discussion addresses important considerations concerning energy balance during transient operation. In steady-state conditions, there is no energy accumulation in the engine. Energy split calculations using mean variables that characterise the system state, such as fluid temperatures and mass flows, result in no significant imbalance except for experimental uncertainties or numerical errors. However, two crucial phenomena affecting the energy balance must be considered in

transient operation. Firstly, there is energy accumulation in different system masses, particularly in the metallic elements of the engine block, pipes, turbo, etc., with the metallic elements being the most significant. Heat accumulation also occurs in the coolant and oil. The accumulation in the metallic element is explicitly considered; in contrast, the fluid accumulation is implicitly considered since the heat rejection to coolant and oil will be internally used for both fluid heating and heat rejection in the exchangers.

Secondly, a significant "delay" phenomenon must be considered when considering the energy balance during transient conditions. The system response is almost instantaneous when focusing on the engine cylinder and ports for calculating energy balance. However, if the complete engine, including heat exchangers and all the gas lines, is considered, an apparent inconsistency between the instantaneous heat release in the cylinders (due to the combustion process) and the addition of the remaining energy terms will appear. This inconsistency becomes negligible when the energy terms are integrated over an extended period.

To perform a comprehensive analysis, two engine boundary limits were considered for cold conditions: the engine block and the complete engine. The "delay" effect will be evident in the latter. Figure 16 shows a detailed view of the energy balance within the engine block, including cylinders and ports, under cold conditions. The graph shows fluctuations in the energy distribution, which are more pronounced at the start of the cycle and gradually become smoother as time passes. This performance can be attributed to the rapid load changes and the progressive accumulation time increase. As the transient progresses, the fast variations have a lower effect on the accumulated energy terms, leading to stabilisation.

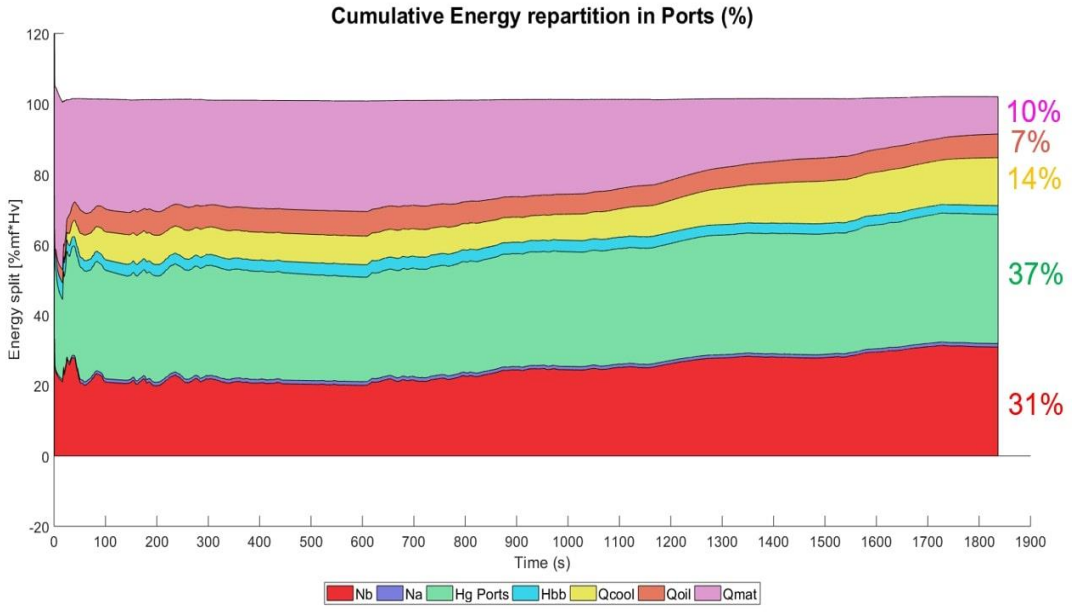

Figure 16. Cumulative energy repartition in the engine block during WLTC at Ambient Cold Start 0 m conditions.

The energy distribution at the end of the cycle reveals some interesting trends. Approximately 31% of the total fuel energy output is converted into brake power, while heat rejected to coolant, oil, and material heating collectively accounts for about 25% of the total energy. The exhaust enthalpy flow, which represents the energy carried away by the exhaust gases, contributing about 37% of the total cumulated energy, plays a crucial role throughout the WLTC.

Interestingly, the energy balance exhibits significant variations during the WLTC evolution. As the different energy terms stabilise gradually with time, the proportions of brake power and heat rejected to coolant, oil, and material also change. Moreover, during the early stages of operation, the heat rejected to the cylinder walls is predominantly utilised to raise the engine block temperature, reducing the heat rejected to coolant and oil. However, as the engine block and fluids reach higher temperatures, the contribution of heat rejected to the coolant tends to increase. A contrary observation applies to heat rejected to oil, which is higher during the first half of the cycle due to the significance of friction losses at the beginning, particularly influenced by the lower oil temperature. The energy to drive the auxiliary systems is lower than 1% throughout the cycle.

Figure 17 shows the energy balance of the entire engine during the WLTC, including the gas path (high and low-pressure EGR lines, turbo, etc.) from ambient to exhaust. Unlike Figure 16, an apparent imbalance is observed at the initial stage of the cycle, but it gradually diminishes over time. This discrepancy arises due to a delay in calculating the enthalpy flows caused by non-synchronized phenomena in the pipes, volumes, and in-cylinder conditions. As a result, there is a temporary lag of energy at the beginning, which diminishes as time progresses and ultimately becomes negligible by the end of the WLTC.

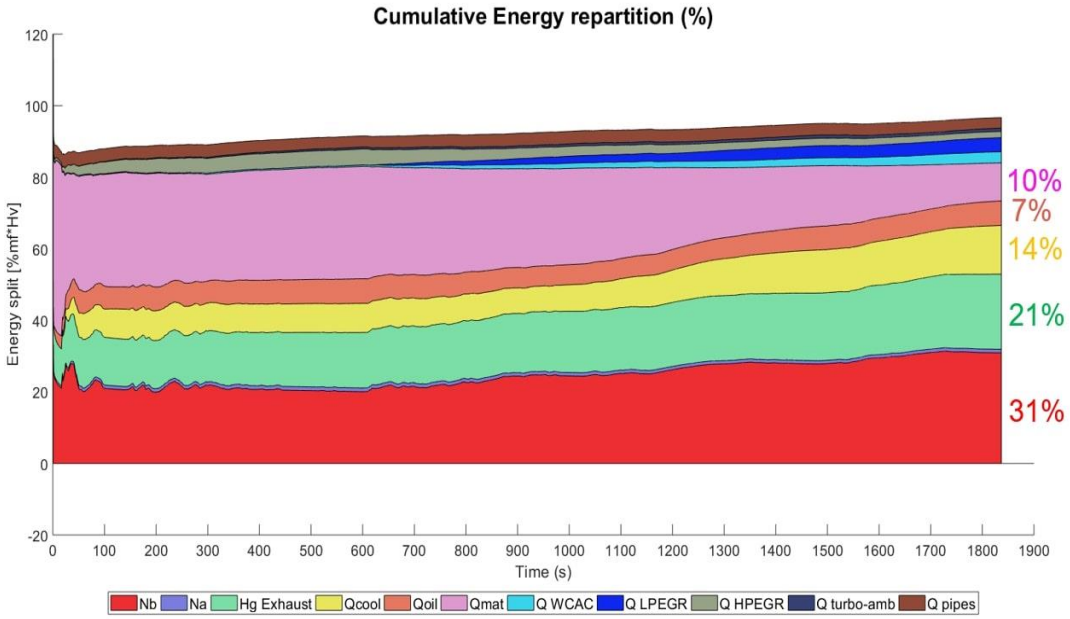

Figure 17. Cumulative energy repartition in the complete engine system during WLTC at Ambient Cold Start 0 m conditions.

Analysing the contributions of different energy terms, the net exhaust enthalpy flow (calculated between the engine intake and downstream the low-pressure EGR pipe) represents approximately 21% of the total engine energy output at the end of the cycle. The difference with respect to exhaust enthalpy flow at the ports (about 16%) can be attributed to the heat rejection in the intercooler, EGR exchangers, and finally, the turbo and pipes to ambient. The heat rejected to intercooler, EGR exchangers, and ambient constitutes about 3% of the total energy output. Furthermore, approximately 6% of the total energy is rejected from the high-pressure and low-pressure exhaust gas recirculation (HPEGR and LPEGR) lines. The utilisation of the HPEGR loop promotes an increase in inlet temperature during the initial operation. In contrast, the LPEGR loop comes into play during later transient phases when the coolant temperature is higher.

Lastly, the turbocharger and pipes reject about 3% of heat to ambient. Considering the complete engine provides additional insights into the various energy contributions and utilisation throughout the WLTC, guiding engine performance optimisation for transient conditions.

Figure 18 compares the energy terms at the end of the WLTC in both Warmed and Cold conditions. The change from Ambient Cold conditions to Warmed conditions brings about noticeable changes in the energy balance of the engine. These changes are particularly evident in the heat transfer accumulated at the metal components ($\dot{Q}_{mat}$) and the heat rejection to the coolant and oil ($\dot{Q}_{cool}$ and $\dot{Q}_{oil}$).

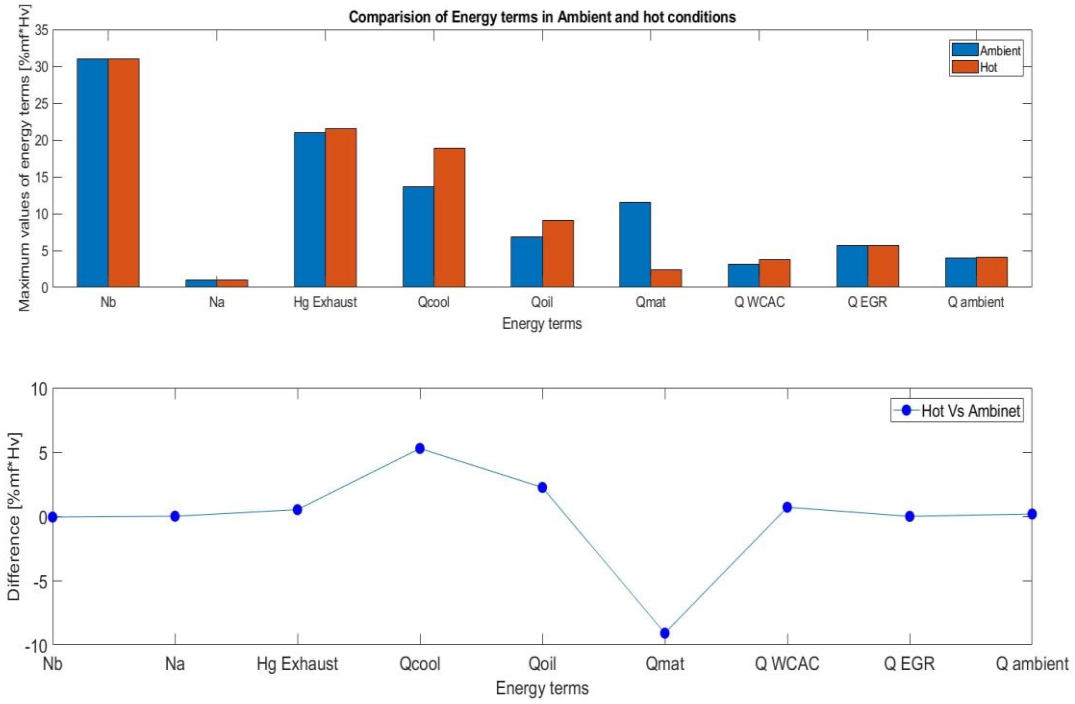

Figure 18. Comparison of energy terms in WLTC in Ambient Cold 0 m and Warmed 0 m conditions at the end of the cycle.

At the beginning of Ambient Cold Start, all the metal and fluids are at around 21°C, and the engine and fluids are considerably low during initial evolution; in Warmed conditions, the coolant, oil, and metal temperatures increase significantly from the beginning, and thus the final cumulated heat rejection to both coolant and oil is higher in Warmed conditions compared to Ambient Cold conditions. Contrarily, less heat accumulation can be seen. Figure 18 shows that the cumulated brake efficiency during Ambient Cold conditions is only slightly lower than during Warmed conditions (less than 1%). This improvement can be attributed to the change in the engine settings and the lower mechanical losses during Warmed conditions, primarily due to the higher engine temperatures, especially in the case of the oil temperature. Other energy terms, such as heat rejection in the EGR coolers and intercooler, show slight variation. The engine operates with low-pressure EGR from the beginning in Warmed conditions, while it starts with high-pressure EGR in Ambient Cold conditions, but the total heat rejected by the EGR coolers remains similar.

Figure 19 presents a comparison of energy terms at the end of the WLTC in Low-Temperature Cold Start (LTCS) and Ambient Cold Start (ACS) at an altitude of 0 meters. When comparing the two scenarios, the higher brake energy in ACS conditions, which is about 30% and 1% higher than in LTCS, can be mainly attributed to the higher mechanical losses in LTCS. However, the higher indicated efficiency in LTCS partially compensates this increase in mechanical losses, as shown in Figure 20. In ACS, friction accounts for about 9%, which is 2% lower than in LTCS, while the indicated efficiency (N_i) is around 43%, slightly lower by 1% compared to LTCS. The slight increase observed in brake efficiency at ACS suggests a balance between the better mechanical losses and the worse indicated efficiency during ACS conditions compared to LTCS.

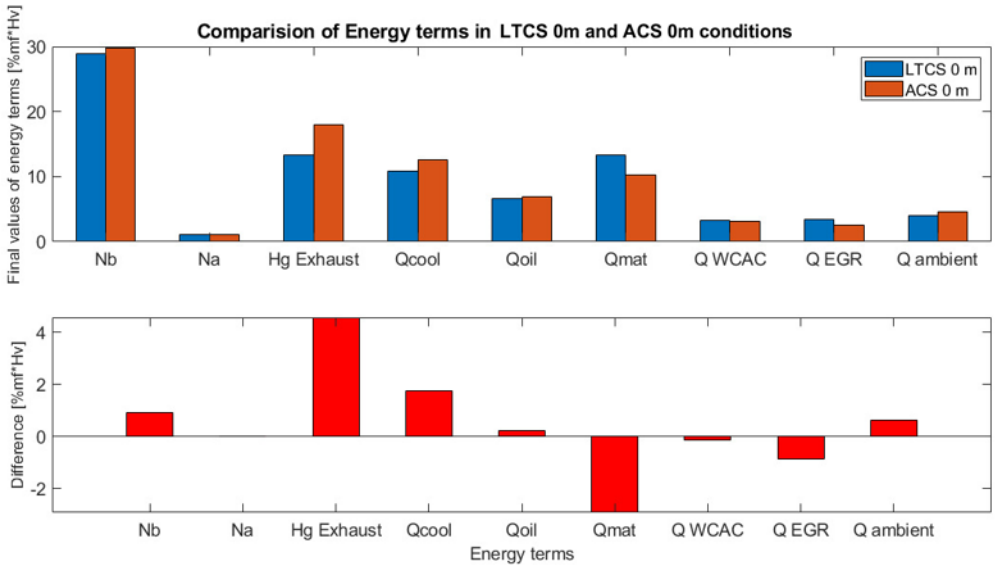

Figure 19. Comparison of energy terms in WLTC in LCTS 0 m and ACS 0 m conditions at

the end of the cycle.

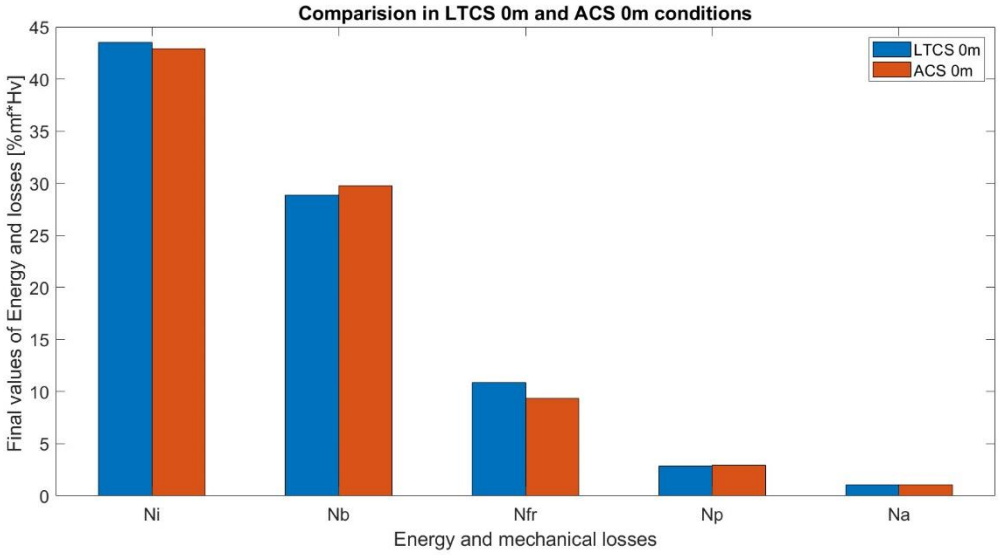

Figure 20. Comparison of energy and losses in WLTC in LCTS 0 m and ACS 0 m conditions.

Significant changes are observed in the heat rejection to coolant, as well as in the heat accumulated in the engine structure. At LTCS conditions, there is higher heat accumulation in the material due to the lower initial temperatures of the fluids and metal. As the temperature of the material increases during operation, the relative weight of the accumulated energy in the metal decreases slightly, leading to a higher heat rejection to the coolant. Additionally, the thermostat opens earlier in ACS, increasing heat transfer to the coolant. Consequently, there is higher heat rejection to the coolant in ACS compared to LTCS (13% vs. 11%). On the other hand, the heat rejection to oil shows a less significant variation (7% in ACS vs. 6.7% in LTCS). The final cumulated values of heat rejected to coolant and oil are slightly higher in ACS conditions. In contrast, the heat rejected to the material ($\dot{Q}_{mat}$) is higher in LTCS (12.5% vs. 10%).

The term with the most significant variation is the net exhaust enthalpy, $H_{g\ Exhaust}$, which is higher in ACS conditions (18% vs. 13.5%). This can be attributed to the reduction of cumulated heat in the block and the EGR coolers in ACS (2.5% vs. 3.5%). Other energy terms, such as heat rejection in the intercooler and to ambient (pipes, turbo), do not show any significant variation between LTCS and ACS conditions. The findings highlight the influence of temperature conditions and EGR on the engine's energy balance and performance during the WLTC cycle.

After examining the impact of starting temperature, this section focuses on assessing the influence of altitude on engine operation. Figure 21 shows the WLTC simulations that were

performed for Low-Temperature Cold Start (LTCS) conditions at altitudes of 0 meters and 1000 meters above sea level, with LTCS at 0 meters serving as the baseline case for analysis.

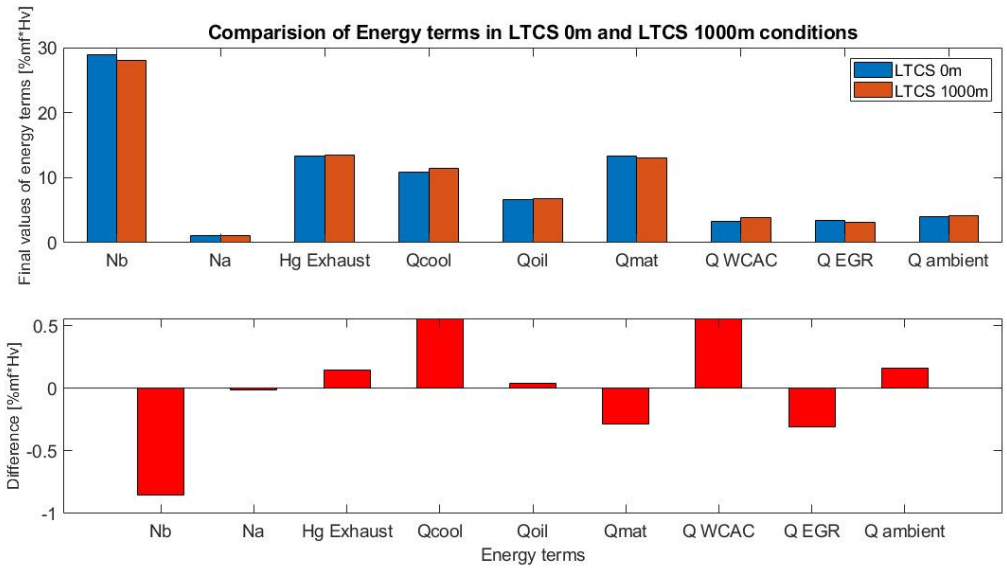

Figure 21. Comparison of energy terms in WLTC in LTCS 0m and LTCS 1000 m conditions at the end of the cycle.

Instantaneous energy balances for both altitudes were obtained, and their evolution was found to be similar to LTCS at 0 meters. Consequently, the analysis is focused on the final results at the end of the WLTC to highlight the main cumulative differences. Overall, the observed differences are relatively small, with only one term changing by more than 0.6%.

When comparing the energy terms at the end of the WLTC between LTCS at 0 meters and 1000 meters, it becomes apparent that the cumulated brake efficiency is slightly lower for LTCS at 1000 meters, with a difference of approximately 0.8%. The lower brake efficiency in this case can be attributed to the pumping losses, which increase (not seen in the plot) from 2.9% to 4% of the total fuel energy.

Two other slight increases are observed in heat rejected to the intercooler and coolant heat exchanger, both rising by approximately 0.5%. The higher heat rejection to the intercooler is due to the elevated compressor outlet temperature resulting from a higher compression ratio of the turbocompressor (to maintain boost pressure with lower compressor inlet pressure due to ambient conditions). The slightly higher intake temperature justifies the slight increase in heat rejection to coolant due to the higher temperature at the compressor outlet.

Considering the findings from the previous section and the analysis presented here, it can be concluded that engine response is primarily affected by ambient temperature, while the impact of altitude is relatively lower.

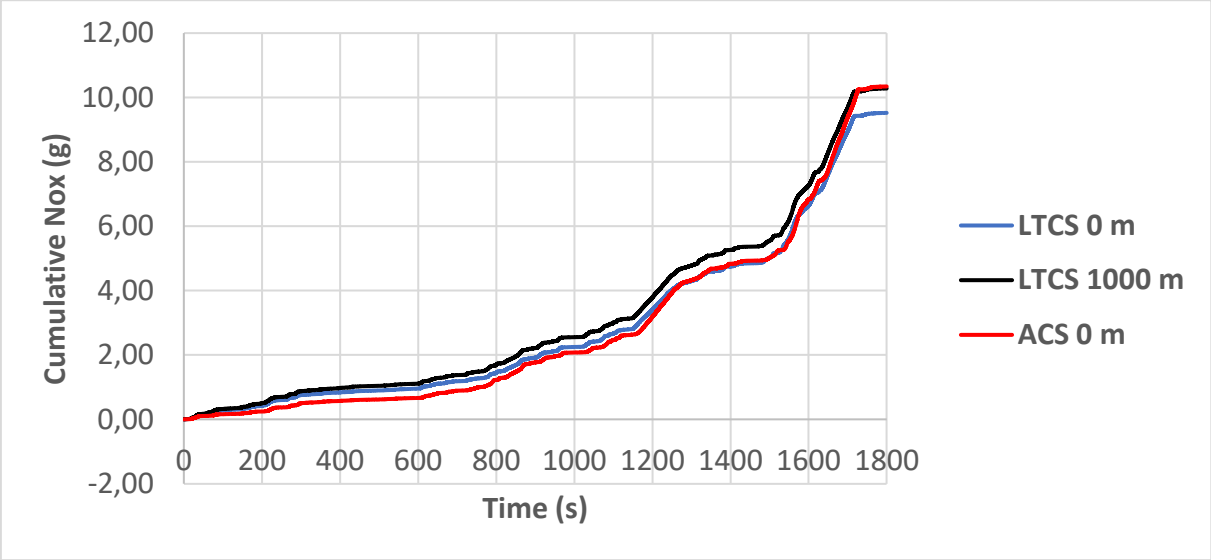

Figure 22. NOx in WLTC at ACS and LTCS conditions.

Finally, Figure 22 illustrates the variations in NOx emissions at different operating conditions. Until about 1300 seconds, Low-Temperature Cold Start (LTCS) at 0 m altitude shows higher NOx emissions than Ambient Conditions Start (ACS) at 0 m. After this point, the trend shifts, and NOx levels decrease until the end of the cycle. This performance can be attributed to the dependence of NOx emissions on temperature and EGR rates.

During LTCS at 0 meters, the lower intake temperature results in higher EGR rates due to the higher intake density, which tends to reduce NOx emissions. However, higher fuel injection is needed in the initial part of the cycle to compensate for increased mechanical losses and maintain torque, leading to higher NOx emissions. As the engine fluid temperatures rise throughout the cycle, the influence of ambient conditions diminishes, and the benefits of LTCS become more evident in the reduction of NOx emissions in the latter part of the WLTC.

When comparing LTCS at 0 meters with LTCS at 1000 meters altitude, a continuous increase in NOx emissions is observed for higher altitudes. This effect can be explained by the lower EGR rate at 1000 meters altitude, as explained in the preceding section. The differences in EGR rate for different altitudes are crucial in influencing NOx emissions during transient engine operations. The positive effect of the low temperature is counteracted by the negative impact of the altitude, so LTCS at 1000 m shows similar final NOx emissions as ACS at 0 m.

This thorough analysis of energy repartition during transient operation is a valuable insight into the engine performance under dynamic conditions, contributing to a deeper understanding of engine performance and potential areas for optimisation. By considering the specific challenges and phenomena involved in transient energy balance, this research aims to enhance the modelling and development of compression ignition engines, supporting the advancement of more efficient and sustainable propulsion technologies for the automotive industry and beyond.

The outcomes presented in this section contribute to a better understanding of engine behaviour under transient conditions. The in-depth analysis of energy repartition enhances our knowledge of engine dynamics during varying loads and speeds, providing a solid foundation for further research and development of compression ignition engines.

By investigating engine performance under transient conditions, this research seeks to pave the way for engine design and optimisation advancements, with potential implications for achieving greater efficiency and reduced emissions. The insights gained from this study and the tool developed can benefit researchers and engineers working towards more sustainable and environmentally friendly propulsion technologies for the automotive industry and beyond.

CHAPTER 4

Conclusions

The simulation tool VEMOD was thoroughly calibrated and validated using a four-cylinder 1.6-L DI Diesel engine. This ensured accurate alignment between modelled and experimental results for key parameters like pressure, heat release, temperatures, and torque.

After focusing on CI combustion with Diesel fuel, the model commissioning was completed with a dual fuel combustion model to model methane-Diesel combustion and extend it to predict hydrogen-Diesel combustion characteristics.

At the outset, a model for the dual fuel engine using methane was built, and it was integrated with Gülder's laminar flame speed model for air-methane mixtures within the software. The validation process involved using experiments and an optimiser to align the in-cylinder pressure profiles with those measured during an experimental campaign conducted on a single-cylinder research engine with optical accessibility. These experimental tests encompassed varying load conditions, specifically 2 and 5 bar of Brake Mean Effective Pressure (BMEP), and different engine speeds, namely 1500 and 2000 rpm.

The results indicate that the model effectively replicates the pressure trends across various load and speed conditions. Furthermore, while there were notable variations in the intensity of the heat release rates, the overall combustion timing exhibited reasonably good agreement with the measurement data.

Two new correlations were developed and integrated into the 0D/1D code for simulations involving hydrogen. One of these correlations was specifically tailored to address the extremely lean operating conditions typical of dual fuel engines. Additionally, the numerical simulations were based on experimental data obtained from the same engine running on hydrogen instead of methane under equivalent BMEP conditions.

The model predicted a significant increase in pressure rise rate and peak pressure levels when hydrogen was utilised. This increase is attributed to a substantial enhancement of the combustion velocity, characteristic of hydrogen as a gaseous fuel. This observation was further supported by the heat release rates, which demonstrated that combustion occurred within a shorter crank angle interval compared to the corresponding methane-Diesel cases. Therefore, it can be concluded that the developed flame model yields result consistent with the characteristics observed in hydrogen combustion.

After completing the commissioning of the 0D/1D tool, a comprehensive analysis of the Gas Exchange and Global Energy Balance (GEB) using VEMOD was conducted for a CI engine. This analysis shed light on engine consumption mechanisms and the influence of

different operating conditions during a WLTC. Unfortunately, due to time limitations and the lack of experimental installations for validation, the analysis could not be applied to a dual fuel engine.

The GEB analysis showed an initial "delay" effect caused by unsynchronised phenomena at the cylinders and gas lines. This led to a temporal imbalance in energy distribution at the cycle start. The "delay" effect gradually decreased over time, thus improving the energy balance.

Each energy term was accumulated, and its relative weight was instantaneously calculated by dividing it by the cumulated fuel energy injected. Key energy terms were compared at Ambient Cold Start (including the analysis at the engine block and complete engine boundaries). Notably, the brake energy term (cumulated brake efficiency) was lower initially due to higher mechanical losses produced by higher oil viscosity because of the low oil temperature. Friction, particularly piston friction, was a key factor.

The analysis also compared energy distribution in Ambient Cold and Warmed engine conditions. Differences in heat rejection to coolant, oil, and engine material were observed due to varying initial temperatures. Warmed conditions exhibited higher heat rejection to exchangers from the start, while in cold conditions, heat initially warmed up the fluids and engine block. Despite some uncertainties like the 'delay' effect, the model's performance was considered good, with a final cumulated unbalance of about 3% in both cold and Warmed conditions.

Later, a comparison of energy terms at the end of the WLTC in Low-Temperature Cold Start (LTCS) and Ambient Cold Start (ACS) at an altitude of 0 meters was carried out. When comparing the two scenarios, the higher brake energy in ACS conditions, about 30% and 1% higher than in LTCS, can be mainly attributed to the higher mechanical losses in LTCS. However, this increase in mechanical losses is partially compensated by the higher indicated efficiency in LTCS: friction accounts for about 9% in ACS, which is 2% lower than in LTCS, while its indicated efficiency (N_i) is around 43%, slightly lower by 1% compared to LTCS. The resulting brake efficiency improvement is only 1% during ACS conditions compared to LTCS.

The GEB analysis was also conducted considering the complete engine under various starting temperatures and altitudes. The comparison between LTCS and Ambient Cold Start (ACS) conditions showed changes such as indicated and brake energies, heat rejection and heat accumulation due to different ambient temperatures. At Low-Temperature Cold Start (LTCS) conditions, indicated efficiency remained stable during the WLTC at about 44%, which is 1% higher than in ACS. However, the brake energy in LTCS is 1% lower than ACS. Also, ACS conditions exhibited higher heat rejection to coolant and oil.

Altitude assessment revealed minor changes except in pumping and brake efficiency: increasing altitude lowered brake efficiency by 0.8%, with a 2.5% rise in fuel consumption

(higher than the efficiency changes because of the higher load required). NOx emissions showed varying trends due to EGR rates and intake temperature: altitude increases NOx because of the higher fuel required and the lower EGR; this worsening can be compensated by the temperature reduction so that LTCS at 1000 m shows similar emission as ACS at 0 m.

References

1. European Commission. (2017). Worldwide harmonized Light vehicles Test Procedure (WLTP).
   Retrieved from https://ec.europa.eu/clima/policies/transport/vehicles/wltp_en
2. WLTP: ACEA. (2021). Worldwide harmonized light vehicle test procedure (WLTP).
3. High altitude effects on engine performance: Mollah, M. A. H., Rakib, A., Anik, M. S. A., & Hossain, M. A. (2019). Influence of high altitude on engine performance: A review. Renewable and Sustainable Energy Reviews, 104, 383-392.
4. High altitude effects on emissions: Chen, H., Xu, Y., Tang, Q., Wang, Y., & Deng, J. (2016). Effect of high altitude on emission characteristics of Diesel engine. Journal of Environmental Sciences, 49, 59-67.
5. Turbocharger performance at high altitude: Liu, X., Liu, Z., Wang, Z., & Yu, L. (2006). Turbocharger performance degradation under high altitude operation conditions. SAE Technical Paper 2006-01-3032.
6. EGR system at high altitude: Zhang, X., Shuai, S., & Zhao, Y. (2015). Study on the influence of high altitude on engine EGR system. Energy Procedia, 75, 346-351.
7. U.S. Environmental Protection Agency. (2022). Altitude Adjustment for Vehicle Emissions Testing. Retrieved from https://www.epa.gov/regulations-emissionsvehicles-and-engines/altitude-adjustment-vehicle-emissions-testing
8. Zhang, J., Wang, Y., Wu, X., & Wang, L. (2015). Altitude Compensation Control for Diesel Engine Based on Boost Pressure and Air Flow. Mathematical Problems in Engineering, 2015. https://doi.org/10.1155/2015/906235
9. Farias, T. L., Diniz, A. L. B., & Silva, M. G. (2017). Effects of altitude on fuel economy and emissions of a gasoline engine. Journal of Cleaner Production, 162, 1020-1027. https://doi.org/10.1016/j.jclepro.2017.06.146
10. Kishore, A., & Dhingra, S. C. (2018). Impact of altitude on combustion and emission characteristics of Diesel engines. Journal of Energy Institute, 91(2), 232-240. https://doi.org/10.1016/j.joei.2017.03.001
11. Zhang, Y., & Ciatti, S. (2017). On the importance of global energy balance in internal combustion engine research and development. Energies, 10(5), 655. doi: 10.3390/en10050655
12. Heywood, J. B. (1988). Internal combustion engine fundamentals. New York: McGraw-Hill.
13. Lapuerta, M., & Armas, O. (2017). Energy balance analysis of Diesel engine using an alternative fuel from biomass. Applied Thermal Engineering, 114, 540-548. doi: 10.1016/j.applthermaleng.2016.11.139

14. Lapuerta, M., & Armas, O. (2016). Energy balance analysis of a Diesel engine using a mixture of Diesel and dimethyl ether (DME) as fuel. Fuel, 167, 329-336. doi: 10.1016/j.fuel.2015.11.080
15. Yang, L., & Ciatti, S. (2015). An investigation of the effect of injection timing on combustion and global energy balance in a HSDI Diesel engine. Energy Conversion and Management, 98, 114-125. doi: 10.1016/j.enconman.2015.04.040
16. Bianchi, G.M., Fontanesi, S., and Cantore, G. (2016). A thorough and integral analysis of the energy balance of a small gasoline engine: The impact of combustion phasing on engine efficiency and emissions. Applied Energy, 174, 1-14.
17. Lapuerta, M., and Armas, O. (2018). Modeling and simulation of internal combustion engines. Cham: Springer.
18. Dempsey, A.B., and Kittelson, D.B. (2010). Combustion processes in compression ignition engines: In-cylinder studies. Progress in Energy and Combustion Science, 36(5), 521-550.
19. Kuo, T.W., Chang, C.W., and Chiang, C.H. (2019). An integrated 1-D engine and cooling system simulation model for fuel consumption and thermal management analysis. Applied Thermal Engineering, 159, 113990.
20. B. Venugopal, S. Renganarayanan, and S. Sankaranarayanan, "Dual fuel engines: A comprehensive review," Renewable and Sustainable Energy Reviews 77 (2017): 1209-1229.
21. M. H. Shojaeefard, M. A. Ommi, and M. Hosseini, "Dual-fuel engines: a comprehensive review with a focus on performance and emissions characteristics," Renewable and Sustainable Energy Reviews 72 (2017): 169-183.
22. J. S. Park, S. K. Choi, and S. S. Park, "Review on the combustion and emission characteristics of dual-fuel combustion engines," Renewable and Sustainable Energy Reviews 96 (2018): 162-172.
23. M. M. Ali, H. H. Masjuki, M. A. Kalam, M. H. Jayed, and S. M. Ashrafur Rahman, "A review on energy, environmental and sustainability aspects of Diesel/natural gas dual fuel engines," Renewable and Sustainable Energy Reviews 69 (2017): 551-565.
24. S. V. Yadav and A. Kumar, "Performance analysis of Diesel-natural gas dual fuel engine: A review," Renewable and Sustainable Energy Reviews, vol. 43, pp. 784-794, 2015. https://doi.org/10.1016/j.rser.2014.11.004
25. A.M. Khalil and A. M. A. Bakar, "Performance and emission characteristics of Diesel engine operating on dual fuel mode with LPG and CNG as alternate fuels - A review," Renewable and Sustainable Energy Reviews, vol. 16, no. 8, pp. 4886-4904, 2012. https://doi.org/10.1016/j.rser.2012.04.051
26. K. S. Kadirgama, M. M. Noor, R. A. Bakar, and K. V. Sharma, "Performance and emission characteristics of compressed natural gas - Diesel dual fuel engine - A review," Renewable and Sustainable Energy Reviews, vol. 16, no. 5, pp. 2686-2695, 2012. https://doi.org/10.1016/j.rser.2012.01.068
27. A. J. Shah, T. H. R. Chan, and S. S. Pang, "A review on the performance and emissions of dual fuel combustion in internal combustion engines," Renewable and Sustainable Energy Reviews, vol. 92, pp. 872-892, 2018. https://doi.org/10.1016/j.rser.2018.04.026

28. "A review on compression-ignition engines as prime movers for natural gas vehicles" by K. S. S. Ramachandra Rao, Renewable and Sustainable Energy Reviews, Volume 14, Issue 9, December 2010, Pages 3039-3047.
29. "Dual-fuel technology for heavy-duty vehicles" by Rui Chen, Yanjun Huang, Xinyan Wang, and Wei Liu, Applied Energy, Volume 228, September 2018, Pages 2366-2386.
30. "Dual-fuel engine performance and emissions: A review" by S. S. Thipse, S. S. Vakkalanka, and S. R. Bhatkar, Renewable and Sustainable Energy Reviews, Volume 72, August 2017, Pages 1157-1173.
31. Gülder, Ö.L., "Combustion: Physical and Chemical Fundamentals, Modeling and Simulation, Experiments, Pollutant Formation," Springer, 2012.
32. Gülder, Ö.L., "Laminar flame speed measurements and modeling: A review," Progress in Energy and Combustion Science, vol. 32, no. 4, pp. 462-537, 2006.
33. M. Sarafraz, S. E. Ghobadian, and T. Najafi, "Hydrogen combustion in dual fuel engines: A review," Renewable and Sustainable Energy Reviews, vol. 51, pp. 15311541, 2015.
34. M. R. Yaacob, M. F. Mohammad, and M. H. Abdullah, "A review of hydrogenDiesel dual fuel combustion, emissions and performance," Renewable and Sustainable Energy Reviews, vol. 62, pp. 1024-1036, 2016.
35. J. A. Caton, B. D. Chenoweth, and S. A. Ciatti, "Development and experimental validation of a reduced kinetic mechanism for hydrogen/Diesel dual-fuel combustion," Fuel, vol. 142, pp. 1-10, 2015.
36. K. G. Raju, M. R. Yaacob, and M. H. Abdullah, "Hydrogen-Diesel dual fuel combustion: An experimental study," International Journal of Hydrogen Energy, vol. 42, no. 13, pp. 8914-8924, 2017.
37. D. B. Rao, "Investigation of hydrogen-Diesel dual-fuel combustion in a compression ignition engine," International Journal of Hydrogen Energy, vol. 41, no. 45, pp. 21270-21277, 2016.
38. Carreno Arango R. "A comprehensive methodology to analyse the Global Energy Balance in reciprocating internal combustion engines. " PhD Thesis, Universitat Politecnica de Valencia, Valencia, September 2016, http://hdl.handle.net/10251/73069
39. Martin J, Arnau F, Piqueras P et al. "Development of an Integrated Virtual Engine Model to Simulate New Standard Testing Cycles." SAE Technical Paper Series 2018; 1: 1–17. DOI:10.4271/2018-01-1413.
40. Olmeda P, Mart´ın J, Arnau FJ et al. Analysis of the energy balance during World harmonized Light vehicles Test Cycle in warmed and cold conditions using a Virtual Engine. International Journal of Engine Research 2019; DOI:10.1177/1468087419878593.
41. Payri F, Martín J, José Arnau F, Artham S. Analysis of temperature and altitude effects on the Global Energy Balance during WLTC. International Journal of Engine Research. 2022;23(11):1831-1849. doi:10.1177/14680874211034292

42. A. Magno, E. Mancaruso and B. M. Vaglieco, “Combustion Analysis of Dual Fuel Operation in Single Cylinder Research Engine Fuelled with Methane and Diesel,” in SAE Technical Paper 2015-24-2461, 2015, https://doi.org/10.4271/2015-24-2461.
43. Payri, F., Olmeda, P., Martin, J. and Carreño, R., "A New Tool to Perform Global Energy Balances in DI Diesel. Engines". SAE Int. J. Engines 7(1):2014, doi:10.4271/2014-01-0665.
44. M. Lapuerta, O. Armas, J.J. Hernandez. Diagnosis of DI Diesel combustion from in-cylinder pressure signal by estimation of mean thermodynamic properties of the gas. Applied Thermal Engineering 19 (1999) 513-529.
45. Benajes, J., Olmeda, P., Martin, J. and Carreño, R. “A new methodology for uncertainties characterization in combustion diagnosis and thermodynamic modelling”. Applied Thermal Engineering 71 (2014) 389-399. doi: 10.1016/j.applthermaleng.2014.07.010
46. Ö. Gülder, “Turbulent Premixed Flame Propagation Models for Different Combustion Regimes,” in Syposium on Combustion, 1990.
47. Ö. Gülder, “Correlations of Laminar Combustion Data for Alternative S.I. Engine Fuels,” in SAE Technical Paper 841000, doi:https://doi.org/10.4271/841000, 1984.
48. N. Marinov, C. Westbrook and W. Pitz, “Detailed and Global Chemical Kinetics Model for Hydrogen,” in 8th International Symposium on Transport Properties, San Fancisco, CA, 1995.

Appendix

0D Laminar Flame Speed Model for Methane Lean Mixture in Dual Fuel Combustion Engine

De Robbio, R., Mancaruso, E., Vaglieco, B.M.
STEMS-CNR
Naples, Italy

Artham, S., Martín, J.
CMT- Motores Térmicos
Valencia, Spain

1 Introduction

For decades, the compression ignition (CI) engines are widespread in the market because of their reliability and efficiency. But, they have high exhaust emissions of particulate matter (PM) and nitric oxides (NO_x) which can be problematic for environment. It is necessary to emphasize on reducing emissions in order to keep up with the latest stringent regulations on emissions [1, 2]. This can be achieved with the implementation of alternative solutions like the usage of after treatment systems, usage of gaseous fuels along with diesel fuel etc. The solution to use after treatment systems is not cost efficient and decreases global efficiency because of the higher pumping work required. Dual fuel operation, where gaseous fuels are used with pilot diesel injection, is considered as one efficient solutions used in diesel engines to improve exhaust emissions. Indeed, part of the diesel liquid fuel is substituted with alternative gaseous fuels [3, 4] that is introduced into the intake manifold to form a premixed charge with air, in this way both PM and NO_x can be significantly reduced. Methane is mostly used gaseous fuel for the dual fuel compression ignition engine. It is an economical fuel with a wide availability across the globe. Methane is well-suited with the high compression ratios of CI engine. It has high auto-ignition temperature, low carbon content and high knock resistivity [5-8]. Nevertheless, dual fuel combustion results extremely complex to model, since it is characterized by the oxidation of two fuels presenting different physical and chemical features. As a matter of fact, a small amount of diesel, burning in a diffusive flame, starts via a multipoint ignition the propagation of a flame in the air-methane premixed charge.

In the present work, a dual-fuel combustion model was built in a commercial software with the aim of simulating the experimental results and investigating the characteristics of methane-diesel combustion. The software used to build and simulate the engine model is GT-Power. Modelling a dual fuel engine with methane is an important task as the model built must respond to the inputs in accordance with experimental results. The main emphasis will be on combustion, which includes a laminar flame speed model. For methane, the combustion model available in GT power does not have pre-defined constants for laminar flame speed model. This work aims to build a laminar flame speed model and incorporate it

Correspondence to: roberta.derobbio@stems.cnr.it

in the combustion model of the GT power. It uses approaches from Heywood [9] and Gülder [10, 11] and it was validated with experimental results.

2 Model setup

The research was carried out in a single cylinder diesel engine. It is a 522 cm^3 four-stroke diesel engine. The specifications of the engine can be seen in Table 1. The engine was modelled in the engine simulation software, according to the specifications from engine test bench, as shown in the Figure 1.

Table 1: Engine specifications.

Engine type	4-stroke, single cylinder
Stroke [mm]	92
Bore [mm]	85
Cylinder volume displacement [cm^3]	522
Combustion bowl volume [cm^3]	19.7
Compression ratio	16.5:1
Number of Valves	4

As it can be seen, the model has two injectors, one at the intake port, where methane will be injected and second one in the engine head, where diesel will be injected within the cylinder to initiate combustion. The stationary tests for calibration were performed at 4 different operating points. The engine model was updated with all the intake and exhaust conditions, initial pressures and temperatures at various locations, fuel mass flow rate for methane, start of injection (SOI) and injected fuel mass for diesel, according to the experimental results of dual fuel methane/diesel engine, for various operating points as shown in Table 2.

Once the model is built, it was simulated to check the air mass flow, to be coherent with the experimental values. The diameter of the orifice connection "VL-out" has been modified accordingly, in order to reach the experimental air mass flow. After initial calibration, the interest has been shifted to the combustion model, where a new laminar flow model was built and incorporated in set-up for methane-diesel dual fuel model.

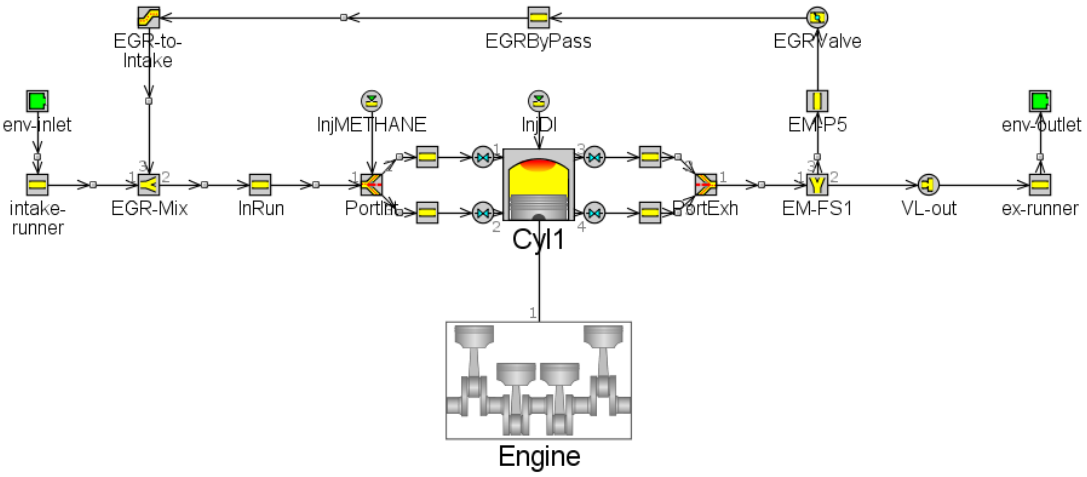

Figure 1: GT-Power model of the compression ignition single cylinder diesel engine in dual fuel mode.

Table 2: Engine operating conditions.

Case	**#1**	**#2**	**#3**	**#4**
Engine Speed [rpm]	1500	1500	2000	2000
Brake Mean Effective Pressure [bar]	2	5	2	5
Start of Injection of pilot [deg]	-16	-11.6	-21.2	-18.6
Start of Injection of main [deg]	-6	0.3	-8	-2.4
Dwell interval [deg]	10	11.9	13.2	16.2
Duration pilot and main [deg]	2.6	2.4	3.4	3.1
Diesel mass injected pilot and main [mg/cycle]	0.711	0.822	0.717	0.833
Methane mass [mg/cycle]	7.58	11.19	7.55	10.15
Rail pressure [bar]	615	867	700	891
Pressure inlet [bar]	1.5	1.7	1.5	1.7
Temperature inlet [°C]	44	46	50	51
Air mass [mg/cycle]	750.9	802.4	679.3	741.2
Methane/air equivalence ratio [-]	0.174	0.240	0.192	0.236
Premixed Ratio [%]	86.10	88.78	85.97	87.62

3 Combustion model

In the software, a specific model is provided for dual fuel combustion. Actually, it consists of two models usually used for conventional diesel combustion and flame propagation in spark ignition engines, respectively. Without considering in this phase, the effects of turbulence, it uses the well-established power law formula [12] to relate the dependency of the laminar flame speed on temperature and pressure:

$$S_L = S_{L,0}\left(\frac{T_u}{T_{ref}}\right)^{\alpha}\left(\frac{p}{p_{ref}}\right)^{\beta}$$

$$\alpha = 2.18 - 0.8(\phi - 1)$$

$$\beta = -0.16 + 0.22(\phi - 1)$$

The main focus of this work is the defining of the $S_{L,0}$ term. It represents the speed of the laminar flame in standard conditions (T_{ref} = 298 K and p_{ref} = 1.03 kPa) that is an intrinsic property of the mixture. The software offers only the standard correlation for its expression [12]:

$$S_{L,0} = B_m + B_\phi(\phi - \phi_m)^2$$

However, the software suggests the use of a "proprietary" model for combustion in methane mixtures. Indeed, this model is acceptable for simulations of mixtures near the stoichiometric value, while below

equivalence ratios of 0.6, the flame speed assumes a negative value (Figure 2). Gaseous fuels usually burn in lean conditions, such as the test cases under investigation (Table 2), therefore, the flame propagation model requires to be adapted.

In order to avoid the negative flame speeds, the second order polynomial correlation was corrected by Gülder [10]:

$$S_{L,0}(\phi) = \omega \phi^{\eta} e^{-\xi(\phi-\sigma)^2}$$

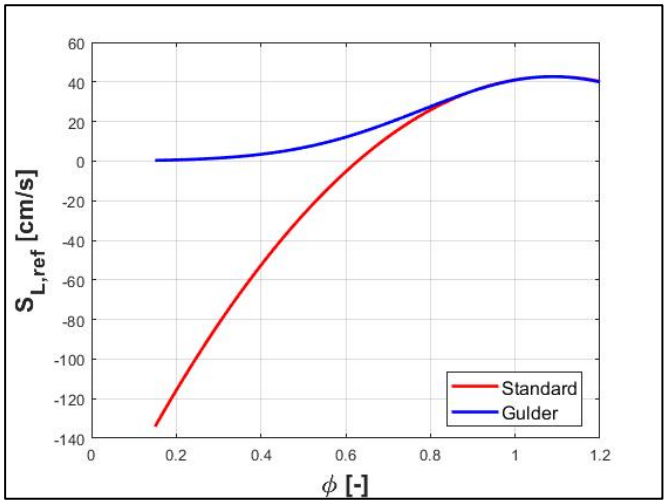

Figure 2: Reference laminar flame speed trends for different equivalence ratios for standard [12] and Gülder [10] correlations.

Table 3: Coefficients of methane [10].

ω [cm/s]	η	ξ	σ
42.2	0.15	5.18	1.075

In order to implement this correlation in the software, it is possible to adapt the standard one by providing to the term B_m a matrix of values, created in Matlab, that reproduces the Gülder laminar flame speed in function of the equivalence ratio, while the quadratic part of the standard correlation is deleted by setting the term B_ϕ equal to 0.

4 Results

Initially, the engine was calibrated with motoring conditions to estimate the correct mass flow rate entering the system. Moreover, the engine is affected by mass loss (blow by) of the premixed charge of air and methane in the crevices region of the cylinder, starting from the results obtained in [13] a calibration of the parameter that regulates this phenomenon for the different cases is necessary. Once the simulated results agreed with the experimental ones, the interest was shifted to the calibration of combustion. Since the blow by model of the software, foresees only the loss of air, to take into account of the methane loss as well, the quantity of methane introduced into the intake manifold was reduced. Regarding the turbulence and combustion setting, the constants were calibrated with reference to the 1500x2 case. In Figure 3, the results in terms of in-cylinder pressure are displayed.

As it is observed in Figure 2, the model is capable to provide a correct estimation of peak pressure levels. In addition, in the numerical simulations the rise to maximum is characterized by two peaks, probably

due to the two injections of diesel fuel; while, the expansion phase is likely driven by the oxidation of the sole methane, that, except for the 1500x2 case, seems to be underestimated. This can be explained, as already highlighted, by the fact that turbulence and combustion conditions were not specifically modelled and the same constants were used for all the cases. On the contrary, they can be significantly affected by the engine speed and load level, considering, also, the mass loss [14].

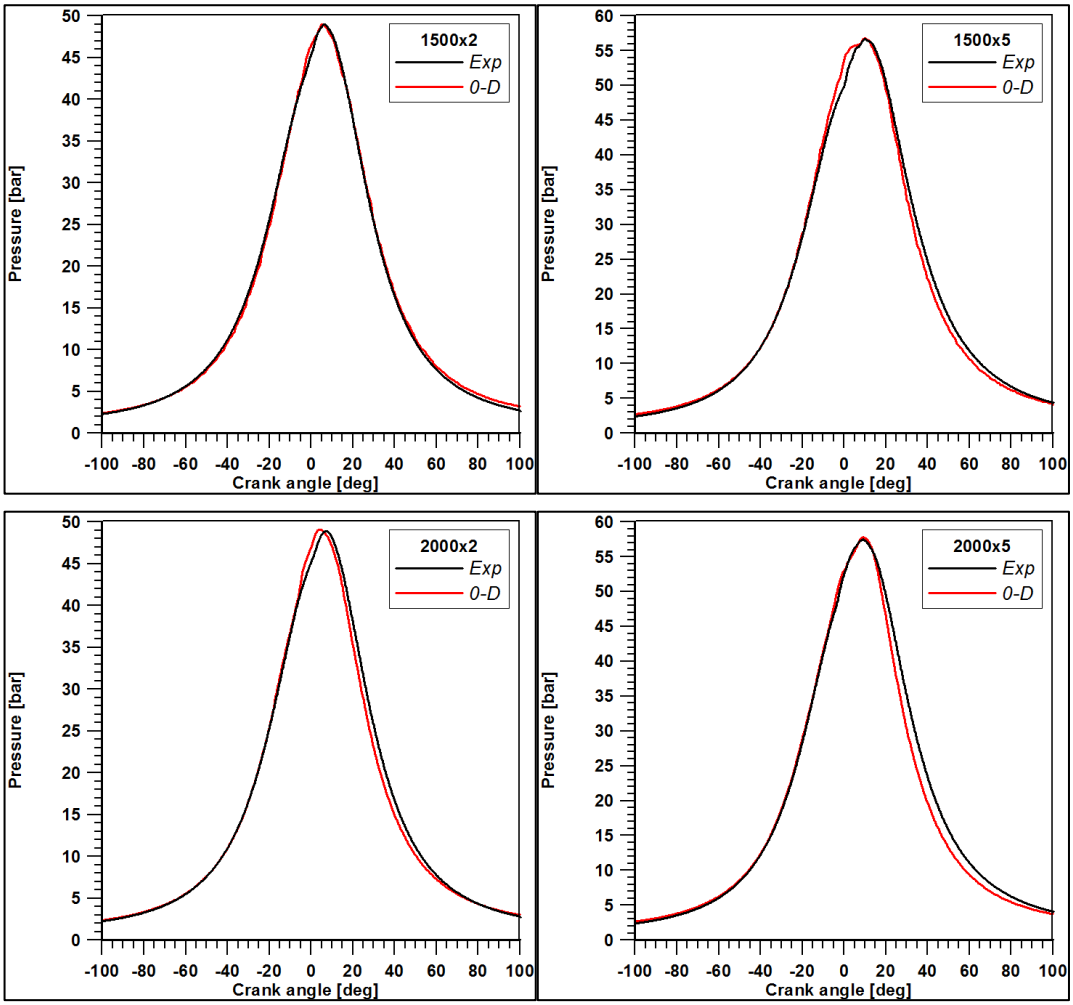

Figure 3: Pressure trends comparison for the different test cases.

In addition, the analysis of the burn rate and heat release, can be helpful to estimate the contribution of each fuel to the different phases of combustion development and to assess the differences with conventional ones.

Finally, the study of methane-diesel dual fuel combustion aims at the correct prediction of combustion process for various operating points with different speed and load conditions, especially for the applications that are difficult to investigate experimentally. As a matter of fact, it represents a feasible solution for the reduction of emissions with accessible costs in heavy-duty engines that require performances levels that only a well-established technology, such as the diesel engine can provide.

References

[1] Payri, F., Martín, J., Arnau, F.J., Artham, S., Analysis of temperature and altitude effects on the Global Energy Balance during WLTC. https://doi.org/10.1177/14680874211034292

[2] Vavra, J., Bortel, I., and Takats, M., "A Dual Fuel Hydrogen - Diesel Compression Ignition Engine and Its Potential Application in Road Transport," SAE Technical Paper 2019-01-0564, 2019, doi:10.4271/2019-01-0564.

[3] Taritaš, I., Sremec, M., Kozarac, D., Blažić, M. i Lulić, Z. (2017). The Effect of Operating Parameters on Dual Fuel Engine Performance and Emissions – An Overview. Transactions of FAMENA, 41 (1), 1-14. https://doi.org/10.21278/TOF.41101

[4] Monsalve-Serrano, J., Belgiorno, G., Di Blasio, G., Guzmán-Mendoza, M., 1D Simulation and Experimental Analysis on the Effects of the Injection Parameters in Methane–Diesel Dual-Fuel Combustion. *Energies* 2020, *13*, 3734. https://doi.org/10.3390/en13143734

[5] Misra, A., Yadav, M., Sharma, A., Singh, G., (2020). Methane–Diesel Dual Fuel Engine: A Comprehensive Review. 10.1007/978-981-15-2647-3_30.

[6] Sahoo, B., Niranjan, S., Saha, U., (2009). Effect of engine parameters and type of gaseous fuel on the performance of dual-fuel gas diesel engines--A critical review. Renewable and Sustainable Energy Reviews. 13. 1151-1184. 10.1016/j.rser.2008.08.003.

[7] Mancaruso, E., Todino, M., Vaglieco, B., (2020). Study on dual fuel combustion in an optical research engine by infrared diagnostics varying methane quantity and engine speed. Applied Thermal Engineering. 178. 115623. 10.1016/j.applthermaleng.2020.115623.

[8] Carlucci, A.P., Laforgia, D., Saracino, R., Toto, G., Combustion and emissions control in diesel–methane dual fuel engines: The effects of methane supply method combined with variable in-cylinder charge bulk motion, https://doi.org/10.1016/j.enconman.2011.04.012.

[9] Heywood, J. B. (1988). Internal Combustion Engine Fundamentals.

[10] Gülder, Ö. (1990). Turbulent Premixed Flame Propagation Models for Different Combustion Regimes. 1990: Syposium on Combustion.

[11] Gülder, Ö., 1984, "Correlations of Laminar Combustion Data for Alternative S.I. Engine Fuels," SAE Technical Paper 841000. https://doi.org/10.4271/841000

[12] Metghalchi M., and Keck J.C., Burning velocities of mixtures of air with methanol, isooctane, and indolene at high pressure and temperature. Combust Flame 1982; 48: 191–210.

[13] De Robbio, R., Cameretti, M.C., Mancaruso, E., Tuccillo, R. et al., "Combined CFD - Experimental Analysis of the In-Cylinder Combustion Phenomena in a Dual Fuel Optical Compression Ignition Engine," SAE Technical Paper 2021-24-0012, 2021, doi:10.4271/2021-24-0012.

[14] De Robbio, R., Cameretti, M.C., Mancaruso, E., Tuccillo, R., Vaglieco B.M., CFD Study and Experimental Validation of a Dual Fuel Engine: Effect of Engine Speed. Energies 2021, 14, 4307. https:// doi.org/10.3390/en14144307

Experimental Validation of Laminar Flame Model for CH4/Diesel Dual Fuel Engine applied to H2/Diesel Combustion

R. De Robbio*[1], E. Mancaruso[1], B.M. Vaglieco[1], S. Artham[2] and J. Martin[2]

[1]STEMS – CNR. Viale G. Marconi 4, 80125, Naples, Italy.

E-mail: roberta.derobbio@stems.cnr.it; ezio.mancaruso@stems.cnr.it; biancamaria.vaglieco@stems.cnr.it

[2]CMT – Motores Térmicos. Universitat Politécnica de Valencia. Camino de Vera s/n, E-46022 Valencia, Spain.

E-mail: susar1@upv.edu.es; jaimardi@mot.upv.es

Abstract.
Despite of having high thermal efficiency and wide range of operation, compression ignition (CI) engines have high exhaust emissions of particulate matter (PM) and nitrogen oxides (NOx) which are harmful for the environment. In order to keep up with the latest stringent regulations on emissions, the CI the engines have been pushed to work with different fuels. In particular, the usage of gaseous fuels along with diesel fuel in dual fuel mode demonstrated to be a valid solution, especially for large bore applications. Indeed, a large part of the diesel liquid fuel is substituted with alternative gaseous fuels that is introduced into the intake manifold to form a premixed charge with air, which reduces PM significantly and, in many cases, NOx. Even though, methane has been the mostly used gaseous fuel for dual fuel CI engine, the necessity to reduce CO_2 emissions as well, has led hydrogen to be one of the most promising alternatives. Because of its faster burning velocity and wide range of air to fuel ratios, a different model for its combustion must be used for predictive purposes. In current work, a dual-fuel combustion model has been implemented in GT-Power, with the aim of simulating and investigating the characteristics of hydrogen-diesel combustion. Initially, a dual fuel model with methane was used and experimentally validated. A laminar flame speed model, with the approaches of Heywood and Gülder studies, was built and incorporated in the software. Design of experiments and design optimizer was used to find the optimal values of the combustion model constants matching in-cylinder pressure curves. Once, the model was validated with methane, the same methodology has been adapted to use hydrogen instead. Two new correlations are built and implemented in the code starting from literature experimental measurements. The simulated results of hydrogen-diesel combustion allow to foresee a burn rate consistent with methane-diesel ones.

Notation

BMEP *Brake mean effective pressure.*
BTE *Brake thermal efficiency.*
CI *Compression ignition.*
DF *Dual fuel.*
ECU *Electronic control unit.*
HC *Unburned hydrocarbons.*
NOx *Nitrogen oxides.*
NG *Natural gas.*
PM *Particulate matter.*
RCCI *Reactivity controlled compression ignition.*
RoHR *Rate of heat release.*
RP *Premixed ratio.*

1. Introduction

Compression ignition (CI) engines cover from large marine to small car applications. Despite of having high thermal efficiency and wide range of operation, it is well-know that CI engines have high exhaust emissions of particulate matter (PM) and nitrogen oxides (NOx). Since they have significant effects on human health and are harmful for the environment, several efforts have been made to improve

the emissions, preserving the performance of modern diesel engines. In order to keep up with the latest stringent regulations on emissions [1] [2], the implementation of alternative solutions is necessary. Some of such alternative solutions such as the usage of after treatment systems, is not cost efficient and decreases global efficiency because of the higher pumping work required [3].

On the contrary, other solutions have been proposed and concern the way of combustion and cleaner fuels that power the engine. In particular, the combustion of the gaseous fuels, usually natural gas (NG) or methane, initiated by pilot injection of diesel fuel, called dual fuel (DF) injection, has demonstrated to be effective in the resolution of the previous mentioned issues. Indeed, in their literature review [4] Lijiang and Peng collected several scientific papers that analyzed DF combustion, emissions, and performance characteristics for different NG/air mass ratios. It is illustrated that dual fuel mode has a lower pressure ratio and a longer ignition delay with respect to diesel mode. More importantly, DF introduces a trade-off between NOx and PM emissions, and unburned hydrocarbons (HC) and carbon monoxide (CO). In fact, the former substantially decrease while the latter increase with a consequent negative effect on engine power and brake thermal efficiency (BTE).

The authors of the present work have studied dual fuel (methane-diesel) combustion both experimentally [5], [6], [7], [8], and numerically [9], [10], [11]. In particular, the experimental activity was carried out on an optically accessible single cylinder diesel engine. Innovative spectroscopic and infrared visualization have been obtained with intensified and fast cameras, respectively, able to investigate different emission wavelength, and therefore, to follow the evolution of fundamental species in the long chain of reactions. Then, experimental results have been utilized for the validation of the CFD calculations. Indeed, three-dimensional codes can be useful tools to deepen the knowledge of the in-cylinder phenomena. However, the main issue of the dual fuel modelling is the description of the combustion development. As a matter of fact, a flame propagates in the premixed charge, such flame is started by the diesel liquid jet. A reliable model is presented in [12] where Amirante et al. analyze the flame propagation of different fuels based on the works of Heywood [13] , Metghalchi [14] and Gülder [15] [16]. This model has been used in the 3D codes and validated in [11]. Nevertheless, the implementation of such model in a 0D/1D code can be decisive for a faster evaluation and optimization of a dual fuel engine performances. This methodology was used by Millo et al. [17] for the simulation of a large bore diesel engine supplied with natural gas, since marine applications seem the most suited for the implementation of dual fuel technology. They developed a phenomenological fast running 0D/1D combustion model, only for natural gas, in GT-Power validated against experimental data.

Particular attention must be paid to low load conditions, since they can be significantly critical for dual fuel combustion; in [18] an in-house 1D code is used to evaluate the influence of the main injection parameters on the efficiency and emissions. It is demonstrated that with respect to single pilot injection, double injection strategies lead to an enhancement of efficiency; increasing the rail pressure promotes a more prominent premixed combustion phase leading to a smoother combustion development; adjusting injection parameters together with methane percentage, it is possible to obtain an improvement of efficiency up to 3.5%.

Even though, methane is the mostly used gaseous fuel with a wide availability across the globe that ensures economical prices, for dual fuel CI engine, hydrogen is one of the most promising alternative fuels, because of its faster burning velocity, wide range of air to fuel ratios and rapid combustion [19], [20]. Therefore, with the use of hydrogen as gaseous fuel more significant drop in CO_2 emissions can be obtained, and the engine can be operated at very lean equivalence ratios as well. Many researchers proposed the addition of hydrogen to diesel in the CI engines as a method to improve the performance as it increases the H/C ratio of the entire fuel and reduce the combustion duration due to the high flame speed of hydrogen in comparison to other fuels.

Miyamoto et al. [21] experimentally investigated the performance and emission characteristics of a diesel engine with small volume percentages of hydrogen added to the intake air at late diesel-fuel injection timings. They focused on the reduction of NOx and PM emissions but keeping an acceptable level of in-cylinder pressure rise to avoid excessive noise. They demonstrated that a right late diesel timing in combination with H_2 addition can lead to low temperature combustion with a decrease of nitrogen oxides emissions without enhancing smoke in the exhaust. In [22] Ghazal simulated the combustion of different hydrogen-diesel blends for different engine speed and different air to fuel ratios. Results demonstrated that small amounts of H_2 reduce the diesel ignition lag and the pressure rise rate providing softer run conditions and improving the durability of the engine. In general, the engine power is improved, and CO emissions are reduced with respect to the base diesel engine. Ultimately, the comprehensive review in [23] summarized the results of different works in literature reporting that the utilization of hydrogen in dual fuel engines, reduces unburned hydrocarbons, carbon monoxide and smoke to near zero level and significantly decreases greenhouse emissions (CO_2 and methane). On the contrary, the high adiabatic flame temperature of H_2 generates high localized in-cylinder temperatures, leading to

increasing emissions of NOx. Moreover, an enhancement of hydrogen substitution advances the start of combustion, and if a critical value is achieved the autoignition of the premixed H_2-air charge could occur and lead to an abnormal combustion (knocking). In the review, solutions to these problems, such as low temperature strategies or water injections are proposed. Also, for dual fuel hydrogen-diesel engine GT-Power can be used. Indeed, Ghazal [24] numerically investigated the performances and emissions of reactivity controlled compression ignition (RCCI) engine in DF mode combined with port water injection. Results demonstrated that engine speed and injection timing affect the efficiency and emissions; in particular, advancing the injection could lead to high in-cylinder temperature, pressure rising rate and NOx emissions, on the contrary the CO emissions are reduced but at the expense of a lower BTE.

In the current work, a dual-fuel combustion model is built in GT-Power, with the aim of simulating and investigating the characteristics of hydrogen-diesel combustion. Initially, dual fuel engine with methane is built and validated. The previously cited approaches of Heywood [13] and Gülder [15] [16] are used and incorporated in the software, to model laminar flame speed. The optimal values of combustion constants are found through design of experiments and design optimizer in order to match in-cylinder pressure curves. The validation of diesel-methane cases is obtained with the aid of an experimental campaign on an optically accessible single cylinder research engine. Experimental tests are characterized by different load levels, 2 and 5 bar of brake mean effective pressure (BMEP), and different engine speeds, 1500 and 2000 rpm. Dual fuel methane-diesel results represent the starting point to foresee a burn rate for hydrogen-diesel combustion consistent with the previous ones, obtained by adapting the same methodology. However, for hydrogen simulations, not only the correlation must be implemented in the software, but it must be built starting from laminar flame speed empirical measurements found in the literature [25] [26]. The numerical cases are based on an experimental campaign forecasted on the same engine supplied with hydrogen instead of methane. Since the main issue regards the correct determination of laminar flame speed in extremely lean conditions, two new correlations are presented in different ranges of equivalence ratio.

2. Engine set-up

The research activity has been carried out on an optically accessible single cylinder diesel engine supplied with methane in the intake manifold. The engine, specifically designed for the optical access, is equipped with the original common rail injection system of the four-cylinder engine, the characteristics are listed in Table 1. The timing of the direct injected diesel fuel can be arbitrarily controlled via a fully flexible Electronic Control Unit (ECU). Instead, the gaseous fuel is port fuel injected in the intake manifold. Gaseous fuel injection is managed by a delay unit synchronized with the engine shaft encoder. The features of the injection systems for the two fuels are reported in Table 2.

Table 1. Engine specifications

Engine type	4-stroke, single cylinder
Stroke [mm]	92
Bore [mm]	85
Cylinder volume displacement [cm^3]	522
Combustion bowl volume [cm^3]	19.7
Compression ratio	16.5:1
Number of Valves	4
Exhaust Valve Opening (EVO)	116°ATDC
Exhaust Valve Closing (EVC)	340°BTDC
Intake Valve Opening (IVO)	344°ATDC
Intake Valve Closing (IVC)	132°BTDC

Table 2. Injection system specifications

Diesel injection system	Common rail
Number of holes	7
Cone angle of fuel jet axis [deg]	148
Hole diameter [mm]	0.141
Methane injection system	PFI
Number of holes	1
Maximum injection pressure [bar]	5

For a better comprehension, in Figure 1 the scheme of the whole system is displayed. It is important to highlight that to make the engine optically accessible, a sapphire window was placed in the bottom part of the combustion bowl, which now presents a flat shape. However, the modification was made without altering the original bowl volume (Table 1).

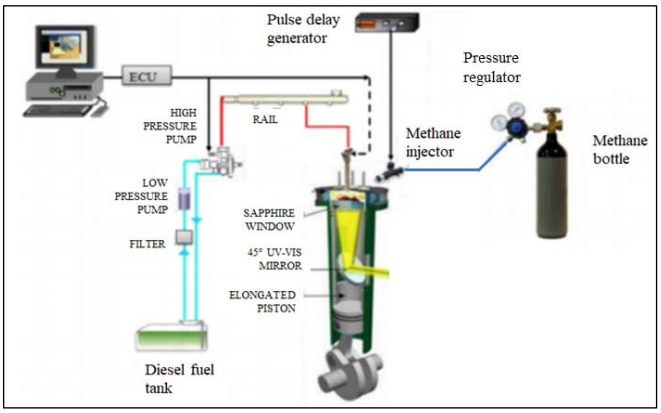

Fig. 1. Experimental set-up scheme

The different signals were measured via a multichannel acquisition system. The diesel injector current of the solenoid was observed by means of a Hall-effect sensor. Instead, a piezoelectric pressure transducer, set in the glow plug seat of the engine head, was used for the acquisition of the in-cylinder pressure both in motored and fired conditions. All the current signals were digitalized and recorded at 0.2° crank angle increments. For each test point, the in-cylinder pressure cycle taken as reference is a calculated average from 200 consecutive combustion cycles through the AVL-Indicom software. Also, the same software used the averaged pressure for the calculation of the heat release rate via the well-known energy balance equation [13].

The experimental tests, used for the validation of the model are characterized by two load levels, 2 and 5 BMEP and two different engine speeds, 1500 and 2000 rpm. The operating conditions for the four cases are listed in Table 3. For each case, the original double (pilot and main) injection timing is maintained with respect to the full diesel case. However, in DF mode the main injection has been reduced until it has same duration as pilot one, so to inject the same amount of liquid fuel. The amount of methane is added with the aim to achieve the same BMEP as the corresponding full diesel case.

Table 3. Engine operating conditions

Case	#1	#2	#3	#4
Engine Speed [rpm]	1500	1500	2000	2000
BMEP	2	5	2	5
SOI pilot	16°BTDC	11.6°BTDC	21.2°BTDC	18.6°BTDC
SOI main	6°BTDC	0.3°ATDC	8°BTDC	2.4°BTDC
Dwell interval [deg]	10	11.9	13.2	16.2
Duration pilot and main [deg]	2.6	2.4	3.4	3.1
Diesel mass injected pilot + main [mg/cycle]	1.42	1.64	1.43	1.66
Methane mass [mg/cycle]	7.579	11.191	7.554	10.148
Rail pressure [bar]	615	867	700	891
Pressure inlet [bar]	1.5	1.7	1.5	1.7
Temperature inlet [°C]	44	46	50	51
Air mass [mg/cycle]	750.9	802.4	679.3	741.2
Methane/air equivalence ratio	0.174	0.240	0.192	0.236
Methane RP [%]	86.1	88.8	86.0	87.6
Hydrogen mass [mg/cycle]	2.457	4.331	2.305	3.904
Hydrogen/air equivalence ratio	0.117	0.189	0.120	0.183
Hydrogen RP [%]	82.8	88.0	81.8	86.7

In addition, Table 3 reports the premixed ratio (RP), that is the ratio of energy input from methane expressed as follows:

$$RP = \frac{(m_p LHV_p)}{(m_p LHV_p + m_d LHV_d)} \times 100$$

Where m_p and m_d are the mass flow rate of premixed fuel (methane) and directly injected fuel (diesel), respectively, LHV_p and LHV_d their lower heating values. All the cases are then characterized by an extremely low equivalence ratio and RP values higher than the 80%. Although a major replacement and reduction of liquid fuel has been accomplished, still a small amount of diesel fuel must be injected to ignite the premixed charge.

Following the same approach, a research activity is forecasted using hydrogen. The four cases are expected to be performed on the same engine supplied with hydrogen instead of methane in order to reach the same BMEP. The values of the mass injected are reported in the Table 3 as well. Moreover, the equivalence ratio and the RP are expected to be lower than methane ones. However, the premixed ratios are still higher than 82%.

The in-cylinder pressures measured for the four cases are displayed in Figure 3. It is possible to see that the main differences are given by the load level. Engine speed has a minor influence on combustion. However, it is important to recall that the injection timing is varied with the operating condition.

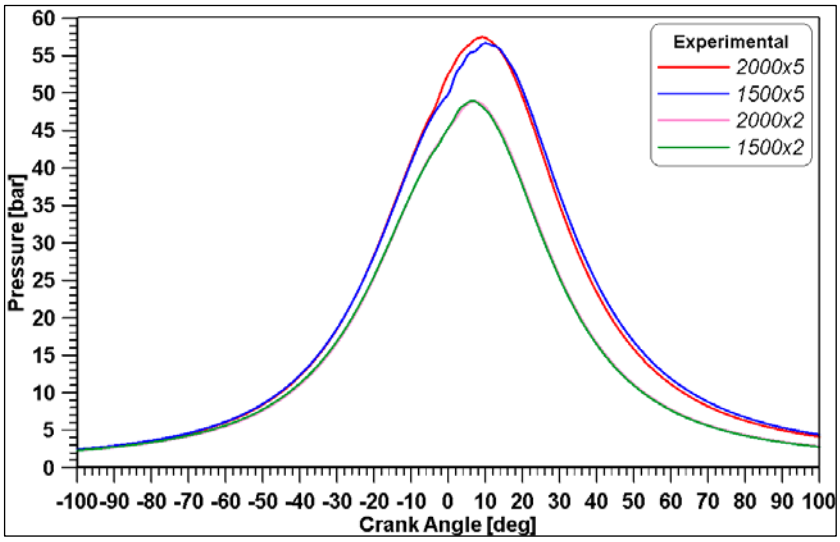

Fig. 2. Experimental in-cylinder pressure curves

3. Model set-up

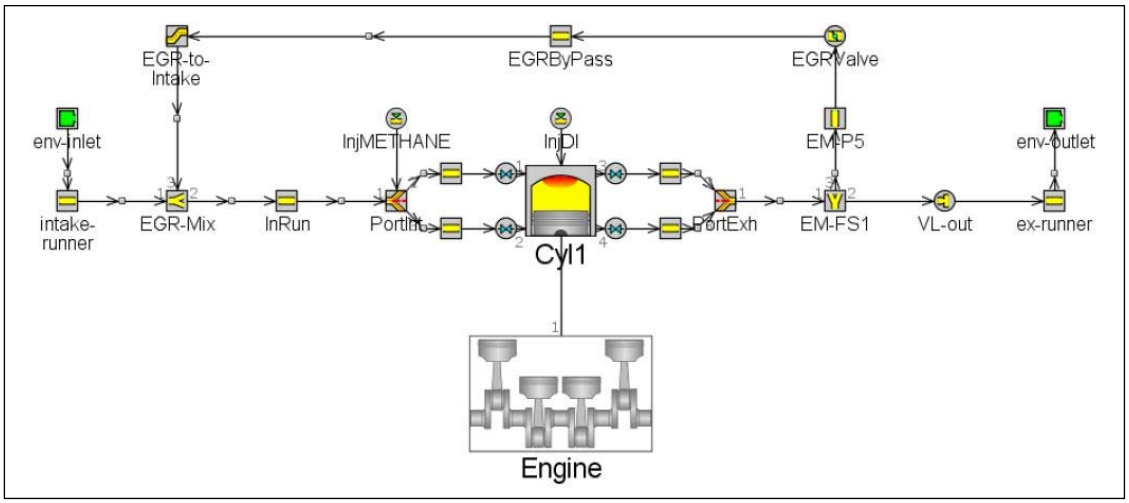

Fig. 3. GT-Power model of the compression ignition single cylinder diesel engine in dual fuel mode

The engine was modelled in the engine simulation software, according to the specifications from engine test bench, as shown in the Figure 3. As it can be seen, the model has two injectors, one at the intake port, where methane or hydrogen fuel is injected and a second one in the engine head, where diesel is injected within the cylinder to initiate combustion. The engine model was updated with all the intake and exhaust conditions, initial pressures and temperatures at various locations, fuel mass flow rate for hydrogen, start of injection and injected fuel mass for diesel, according to the experimental results of dual fuel methane-diesel engine, for various operating points as shown in Table 3. After initial calibration, the interest was shifted to the combustion model, where a new laminar flame model was built and incorporated in the set-up for methane-diesel dual fuel model.
In the software, a specific model is provided for dual fuel combustion named “EngCylCombDualFuel”. It consists of two models, “DIPulse” and “SITurb”, usually used for conventional diesel combustion and flame propagation in spark ignition engines, respectively.

3.1 DI Pulse

This combustion model predicts the combustion rate for direct-injection diesel engines with single and multi-pulse injection events. It tracks the evaporation, mixing with surrounding gas and burning of the fuel jet. The DIPulse model benefits from faster runtime while maintaining or exceeding the predictive accuracy seen by other predictive models. It requires an accurate injection profile to achieve good results.
The DIPulse model includes several submodels which simulate the relevant physical processes taking place during injection and combustion. There are four attributes in the 'DIPulse' template which should be used for calibration.

3.1.1 Entrainment

As the spray penetrates, it slows down as the surrounding unburned and burned gases are entrained into the pulse. The intermixing of pulses occurs through entrainment. The entrainment rate can be modified by the Entrainment Rate Multiplier (C_{ent}).

3.1.2 Ignition

The fuel mixture in each pulse undergoes an ignition delay modelled with an Arrhenius expression which can be modified by the Ignition Delay Multiplier (C_{ign}).

$$\tau_{ign} = C_{ign}\,\rho^{-1.5}\exp\left(\frac{3500}{T}\right)[O_2]^{-0.5}$$

Where, τ_{ign} is ignition delay, T is pulse temperature, ρ pulse gas density and $[O_2]$ is oxygen concentration.

3.1.3 Premixed Combustion

When the pulse ignites, the mixture present at that time is set aside for premixed combustion. The rate of this combustion is assumed to be kinetically limited and can be modified by the Premixed Combustion Rate Multiplier (C_{pm}).

$$\frac{dm_{pm}}{dt} = C_{pm}m_{pm}\mathrm{k}\left(\mathrm{t}-t_{ign}\right)^{2} f([O_2])$$

Where, t_{ign} is the time at ignition, m_{pm} is premixed mass, k is turbulent kinetic energy and t is the time.

3.1.4 Diffusion Combustion

After the pulse ignites, the remaining unmixed fuel and entrained gas in the pulse continue to mix and burn in a primarily diffusion-limited phase. The rate of this combustion can be modified by the Diffusion Combustion Rate Multiplier (C_{df}).

$$\frac{d\mathrm{m}}{dt} = C_{df}\mathrm{m}\,\frac{\sqrt{k}}{\sqrt[s]{V_{cyl}}}\,f([O_2])$$

3.2 SI Turb

This model predicts the burn rate for homogeneous charge, spark-ignition engines. This prediction considers the cylinder's geometry, spark locations and timing, air motion, and fuel properties. There are four important attributes in the 'EngCylCombSITurb' template which should be used for calibration.

3.2.1 Laminar Flame Speed

The laminar flame speed is calculated by an equation, except for the hydrogen and methane options which use different proprietary equations to quantify the flame speed [13]. Detailed explanation of Laminar flame speed model is given in further sections.

3.2.2 Entrainment and Burn-up

The unburned mixture of fuel and air is entrained into the flame front through the flame area at a rate proportional to the sum of the turbulent and laminar flame speeds as shown in formula (1). The burn rate is proportional to the amount of unburned mixture behind the flame front, $(M_e - M_b)$, divided by a time constant, τ, as shown in formula (2). This model requires that in-cylinder flow is described by an 'EngCylFlow' reference object so the turbulent intensity and length scale will be provided. The effects of turbulent intensity and length scale can be modified using the Turbulent Flame Speed Multiplier (C_{TFS}) and Taylor Length Scale Multiplier (C_{TLS}). Additionally, the Flame Kernel Growth Multiplier (C_{FKG}) can be used to adjust the initial growth rate of the flame kernel. All the related equations are shown in the formulas (3), (4) and (5).

$$\frac{dM_e}{dt} = \rho_u A_e (S_T + S_L) \tag{1}$$

$$\frac{dM_b}{dt} = \frac{M_e - M_b}{\tau} \tag{2}$$

Here, turbulent flame speed S_T can be calculated with the help of C_{TFS} and C_{FKG} as shown below

$$S_T = C_{TFS}\, u' \left(1 - \frac{1}{1 + C_{FKG}\left(\frac{R_f}{L_i}\right)^2}\right) \tag{3}$$

$$\tau = \frac{\lambda}{S_L} \tag{4}$$

$$\lambda = \frac{C_{TLS} L_i}{\sqrt{Re_t}} \tag{5}$$

3.3 Calibration and optimization

In the current work, C_{ign} C_{ent} C_{df} C_{pm} C_{TFS} C_{FKG} and C_{TLS} have been calibrated. The aim of calibration is to find the optimal set of constants that will provide the best possible match to various of operating points. The calibration was performed using design of experiments (DOE) and design optimizer in GT power. Initially, the operating point with low speed and low load (1500 rpm engine speed and 2 bar BMEP) was considered and DOE was performed for the individual constants. Once, a set of values were obtained for the combustion constants, they were used for the other operating points to test the consistency. After further tuning, a pre-final set of values for the combustion constants were obtained for all the operating points. In order to be precise with the required targets, design optimizer was used and a final set of values for all the combustion constants are obtained. It is seen that C_{ent} C_{df} C_{FKG} and C_{pm} have low influence on the peak pressures and their lower limits (ranging from 0.05 to 1) give good results. C_{TFS} and C_{TLS} have high influence and the values range from 1.3 to 1.6.
The ignition Delay Multiplier, C_{ign} has high influence on combustion and has a strong dependence on speed and load. Hence it was decided to use a table with a 14x38 matrix, for the C_{ign}, instead of giving a constant value for all the operating points. The table was created using the values obtained through design optimizer. This table consists of the values of the constants for various operating points, with engine speed starting from 1200 until 2500 rpm, along with a load starting from 0.3 until 4 bars. This table interpolates the required constant according to the operating point. The values of the parameters after the optimization are reported in Table 4.

Table 4. Values of the constants

C_{ing}	-
C_{ent}	???
C_{df}	1.4
C_{pm}	0.07
C_{TFS}	3
C_{FKG}	3
C_{TLS}	0.5

4. Laminar Flame Speed model

As already stated in the introduction section, the aim of this work is to model dual fuel combustion through a model of flame propagation. The main issue is that in the GT-Power a specific flame model for methane and hydrogen is not present.

In general, the laminar flame speed is calculated proportionally to the laminar flame speed in standard conditions, i.e. T_{ref} = 298 K and p_{ref} = 1.03 kPa. In order to account for the different temperature and pressure condition the dependency is expressed via the power law formula (6) [14]:

$$S_L = S_{L,0}\left(\frac{T_u}{T_{ref}}\right)^{\alpha}\left(\frac{p}{p_{ref}}\right)^{\beta} \tag{6}$$

$$\alpha = 2.18 - 0.8(\phi - 1) \tag{7}$$

$$\beta = -0.16 - 0.22(\phi - 1) \tag{8}$$

From equations (6) it is observed that the laminar flame speed depends on the temperature of the unburned charge (T_u) and pressure (p) via two constants, α and β, which are a function of the equivalence ratio ϕ, eq. (7) and (8).

The laminar flame speed in standard condition $S_{L,0}$ is an intrinsic property of the mixture. The software makes use only of the standard correlation (eq. 8) by Metghalchi [14] expressed as follows:

$$S_{L,0} = B_m + B_\phi(\phi - \phi_m)^2 \tag{9}$$

Therefore, reference laminar flame speed and the equivalence ratio are linked via a second order polynomial equation. Nevertheless, such correlation assumes negative values below an equivalence ratio of 0.6, as it is possible to observe from Figure 4 (red dotted line).

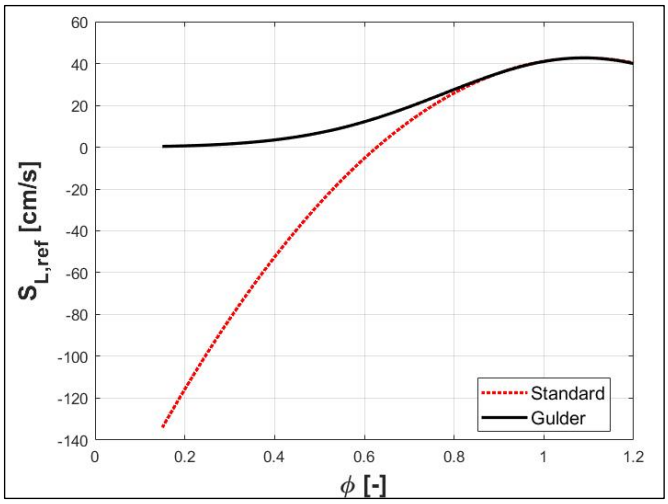

Fig. 4. Reference laminar flame speed vs equivalence ratio for standard [14] and Gülder [16] correlations

Generally, gaseous fuels burn in lean conditions, like the engine under investigation. As already pointed out in Table 3 the equivalence ratio of air-methane mixture ranges between 0.17 and 0.24, far below 0.6 where the laminar flame speed is passing the zero value. Therefore, under such circumstances the software would provide a negative flame speed, and this is not acceptable. For this reason, Gülder proposed an exponential correlation (eq. 10), still illustrated in Figure 4 (black continuous line), that never assumes negative values. The values for the different constants are listed in Table 4.

$$S_{L,0}(\phi) = \omega\phi^{\eta}exp(-\xi(\phi - \sigma)^2) \tag{10}$$

Table 4. Coefficients of methane [16]

ω [cm/s]	η	ξ	σ
42.2	0.15	5.18	1.075

This correlation can be provided to the software by setting the B_ϕ term equal to 0 so to nullify the second term of the polynomial and by providing to the B_m a matrix, created in Matlab, with the Gülder laminar flame speed values in function of the equivalence ratio.

For hydrogen, the same approach was used. However, the correlations found in literature refers to different conditions than the standard ones. Moreover, particular attention must be paid to the estimation of the laminar flame speed for low equivalence ratio, which in the simulations with hydrogen is even lower than methane's one (Table 3). To overcome this problem, a new correlation must be elaborated. To this scope the values listed by Taylor [25] and Marinov et al. [26], respectively black circles and red squares displayed in Figure 5, are used as starting point.

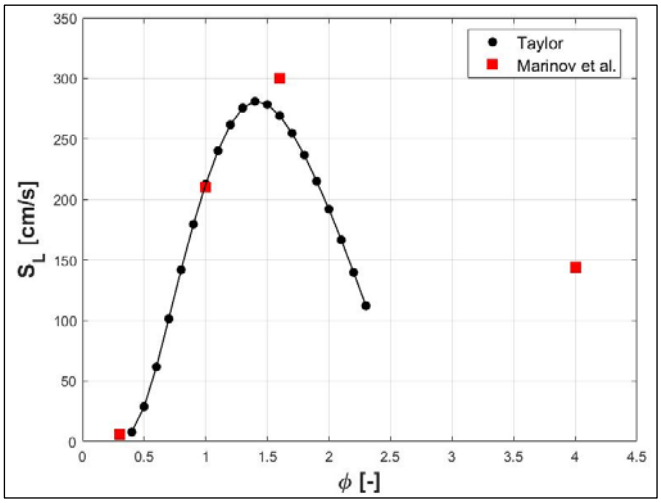

Fig. 5. Hydrogen reference laminar flame speed vs equivalence ratio from Taylor [25] and Marinov et al. [26]

The necessity to use values proposed by Marinov et al. is due to the impossibility to find an exponential correlation that approximates the Taylor curve for the complete range of air/gaseous fuel ratio. Indeed, an exponential correlation seems the right choice two link flame speed and equivalence ratio with the aim to avoid negative flame speeds for lean conditions. For these reasons, a first 4th order polynomial is built to follow the trend proposed in [25] (red dotted line in Figure 6) for ϕ>0.5 and a second exponential correlation valid for ϕ<0.5 is added by integrating the values proposed in [26] (black continuous line in Figure 6). Therefore, two new correlations (eq. 11 and 12) are proposed to describe the laminar flame speed trend with particular attention to the extremely low conditions.

$$S_{L,0}(\phi) = 62.02\phi^4 - 417.85\phi^3 + 728.9\phi^2 - 163.1\phi \qquad \phi = 0.5 \div 2 \qquad (11)$$

$$S_{L,0}(\phi) = 217exp\{-[(\phi - 093)/0.3572]^2\} \qquad \phi = 0 \div 0.5 \qquad (12)$$

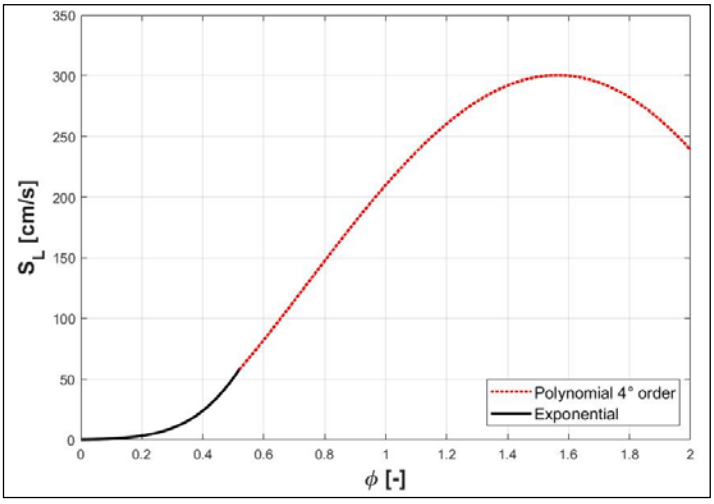

Fig. 6. Hydrogen reference laminar flame speed vs equivalence ratio curve

5. Results

In this section, at first, the validation of dual fuel diesel-methane numerical calculations is presented; then the hydrogen cases are performed using the new presented correlations with the aim to foresee the engine behaviour when supplied with this different gaseous fuel. In particular, the comparison of pressures is necessary to check that the model is capable to provide a good prediction of the original engine performances, while the apparent rate of heat release (RoHR) is a fundamental result to demonstrate that the combustion development is correctly described by the model.

5.1 Diesel-methane model validation

From the comparison of experimental and numerical pressure curves in Figures 7-10 (a) it is possible to observe that the laminar flame model is capable to describe dual fuel combustion; indeed, among all the cases, only the 1500x5 case evidences light differences between the measurements and the calculations. As already illustrated, all the cases have been calibrated to obtain the same air and methane masses, and the correct equivalence ratio as the experimental tests carried out at the bench, considering the blow-by as well. The calibration seems adequate since compression curves perfectly match in each case. Also, with the only exception of the 1500x5 case, the table constant allows to correctly detect the start of diesel fuel ignition, as demonstrated by the fair correspondence of pressure rises. Moreover, the good agreement of the expansion phases evidences the validity of the flame propagation model. This consideration can be confirmed in the 1500x5 case as well, that, although it shows an anticipated start of combustion, the expansion trend follows the experimental one.

Both experimental and numerical apparent rates of heat release, displayed in Figures 7-10 (b), are postprocessed and calculated via the first law of thermodynamic, the energy equation, starting from the pressure curve and using the same value for the different constants:

$$\frac{dQ}{dt} = \frac{\gamma}{\gamma-1} p \frac{dV}{dt} + \frac{1}{\gamma-1} V \frac{dp}{dt} \tag{13}$$

Even though simple, Equation (13) allows to catch the main details of the development and the different phases of combustion, identifying the role of diesel and methane. From Figures 7-10 (b) it is also possible to observe that an acceptable accordance of overall combustion is achieved, the start of combustion, the maximum intensity and the duration of the whole process match in all four cases. Again, the 1500x5 case presents some deviations, but it is likely that they are due to the higher noise of the experimental acquisition.

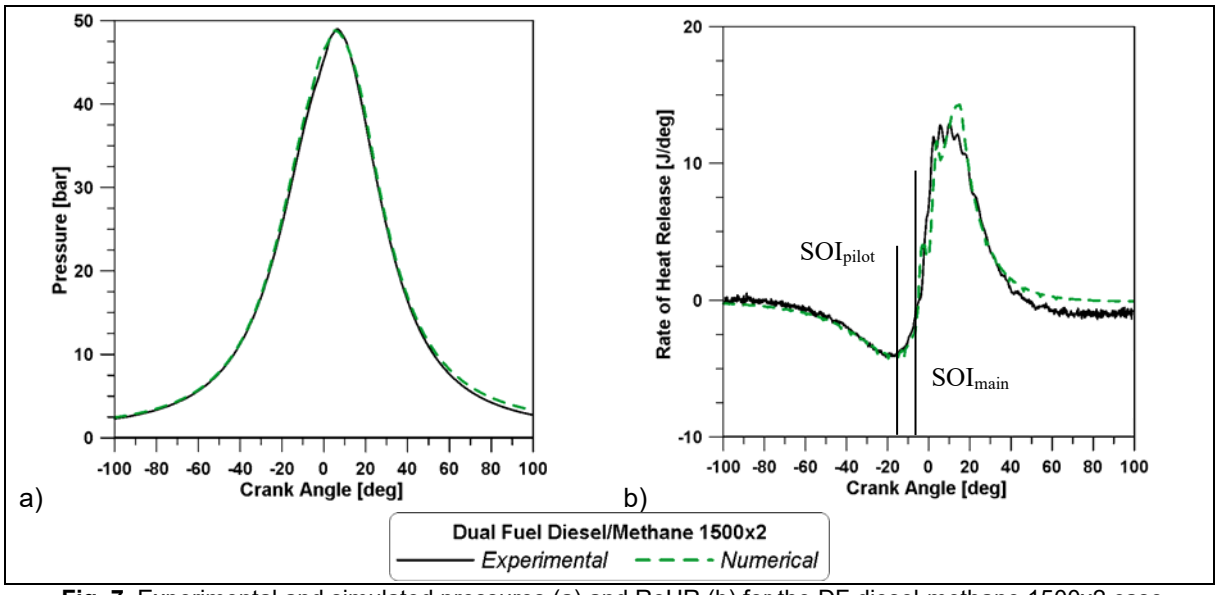

Fig. 7. Experimental and simulated pressures (a) and RoHR (b) for the DF diesel-methane 1500x2 case

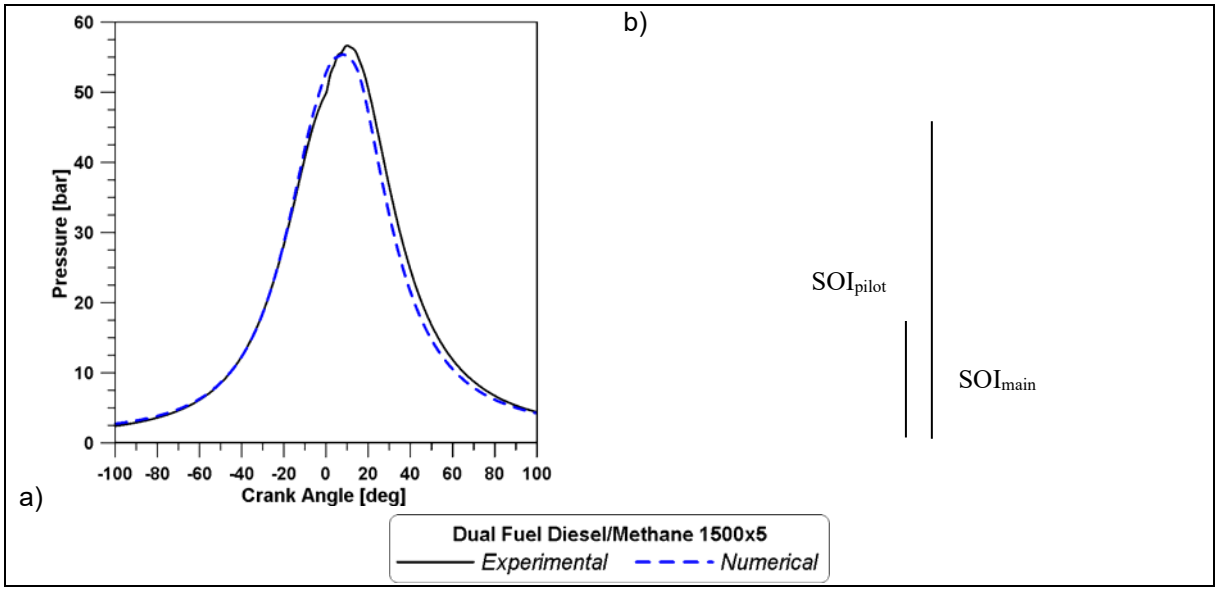

Fig. 8. Experimental and simulated pressures (a) and RoHR (b) for the DF diesel-methane 1500x5 case

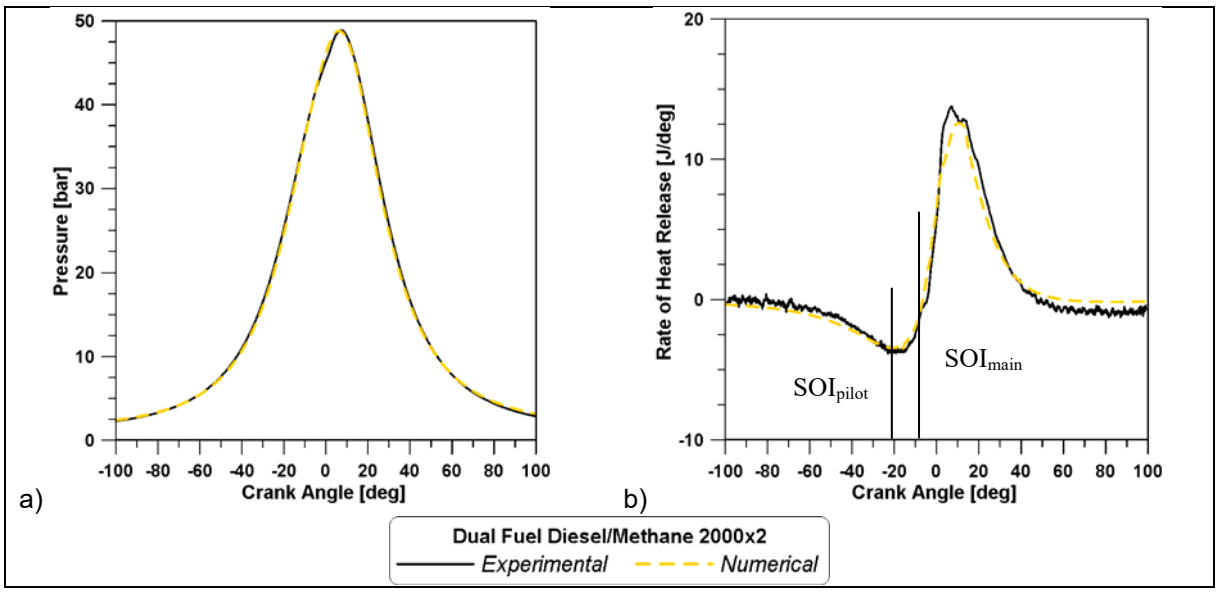

Fig. 9. Experimental and simulated pressures (a) and RoHR (b) for the DF diesel-methane 2000x2 case

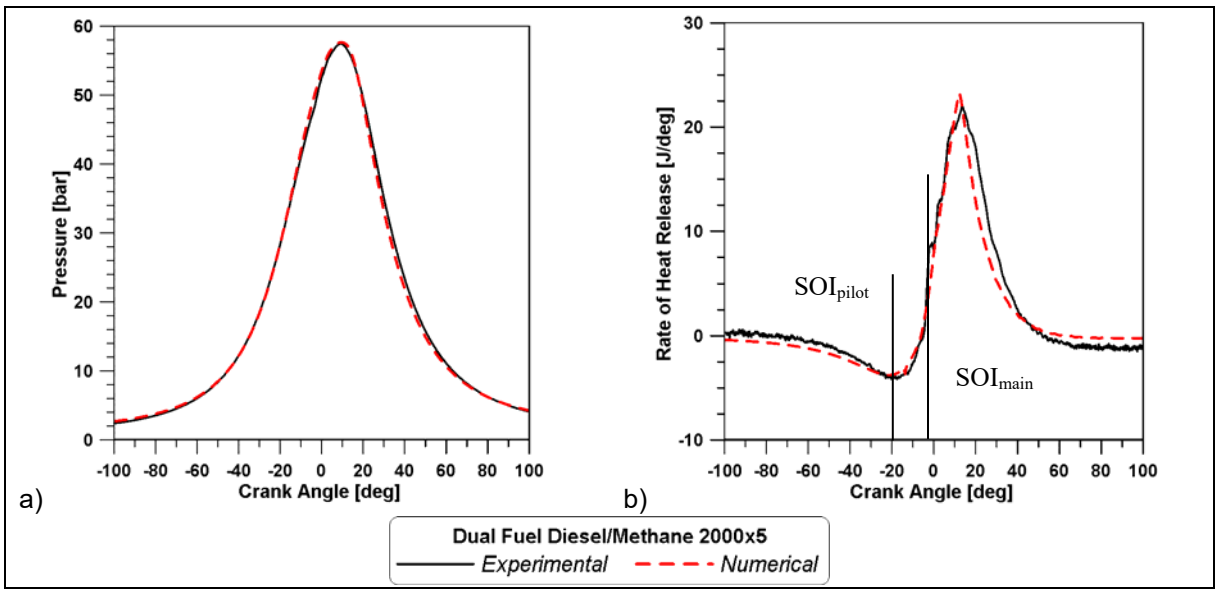

Fig. 10. Experimental and simulated pressures (a) and RoHR (b) for the DF diesel-methane 2000x5 case

The rates of heat release reveal that combustion can be divided in different parts. Firstly, heat is transferred to the cylinder walls due to the high temperature achieved by the mixture at the end of the compression phase; on the other hand, the vaporization of the injected liquid fuel produces a significant heat subtraction, as observed by the negative values of the RoHR during this phase. Secondly the low temperature reactions are activated and the RoHR starts to increase and assumes a positive value. Then three bumps can be identified: the first two combustion events after the pilot and main injections are mainly due to the diesel combustion, while the third, and largest event, is mainly due to the combustion flame through air-methane premixed mixture. Although more evident in the low engine speed cases (Figures 7(b) and 8(b)), this effect can be seen in both experimental and simulated results, thus illustrating the good model performance. Moreover, the aim to catch the general timing can be considered accomplished. Indeed, it is noted that the major contribution to combustion activation and consequently to the rising slopes of RoHR is associated with the main injection ignition. In all four cases, during this phase the two curves present a satisfying timing agreement and matching slope during the rising phase. The same consideration can be made regarding the peak related to the flame propagation. Even though the model tends to underestimate the RoHR during the compression and overestimate the RoHR during the last part of the expansion, this must be mainly attributed to the uncertainties in the heat transfer calculation during the simulation, and thus it is not due to the combustion model performance..

5.2 Diesel-hydrogen predictions

The numerical results previously illustrated are reported in Figures 11-14 together with the simulations relative to the forecasted cases using hydrogen instead of methane. The operating conditions have been already illustrated in Table 3. Figures 11-14 (a) demonstrate that in all cases the use of hydrogen causes an important enhancement of the peak pressure. A likely explanation is the well-known higher flame speed of hydrogen, that not only leads to a general fast consumption of fuel but to an anticipated increased pressure rise right after the start of pilot ignition.

All the above assumptions are confirmed by the apparent rates of heat release in Figures 11-14 (b). Differently from methane cases, where gaseous combustion was activated by the main injection ignition and three bump could be observed, the high reactivity and fast combustion of hydrogen lead to a massive oxidation process started right after diesel pilot ignition. In each case the experimental and numerical rising slopes of RoHR do not match anymore but a steeper increase is observed when hydrogen is involved. The fast consumption of gaseous fuel accelerates the whole process: a single peak of enhanced intensity is produced reducing the gaseous combustion duration. As consequence of the faster consumption of hydrogen, in all cases the expansion phase is below the corresponding one with methane.

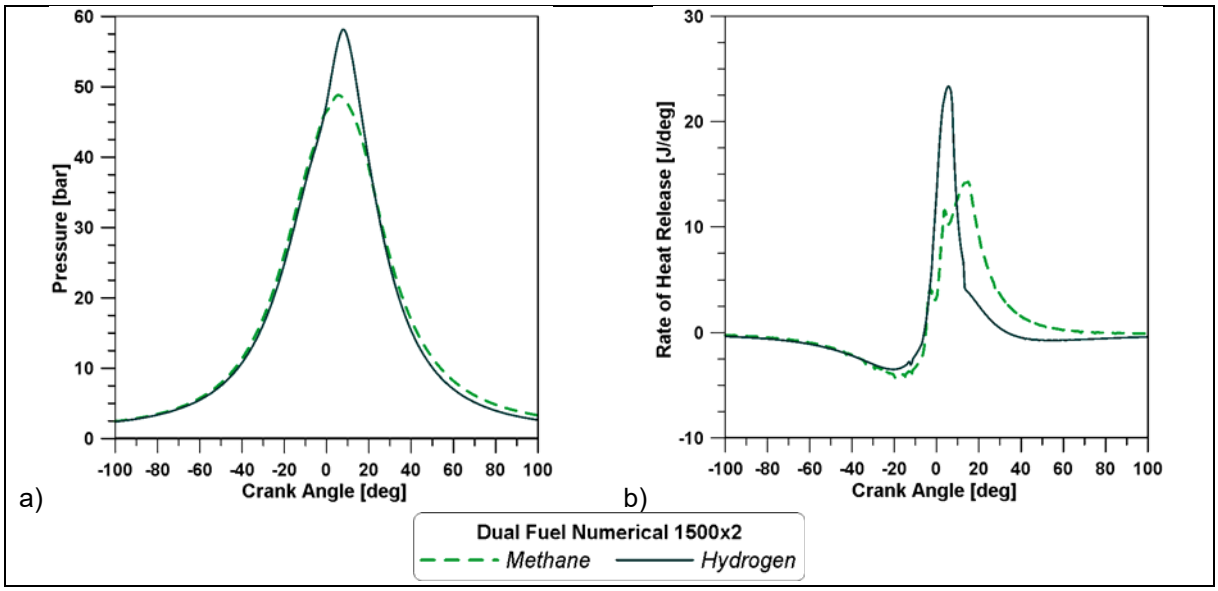

Fig. 11. Pressure (a) and Rate of heat release (b) for the DF 1500x2 numerical cases

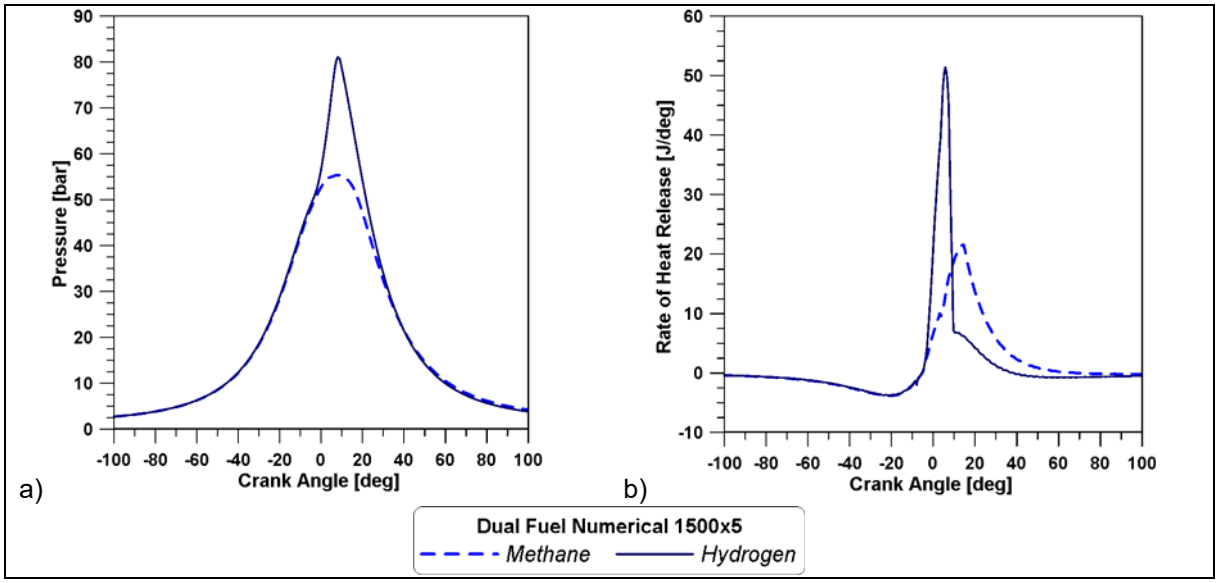

Fig. 12. Pressure (a) and Rate of heat release (b) for the DF 1500x5 numerical cases

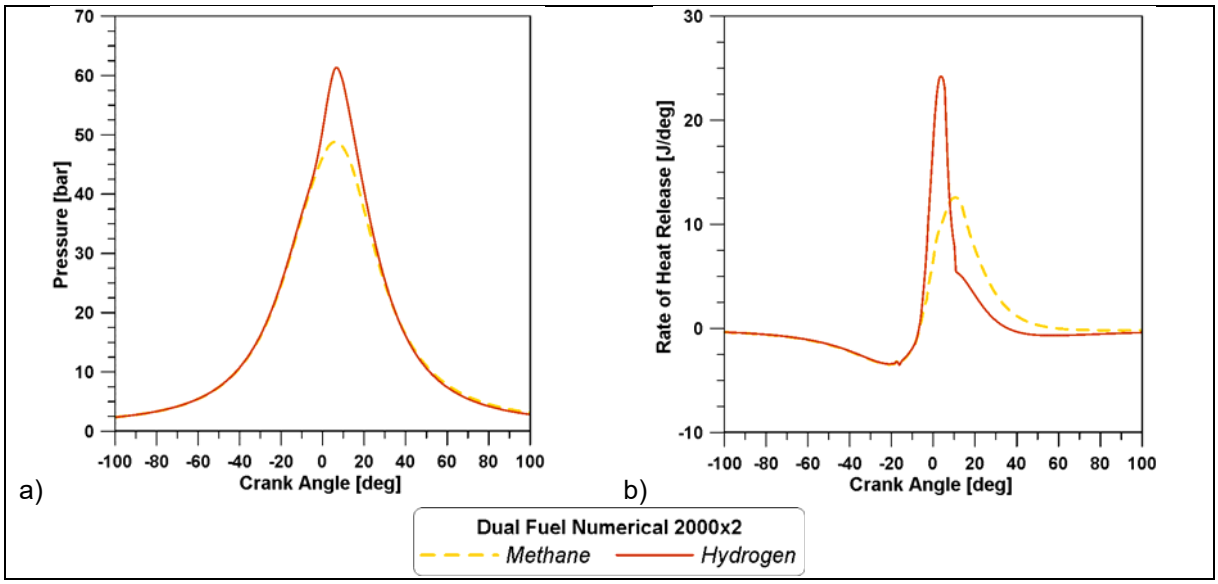

Fig. 13. Pressure (a) and Rate of heat release (b) for the DF 2000x2 numerical cases

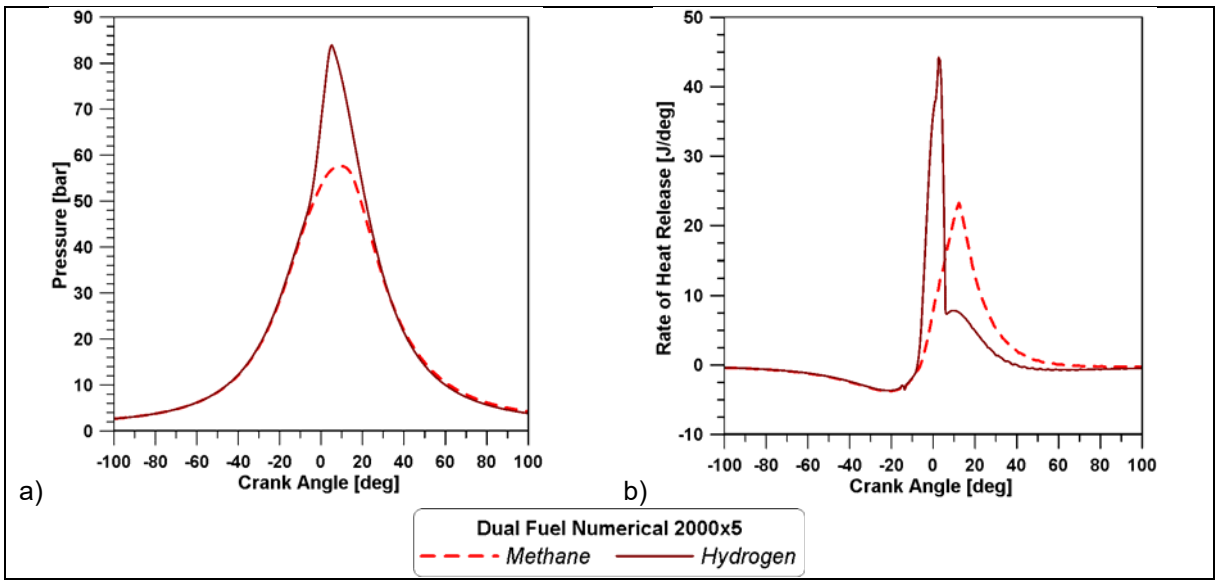

Fig. 14. Pressure (a) and Rate of heat release (b) for the DF 2000x5 numerical cases

Conclusions

In the present work, a dual-fuel combustion model was built in GT-Power, with the aim to validate a methodology for the simulation of diesel-methane combustion and to use the same methodology for the prediction of hydrogen-diesel combustion characteristics.

Initially, the model of the dual fuel engine with methane was built and the laminar flame speed model by Gülder for air-methane mixture was incorporated in the software. The validation was obtained through design of experiments and design optimizer in order to match in-cylinder pressure curves measured during an experimental campaign on an optical accessible single cylinder research engine. Experimental tests are characterized by different load levels, 2 and 5 bar of BMEP, and different engine speeds, 1500 and 2000 rpm.

Results demonstrated that the model is capable of reproducing the pressure trends for different loads and speeds. In addition, although the rates of heat release displayed significant differences in terms of intensity, the overall combustion timing showed an acceptable accordance with the measurements' elaborations.

For the simulations with hydrogen two new correlations were built and implemented in the 0D code, one of them specifically accounts for the extremely lean conditions of dual fuel engines operating conditions. Also, the numerical cases are based on an experimental campaign forecasted on the same engine supplied with hydrogen instead of methane at the same BMEP.

The model foresaw a substantial enhancement of pressure levels with the use of hydrogen. They were mainly caused by a strong enhancement of pressure rise rate due to the higher burn velocity, typical of this gaseous fuel. This consideration is also confirmed by rates of heat release, that evidenced how combustion developed in a shorter crank angle interval with respect to the diesel-methane corresponding cases. Therefore, it can be affirmed that this innovative flame model provides results consistent with the characteristics observed on hydrogen combustion.

Funding

Sushma Artham disclosed receipt of financial support for the research of this work that has been partially supported by FPI grant with reference PRE2018-084411.

References

[1] *REGULATION (EC) No 595/2009 OF THE EUROPEAN PARLIAMENT AND OF THE COUNCIL,* 18 June 2009.

[2] *REGULATION (EU) 2019/631 OF THE EUROPEAN PARLIAMENT AND OF THE COUNCIL,* 17 April 2019.

[3] J. Hu, J. Liao, Y. Hu, J. Lei, M. Zhang, J. Zhong, F. Yan and Z. Cai, "Experimental investigation on emission characteristics of non-road diesel engine equipped with integrated DOC + CDPF + SCR aftertreatment," *Fuel,* vol. 305, no. 121586, 2021, https://doi.org/10.1016/j.fuel.2021.121586.

[4] W. Lijiang and G. Peng, "A review on natural gas/diesel dual fuel combustion, emissions and performance," *Fuel Processing Technology,* no. 142, p. 264–278, 2016, http://dx.doi.org/10.1016/j.fuproc.2015.09.018.

[5] E. Mancaruso and B. M. Vaglieco, "Spectroscopic measurements of premixed combustion in diesel engine," *Fuel,* vol. 90, p. 511–520, 2011, doi:10.1016/j.fuel.2010.09.052.

[6] A. Magno, E. Mancaruso and B. M. Vaglieco, "Combustion Analysis of Dual Fuel Operation in Single Cylinder Research Engine Fuelled with Methane and Diesel," in *SAE Technical Paper 2015-24-2461*, 2015, https://doi.org/10.4271/2015-24-2461.

[7] S. Di Iorio, A. Magno, E. Mancaruso and B. M. Vaglieco, "Diesel/Methane Dual Fuel Strategy to Improve Environmental Performance of Energy Power Systems," *International Journal of Heat and Technology,* vol. 34, no. 2, pp. S581-S588, 2016, doi: https://doi.org/10.18280/ijht.34S254.

[8] E. Mancaruso, M. Todino and B. M. Vaglieco, "Study on dual fuel combustion in an optical research engine by infrared diagnostics varying methane quantity and engine speed," *Applied*

Thermal Engineering, vol. 178, no. https://doi.org/10.1016/j.applthermaleng.2020.115623, 2020, https://doi.org/10.1016/j.applthermaleng.2020.115623.

[9] E. Mancaruso, L. Sequino, B. M. Vaglieco, M. C. Cameretti, R. De Robbio and R. Tuccillo, “CFD Analysis of the Combustion Process in Dual-Fuel Diesel Engine,” in *SAE Technical Paper 2018-01-0257*, 2018, doi:10.4271/2018-01-0257.

[10] R. De Robbio, M. C. Cameretti, E. T. R. Mancaruso and B. M. Vaglieco, “CFD Study and Experimental Validation of a Dual Fuel Engine: Effect of Engine Speed,” *Energies,* vol. 14, no. 4307, 2021, https://doi.org/10.3390/en14144307.

[11] R. De Robbio, M. C. Cameretti, E. Mancaruso, R. Tuccillo and B. M. Vaglieco, “Combined CFD - Experimental Analysis of the In-Cylinder Combustion Phenomena in a Dual Fuel Optical Compression Ignition Engine,” in *SAE Technical Paper 2021-24-0012*, 2021, doi:10.4271/2021-24-0012.

[12] R. Amirante, E. Distaso, P. Tamburrano and R. D. Reitz, “Laminar flame speed correlations for methane, ethane, propane and their mixtures, and natural gas and gasoline for spark-ignition engine simulations,” *International Journal of Engine Research,* vol. 18, no. 9, p. 951–970, 2017, doi: 10.1177/1468087417720018.

[13] J. B. Heywood, Internal Combustion Engine Fundamentals., 1988.

[14] M. Metghalchi, “Burning Velocities of Mixtures of Air with Methanol, Isooctane, and Indolene at High Pressure and Temperature,” *Combustion and Flame,* vol. 48, pp. 191-210, 1982.

[15] Ö. Gülder, “Turbulent Premixed Flame Propagation Models for Different Combus-tion Regimes,” in *Syposium on Combustion*, 1990.

[16] Ö. Gülder, “Correlations of Laminar Combustion Data for Alternative S.I. Engine Fuels,” in *SAE Technical Paper 841000, doi:https://doi.org/10.4271/841000*, 1984.

[17] F. Millo, F. Accurso, A. Piano, G. C. A. Caputo and J. Hyvonen, “Experimental and numerical investigation of the ignition process in a large bore dual fuel engine,” *Fuel,* vol. 290, no. 120073, 2021, https://doi.org/10.1016/j.fuel.2020.120073.

[18] J. Monsalve-Serrano, G. Belgiorno, G. Di Blasio and M. Guzmán-Mendoza, “1D Simulation and Experimental Analysis on the Effects of the Injection Parameters in Methane–Diesel Dual-Fuel Combustion,” *Energies,* vol. 13, no. 3734, 2020, doi:10.3390/en13143734.

[19] C. White, R. Steeper and A. Lutz, “The hydrogen-fueled internal combustion engine: a technical review,” *International Journal of Hydrogen Energy,* vol. 31, pp. 1292-1305, 2006, doi:10.1016/j.ijhydene.2005.12.001.

[20] S. Ravi and E. L. Petersen, “Laminar flame speed correlations for pure-hydrogen and high-hydrogen content syngas blends with various diluents,” *International Journal of Hydrogen Energy,* vol. 37, pp. 19177-19189, 2012, http://dx.doi.org/10.1016/j.ijhydene.2012.09.086.

[21] T. Miyamoto, H. Hasegawa, M. Mikami, N. Kojima, H. Kabashima and Y. Urata, “Effect of hydrogen addition to intake gas on combustion and exhaust emission characteristics of a diesel engine,” *International Journal of Hydrogen Energy,* vol. 36, pp. 13138-13149, 2011, doi:10.1016/j.ijhydene.2011.06.144.

[22] O. Ghazal, “Performance and combustion characteristic of CI engine fueled with hydrogen enriched diesel,” *International Journal of Hydrogen Energy,* vol. 38, pp. 15469-15476, 2013, http://dx.doi.org/10.1016/j.ijhydene.2013.09.037.

[23] V. Chintala and K. Subramanian, “A comprehensive review on utilization of hydrogen in a compression ignition engine under dual fuel mode,” *Renewable and Sustainable Energy Reviews,* vol. 70, p. 472–491, 2017, http://dx.doi.org/10.1016/j.rser.2016.11.247.

[24] O. Ghazal, “Combustion analysis of hydrogen-diesel dual fuel engine with water injection technique,” *Case Studies in Thermal Engineering,* vol. 13, no. 100380, 2019, https://doi.org/10.1016/j.csite.2018.100380.

[25] S. Taylor, “Burning Velocity and the Influence of Flame Stretch,” PhD Thesis, University of Leeds, 1991.

[26] N. Marinov, C. Westbrook and W. Pitz, “Detailed and Global Chemical Kinetics Model for Hydrogen,” in *8th International Symposium on Transport Properties*, San Fancisco, CA, 1995.

Analysis of the energy balance during WLTC in warmed and cold conditions using a Virtual Engine

Pablo Olmeda, Jaime Martín*, Francisco J. Arnau and Sushma Artham

Abstract

In recent years, the interest on transient operation and real driving emissions have increased because of the global concern about environmental pollution that has led to new emissions regulation and new standard testing cycles. In this framework, it is mandatory to focus the engines research on the transient operation, where a Virtual Engine has been used to perform the Global Energy Balance (GEB) of a 1.6 L Diesel engine during a World harmonized Light vehicles Test Cycle (WLTC). Thus, the energy repartition of the chemical energy has been described with warmed engine and cold start conditions, analyzing in detail the mechanisms affecting the engine consumption. The fist analysis focusses on the "delay" effect affecting the instantaneous energy balance due to the time lag between the in-cylinder processes and pipes: as main conclusion it is obtained that it leads to an apparent unbalance than can reach more than 10% of the cumulated fuel energy at the beginning of the cycle, becoming later negligible. Energy split analysis in cold starting WLTC shows that in this conditions the energy accumulation in the block is a key term at the beginning (about 50%) that diminishes its weight until about 10% at the end of the cycle. In warmed conditions energy accumulation is negligible but the heat transfer to coolant and oil are higher than in cold starting (21% vs 28%). The lower values of the mean brake efficiency at the beginning of the WLTCs (only about 20%), is affected, especially in cold starting, by the higher mechanical losses due to the higher oil viscosity, and the heat rejection from the gases. The friction plays an important role only during the first half of the cycle, with a percentage of about 65% of the total mechanical losses and 10% of the total fuel energy at the end of the WLTCs. However, at the end of the cycle it does not affect dramatically the mean brake efficiency which is about 31% both in cold starting and warmed WLTC.

Keywords
Transient, Global Energy Balance, Virtual Engine, WLTC

Corresponding author:
Martín Díaz Jaime, CMT-Motores Térmicos, Universitat Politècnica de València, Camino de Vera s/n. 46022 València, Spain, www.cmt.upv.es, Tel: +34963877650, fax: +34963877659
Email: jaimardi@mot.upv.es

Nomenclature

DI	Direct Ignition
ECU	Engine control unit
EGR	Exhaust gas recirculation
GEB	Global Energy Balance
HPEGR	High pressure exhaust gas recirculation
HSDI	High speed direct injection
ICE	Internal combustion engines
IMEP	Indicated mean effective pressure
LPEGR	Low pressure exhaust gas recirculation
1D	One-dimensional
VEMOD	Virtual Engine Model
WLTC	World harmonized light vehicles test cycle
WLTP	World harmonized light vehicles test procedure
0D	Zero-dimensional

Introduction

Current internal combustion engines (ICE) has to overcome several problems and demands, one of the most important challenges include the improvement of fuel economy without compromising the engine performance, along with reduced engine emissions at wide range of operating conditions. Thus, automotive manufacturers are facing many challenges to meet government regulations while satisfying the demands of the consumer on outstanding performance, high fuel economy and low cost by means of a number of different approaches. It should also be noticed that even though during the last decades ICEs have been forced to an impressive reduction in pollutant emissions of around 95% in European emission regulations (Euro 1–6), the restrictions to the emissions and consumption will continue in the next years. In this scenario, even though new power plants are being explored for transport applications, the ICE is estimated to continue being the main power plant during the next decades both as main power plant (specially for middle size and large engines) or as part of hybrid power plants in smaller vehicles.

Some years ago, the trend for studying internal combustion engines operation was focused on the steady-state performance, with low attention paid to the transient operation. However, the most of new driving cycles involves transient conditions and it is not usual running at stationary conditions in real-world engine operation [1]. Moreover, transient engine operation contributes much more to the total amount of emissions over a driving cycle than steady-state engine operation [2].

In recent years, the interest on transient operation and real driving emissions have increased because of the global concern about environmental pollution that has led to important changes in the regulation. The increasingly rigorous regulation on pollutants and CO2 emissions have led to the World harmonized Light vehicles Test Procedure (WLTP) [3], which came into force in September 2017 in Euro 6d-Temp, which has more

realistic testing conditions including extended ambient temperature ranges covering low temperature conditions[4]. This WLTC is forcing the automotive industry to optimize different technologies such as engine rightsizing, turbocharging, direct injection, flexible valve actuation or after-treatment systems that are standard solution for emissions reduction and fuel economy improvement of passenger cars and light-duty trucks [4,5].

When facing the engine behavior in a WLTC, the ambient and fluid (coolant and oil) temperatures are important because they will affect heat rejection and in-cylinder conditions, thus affecting combustion and emissions formation and mechanical losses [6]. Moreover, when changing the fluids temperatures the engine calibration change the settings in order to adapt the engine performance. As an example, when in cold start friction increases due to the higher oil viscosity, the fuel mass injected need to be increased and hence the air management settings also change. Heat transfer in the chamber is higher at cold start due to the low fluid and wall temperatures. Regarding emissions, in the cold start, CO are higher compared to warmed operation and NOx emissions, which are very dependent on temperature, are expected to gradually increase [1], when engine temperature increases. Also, the thermal state of the engine is going to be an issue when dealing with the after-treatment performance because the chemical reactions in this elements requires reaching an activation temperature.

Since understanding and assessing different technologies in transient operation has became a key issue to face emissions formation and consumption, experimental and simulation methodologies in this field have increased their importance. In order to evaluate the benefits of a specific engine strategy, performing a Global Energy Balance (GEB) [7,8] is a useful methodology to identify the paths followed by the chemical energy, thus contributing to understand the mechanism affecting the engine consumption. The identification of the energy repartition allows determining the effect of different processes inherent to ICE operation such as cooling, lubricating, fuel injection and air management. Some works dealing with experimental GEB can be found in the literature [9–11]. They are performed to assess the effect of fuels blends [12] and alternative fuels [10] or the heat transfer variation by insulating the combustion chamber walls [13] or to analyze the engine operating conditions in the energy repartition [14,15]. Generally, the energy balance is carried out by considering the brake power, mechanical losses and the exhaust gas energy. It can be performed in a more detail way by considering the heat transfers in the coolant and oil [14]. The terms that account for energy losses with minor impact such as un-burned fuel, heat rejection to the ambient and blow-by enthalpy [13] use to be neglected.

Transient operation is characterized by quick changes in the operating conditions, which can be particularly demanding in terms of engine response and control that requires specific simulation analysis to improve and accelerate the engine development. In this framework, the use of 0D/1D tools to simulate the complete engine behavior (system modeling) has shown to be really useful. The theoretical modeling is a useful way to predict trends and allows simulating multiple engine configurations at a lower cost than the experimental work, thus providing guidelines for further engine improvement. Few works dealing with the complete simulation of the engine energy balance can be found in the literature; the available ones show different points of view that can range from performing the analysis on the combustion chamber [16,17], simulating the heat transfer at

different engine sub-systems [18] or focusing in specific process such as engine cooling [19]. However, the complex phenomena involved in real operation makes difficult to face accurately the simulation of the complete system. For this reason, it is usual to combine simulation with experimental information. An example of a through and integral analysis of the energy balance combining experimental and simulated information was provided in a previous work [20].

However, all the works described are focused on the engine operation in stationary conditions. In fact, there is a lack of works dealing with the GEB in transient operation and only a limited number can be found in the literature [21]. As an example, Romero et al [21] performed the thermal balance of a Diesel engine under transient conditions, exploring the instantaneous energy split during real driving conditions, with the objective of showing the dynamics of energy split, and providing an estimate of the energy losses averaged along the cycle.

To fill this gap, this work is aimed at analyzing the energy balance in transient operation with different fluid temperatures. Thus the study will focus on the WLTC analysis in a 1.6 L diesel engine with two initial conditions: warmed engine and cold start (with an initial temperature of 20ºC). The methodology followed will be basically based on the use of a 0D-1D modelling tool called VEMOD [4] that is previously calibrated in stationary conditions and will be validated in the WLTC by comparing some key variables to characterize the thermal behavior of the engine. Once the model is validated, a complete discussion of the energy split will be provided, using the tool to calculate the different terms that can hardly be obtained experimentally. The discussion includes the comparison of the energy split at cold conditions with warmed conditions.

Experimental and modeling tools

Experimental tool

In order to reproduce the repartition of the energy at each sub-system in realistic operating conditions, the research was carried out in a multi-cylinder, HSDI Diesel engine. The engine is a 1.6L four-stroke engine compliant with Euro 5 emissions regulations. The specifications of the engine can be found in Table 1. The engine includes an electro valve that blocks coolant flow through the engine block during engine warming, which reduces the warm-up time. The intake air to the cylinders is cooled by air-water heat exchangers [4].

The test cell as shown in Figure 1, is fully equipped to measure main operation mean variables (e.g. air and fuel mass flows, temperature and pressure at intake and exhaust lines, etc.), some liquids .), oil and coolant temperatures, coolant mass flows and in-cylinder pressures in the four cylinders. It includes a Horiba MEXA exhaust gas analyzer along with an AVL439 Opacimeter. Table 2 summarizes the relevant instrumentation used for this study. Mean variables were acquired at a frequency of 10Hz with Horiba Stars test automation system, while instantaneous signals were measured at 0.5°.

The stationary tests for calibration were performed at 26 operating points with low to high engine speed (850 rpm to 4000 rpm) and from low to high load (idle to full load).

Table 1. Engine specifications

Type	HSDI Diesel engine
Displacement	1598 cm³
Bore	80 mm
Stroke	79.5 mm
Compression ratio	14.5:1
Number of valves	4 / cylinder
Number of cylinders	4
Air management	VGT, HP-EGR, LP-EGR
Maximum power @ speed	96 kW @ 4000 rpm
Maximum torque @ speed	320 Nm @ 1750 rpm

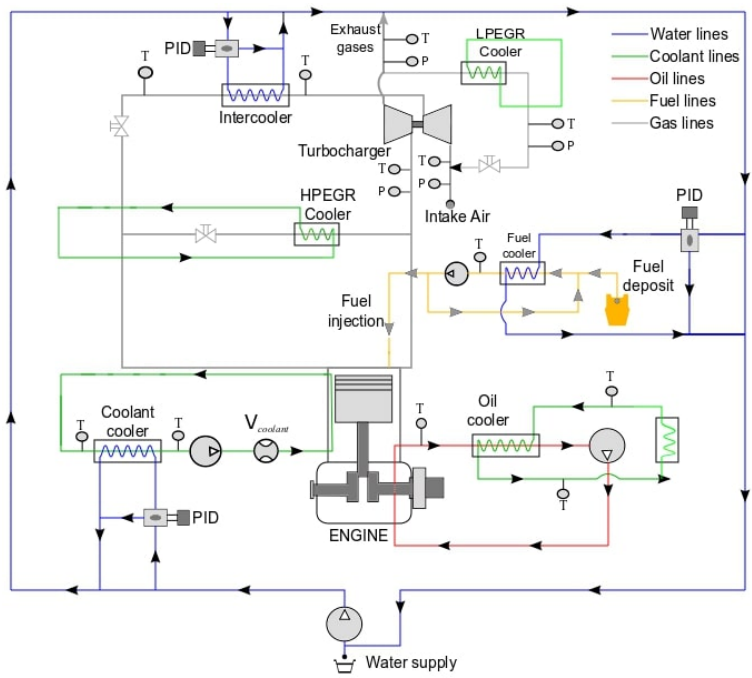

Figure 1. Test cell scheme

Table 2. Test cell instrumentation

Variable	Instrument	Range	Accuracy
Crank angle	Encoder	0-360°	±0.02º
Torque	Dynamometer	0-400 Nm	±0.5 Nm
Gas/wall temperature	k-type thermocouple	70-1520 K	±2 K
Air mass flow	Sensyflow DN80	0-1700 kg/h	±2 %
Coolant flow	Krohne 4010 Optiflux	4.5-90 L/min	±0.5 %
Oil pressure	Piezoresistive transducer	0-10 bar	±25 mbar
In-cylinder pressure	AVL GH13P	0-200 bar	Linearity 0.3%

Some of them were measured at low temperature cold conditions (-7°C). They cover a wide range of the engine map and testing points belonging to the WLTC as shown in Table 3. Engine operating parameters were set according to the calibration included in the engine control unit (ECU).

Table 3. Stationary tests performed

Engine speed in rpm	Load in %
1000	Motoring
2000	Motoring
3000	Motoring
4000	Motoring
850	idle
1000	21, 44, 66, 88
1250	13, 26, 50, 76, 100
1500	11, 25*, 50, 75*, 100
2500	25, 50, 75, 100
3500	25*, 50, 75, 100

* Both conventional and Cold ambient conditions (-7°C)

Table 4. Initial temperatures in the WLTC tests performed

Test conditions	Room temperature	Initial block temperature	Initial Coolant temperature	Initial Oil temperature
Cold start	20°C	20°C	20°C	20°C
Warmed start	20°C	≈ 80°C	≈ 80°C	≈ 85°C

The transient analysis is performed in two WLTC tests, measured with warmed engine and cold start conditions(starting at 20°C). Table 4 summarizes the different engine

temperatures at these conditions at the beginning of the test. Three repetitions of each WLTC and stationary point were measured.

Predictive tool

The Virtual Engine Model (VEMOD)[4] is a standalone tool aimed at simulating new standard testing cycles. This computational tool was developed as a response to limiting requirements of new standards, closer to real-world driving conditions. VEMOD is able to predict engine performance and emissions along with the complete thermo and fluid dynamic condition in the different fluid circuits including gas and liquids (coolant and oil). It covers the calculation of different processes as shown in Figure 2. Various sub-models are used to obtain heat rejection to chamber walls, brake power, perform calculations of flow properties, prediction of various emissions, in-cylinder conditions based on combustion process, heat transfer and wall temperatures. The core of VEMOD is the combustion model, a 1D model based on the concept of Apparent Combustion Time (ACT)[22,23], which provides VEMOD with the capacity of predicting heat release rate and emissions through the calculation of local conditions in the combustion chamber. It is an upgraded version of a combustion model developed at the research group [24]. The whole set of sub-models, marked with a blue box in Figure 2, make up the engine model. The red boxes in Figure 2 represent the different control sub-models, which have been developed in Matlab/Simulink[4].

VEMOD will be used to model the different energy terms to complete the energy balance of the system.

Combustion diagnosis tool

A combustion diagnosis tool called CALMEC [7,25], developed at CMT-Motores Térmicos was used to calculate the heat release and to calibrate the in-cylinder heat transfer in VEMOD[25–27], based on the experimental measurements in stationary conditions.

Methodology

The scheme of the methodology followed is shown in Figure 3. It was structured as follows:

1. The stationary and WLTC transient tests were conducted in the installation described in the experimental tool section. The parameters required for analyzing were measured as described.

2. Calibration of the combustion and emission sub-models, in-cylinder heat transfer and mechanical losses were carried out using the set of stationary points and the characterization methodology described by Benajes et al [26].

3. The VEMOD validation in transient test is performed using experimental data of the evolution of fluid temperatures and brake torque.

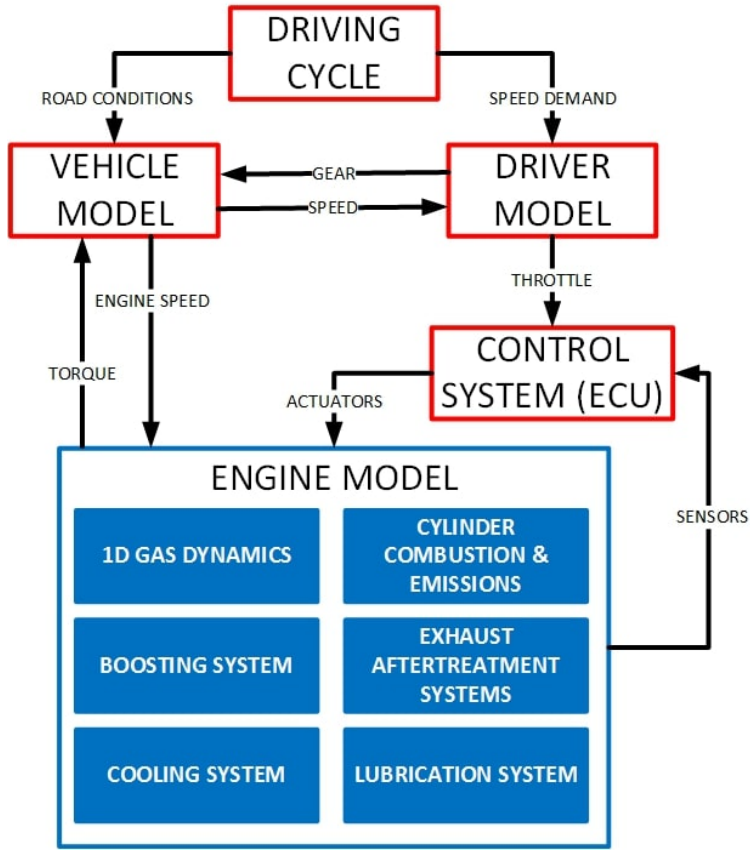

Figure 2. Flow-chart of Virtual Engine Model (VEMOD) modules

4. An extensive analysis of the energy repartition was carried out to assess the effect of different variables on the Global Energy Balance and engine performance. GEB during WLTC was obtained at different thermal conditions, using some experimental data to set target conditions during simulation, as detailed below.

The above mentioned methodology allows achieving the objective of analyzing the GEB in transient tests at different thermal conditions.

For the calculation of both stationary points and the WLTC, the experimental values of air mass flow, fuel mass, fuel rail pressure, engine speed, injection settings and boost pressure were set as targets or directly imposed at every instant.

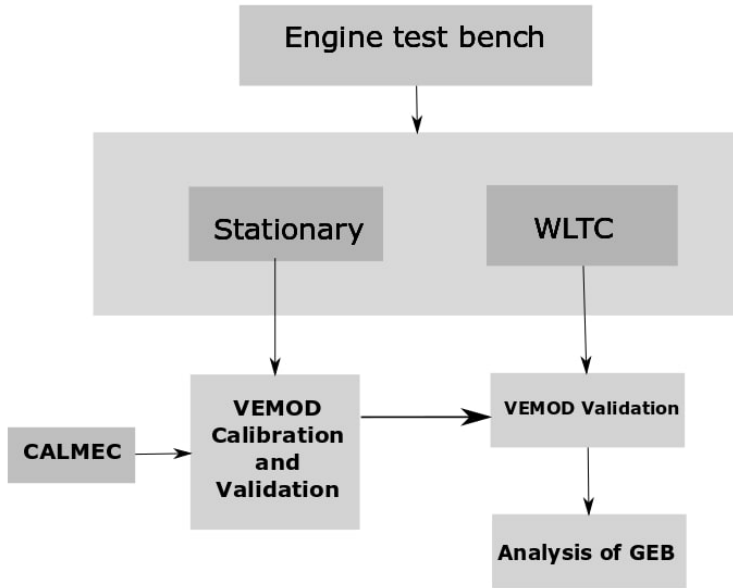

Figure 3. Methodology

Global Energy Balance (GEB) description

The basis of the analysis is the first law of thermodynamics. There must be an energy balance between engine input (mainly fuel chemical power) and output. Different paths followed by energy terms and energy distribution are represented in Figure 4. Where, all the energy transformations taking place in a diesel engine, are taken into account [7,8,20,28].

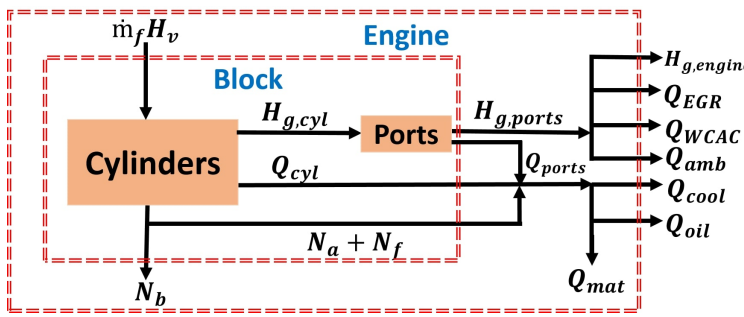

Figure 4. Energy distribution

The energy flows entering the engine are the sensible enthalpy of air, $\dot{m}_a h_a^{sens}$, the sensible enthalpy of fuel, $\dot{m}_f h_f^{sens}$ and the chemical energy of the fuel with its heating

value $\dot{m}_f H_v$. The outlet energy flows are the brake power, N_b, the heat flow to the coolant, $\dot{Q}_{cool}$, the flow of sensible enthalpies of the exhaust gases $\dot{m}_{exh} h_{exh}$, the heat rejection to oil, $\dot{Q}_{oil}$ (which at the end will be rejected to coolant in the oil exchanger), the heat cumulated in the engine structure, $\dot{Q}_{mat}$, the heat rejection in the intercooler, $\dot{Q}_{WCAC}$, the heat rejection in the EGR heat exchangers, $\dot{Q}_{LPEGR}$ and $\dot{Q}_{HPEGR}$ (for the sake of rigor there is not a heat exchanger for the HPEGR but the block itself acts as a cooler when the HPEGR passes through it), which are also considered explicitely even though they are finally cooled by the engine coolant, the heat from the external walls of the engine to the ambient, considered through the heat rejection in the pipes, $\dot{Q}_{pipes}$ and turbo case, $\dot{Q}_{turbo-amb}$ and finally, the enthalpy flow of blow-by losses, H_{bb} [7,8,28].

In order to perform the detailed analysis of energy repartition, some energy terms are rearranged and the first law of thermodynamics can be expressed as:

$$\begin{aligned}\dot{m}_f H_v =& N_b + N_a + H_{exh} + \dot{Q}_{cool} + \dot{Q}_{oil} + \dot{Q}_{mat} + \dot{Q}_{WCAC} + \dot{Q}_{HPEGR} \\ &+ \dot{Q}_{LPEGR} + \dot{Q}_{pipes} + H_{bb} + \dot{Q}_{turbo-amb}\end{aligned} \tag{1}$$

The description of the terms and how they are determined in the GEB analysis is the following:

- $\dot{m}_f H_v$ is the chemical power of the fuel. It is determined from the measurement of fuel mass flow $\dot{m}_f$(which is imposed in VEMOD) and its heating value, H_v. The heating value of diesel fuel used in this work is 42.92 MJ/kg.

- N_b is the brake power is determined by VEMOD, by subtracting mechanical losses from indicated power.

- N_a is power to run the auxiliaries elements that is determined in VEMOD with the models of the fuel, coolant and oil pumps [29].

- H_{exh} is the net flow of the gases sensible enthalpy determined through balance between incoming and outgoing enthalpy flows.

$$H_{exh} \simeq \dot{m}_{exh} h_{exh}^{sens} - \dot{m}_a h_a^{sens} - \dot{m}_f h_f^{sens} \tag{2}$$

$$\dot{m}_{exh} = \dot{m}_a + \dot{m}_f + \dot{m}_{bb} \tag{3}$$

  where $\dot{m}_a$, $\dot{m}_f$, $\dot{m}_{bb}$ and $\dot{m}_{exh}$ are the intake air, injected fuel, blow by flow rate and exhaust mass flow rates. h_a^{sens}, h_{fuel}^{sens}, h_{exh}^{sens} are the specific sensible enthalpies of air, fuel and exhaust gases, determined from the corresponding specific heats.

- H_{bb} is the net flow of blow-by sensible enthalpy. It is determined by the balance between incoming and outgoing blow-by enthalpy flows. The final expression for

net flow of blow-by sensible enthalpy is:

$$H_{bb} = \dot{m}_{bb} h_{bb}^{exh} - \dot{m}_a^{bb} h_a^{sens} - \dot{m}_f^{bb} h_f^{sens} \tag{4}$$

where $\dot{m}_{bb}$ is the mass flow leakage due to blow-by. h_{bb}^{exh}, h_a^{sens}, h_f^{sens} are the sensible enthalpies corresponding to blow.by leakage, fresh air and fuel.

- $\dot{Q}_{cool}$ is the total heat transfer to the coolant that is obtained by means of a lumped conductance model[30,31]. It is mainly due to the heat transfer from the chamber, but the engine coolant refrigerates the complete engine block, which also includes heat transfer from engine ports, $\dot{Q}_{ports}$. As commented, specific terms for oil heat rejection and EGR are independently considered.
- $\dot{Q}_{oil}$ is the heat rejection to the oil in the engine block and turbocharger. As in case of $\dot{Q}_{cool}$, it is obtained by means of two lumped conductance models, the first considers the engine block and second the turbo[30]. It is mainly due to the heat rejection from the chamber to piston, but also friction and in lower extent turbo cooling has a relevant role.
- $\dot{Q}_{mat}$ is the heat cumulated in engine structure during the transient evolution. It is obtained in VEMOD taking into account the thermal capacity of the whole engine structure.
- $\dot{Q}_{WCAC}$ is the heat rejection in the intercooler. It is determined from the air mass flow and its temperature variation.

$$\dot{Q}_{WCAC} = \dot{m}_{wcac} c_{p,a} (T_{a,out} - T_{a,in}) \tag{5}$$

where $T_{a,in}$ and $T_{a,out}$ are the temperatures at inlet and outlet of the intercooler, and $c_{p,a}$ is the specific heat of the air.

- $\dot{Q}_{HPEGR}$ and $\dot{Q}_{LPEGR}$ are the heat transfers in the high pressure and low presure EGR heat exchangers. They are obtained in VEMOD using the following expression and difference of temperatures of the fluid at the inlet and outlet of the heat exchanger.

$$\dot{Q}_{EGR} = \dot{m}_{EGR} c_{p,EGR} (T_{EGR,out} - T_{EGR,in}) \tag{6}$$

where $\dot{m}_{EGR}$ is the EGR mass flow, $T_{EGR,in}$ and $T_{EGR,out}$ are the temperatures at inlet and outlet of the exchanger, and $c_{p,EGR}$ is the specific heat of the fluid.

- $\dot{Q}_{turbo-amb}$ is the heat rejected from turbocharger to ambient. It is determined in VEMOD using a lumped conductance model in which the ambient is a node used as boundary conditions [30,31].
- $\dot{Q}_{pipes}$ is the heat rejection to the ambient in the pipes. It is obtained with the help of simple lumped model, considering gas inside the pipes and ambient air as boundary conditions.

Model calibration and validation

Calibration in stationary conditions

In order to proceed with the analysis of energy balance, the calibration of the Virtual Engine, VEMOD, was previously performed. The calibration includes the determination of the fitting constants of different sub-models of VEMOD. Thus, it is necessary to determine the calibration constants of the heat transfer, combustion and mechanical losses models. Moreover, it is also necessary to accurately determine some engine characteristics such as the static and dynamic compression ratios (VEMOD includes a simple deformation model). The calibration was performed using motoring and combustion tests in stationary conditions as detailed in Table 3.

Motoring test was used to adjust engine uncertainties and to perform an initial convective heat transfer tuning [26]. Later, the warm and cold test indicated in Table 3, covering the complete engine map, were used for commissioning the rest of sub-models.

In short, the tool calibration includes the following points:

- Real compression ratio, deformations model and in-cylinder heat transfer model calibration was performed by means of an in house developed methodology in which a combination of experimental and simulated in-cylinder cycles are used. The complete description can be found in [26]. The heat transfer model refinement method is described in [28].

- The injector model was calibrated with a complete experimental matrix in an injector test rig. The calibration of the injection rate model was carried out following the methodology detailed in [32].

- The combustion model calibration was performed after the heat transfer model calibration, which affects the experimental heat release (main input for the combustion model). The calibration of the combustion model includes the determination of the different constants of the three sub-models: ignition delay, premixed and diffusion sub-models. The criterion for the determination of the models constant was to minimize the difference between the experimental heat release and the simulated one.

- Even though out of the scope of this work, aftertreatment models were calibrated (and validated) in stand-alone executions. The detailed description of the complete process and the experimental condition used for the calibration can be found at [33].

- The friction model calibration, aimed at obtaining an accurate prediction of the brake efficiency, was performed with stationary operating points in the complete engine map both at cold and warm conditions. The methodology is described at [34].

Following, some key results that allow characterizing the model performance are shown.

Figure 5 shows the experimental and modeled in-cylinder pressure and heat release at engine speed of 2500 rpm at different loads (25%, 50%, 75% and 100%). The dotted

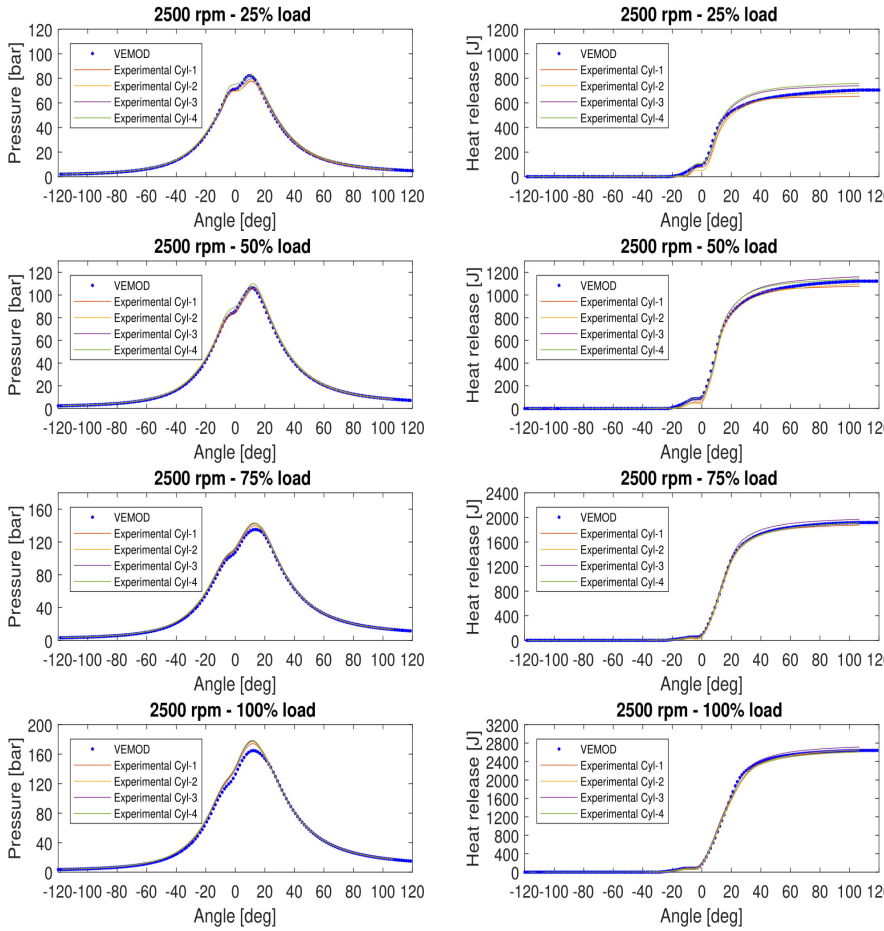

Figure 5. In-cylinder pressure and Heat release at different loads in stationary

lines represent the modeled values of VEMOD for one cylinder (no relevant dispersion between cylinders exists) and the solid lines represent the experimental values of the four cylinders. As it can be seen, the pressure and heat release evolutions are quite well predicted even though it can be identified a slight trend to underestimate the combustion velocity, especially at high load conditions. Also an overestimation of the blow-by in these conditions high loads contribute to underestimate the pressure peak. In any case, the global performance is good with slight uncertainty.

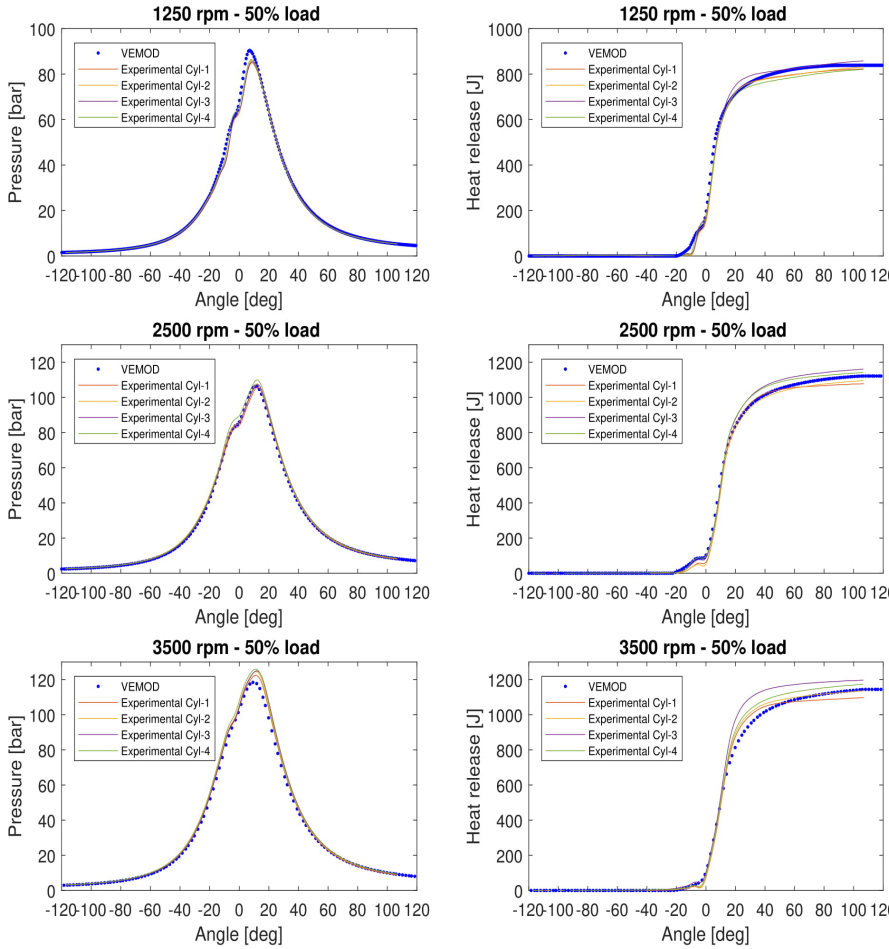

Figure 6. Pressure and Heat release at different speeds at 50% load in stationary

Figure 6 represents the pressure and heat release at engine speeds of 1250 rpm, 2500 rpm and 3500 rpm and 50% load. As it can be seen, the modeled results shows a good global agreement with experimental data. However, the modeled heat release are slightly lower than the experimental ones at high speed and load, even though at the end, the simulated heat release is in the range of experimental dispersion. The reason for the slightly poorer performance at high speed and load is due to the fact that the priority was put on the low-mid ranges because they are critical for the test cycle simulation,

main objective of the work. In any case, as shown in the next paragraph, if the analysis is extended to other key outputs, global performance of the model is good.

It has to be highlighted that, due to the physical approach of the tool, no correction or lookup table is used in any sub-model to take into account specific characteristic of the operating conditions.

Figure 7, Figure 8 and Figure 9 represents the IMEP, turbine inlet temperature and coolant temperature for all the selected points in steady-state at various engine speeds and loads. In the case of IMEP, the mean relative error is about 2%, for turbine inlet temperature the mean relative error is 1.5% and in the case of coolant temperature, the mean relative error is 0.5%.

For the sake of brevity, other variables that will be later shown in transient, have been omitted, but their global performance is similar to the shown variables, thus brake mean error is 4.5%, turbine outlet temperature is 2.5% and oil temperature is 1.5%.

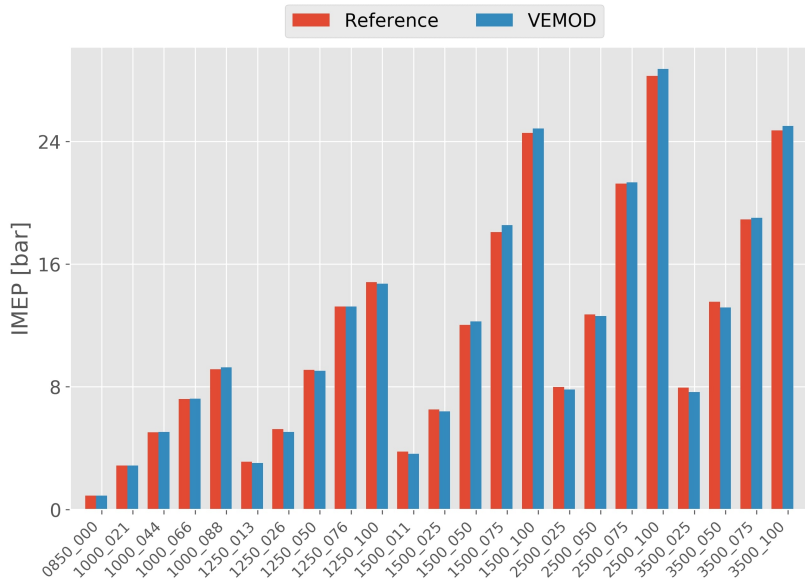

Figure 7. IMEP at different speeds and load in stationary conditions

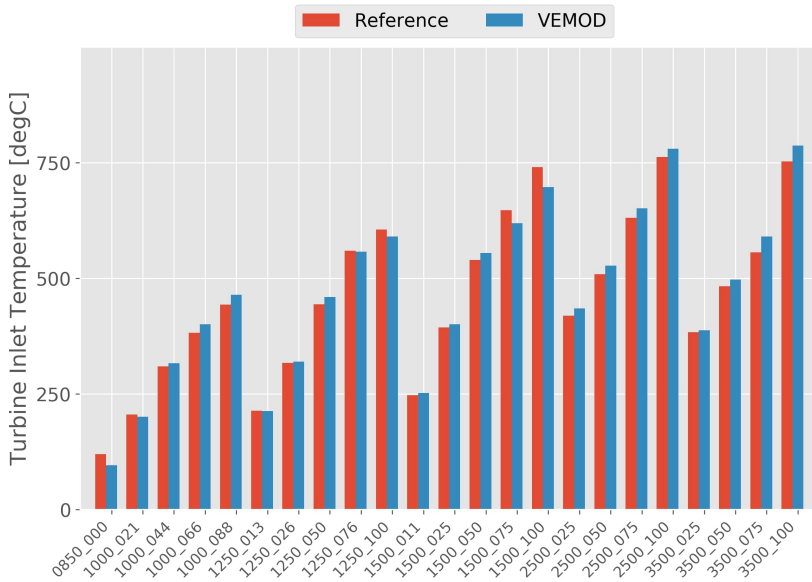

Figure 8. Turbine inlet temperature at different speeds and load in stationary conditions

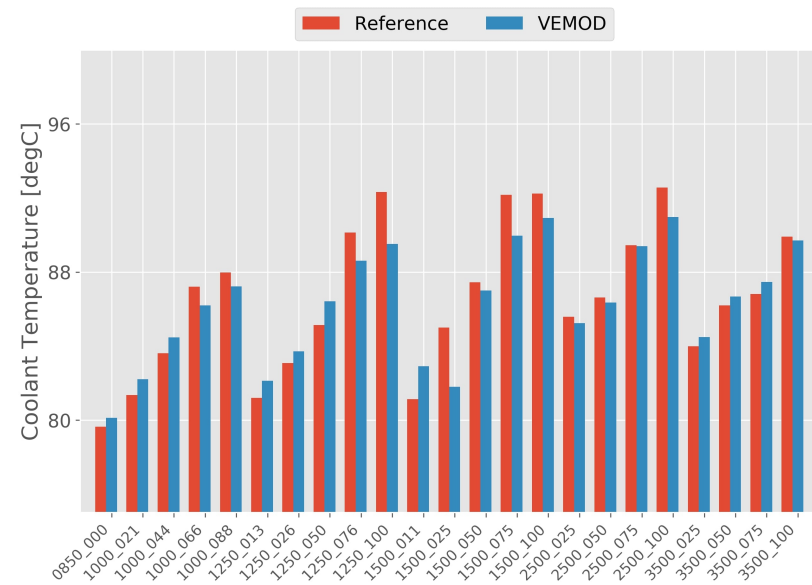

Figure 9. Coolant temperature at different speeds and load in stationary conditions

Transient validation

Before facing the energy balance in transient operation it is necessary to ensure the good performance of the model, also in this conditions. For this purpose the experimental speed, injection settings, air demand and boost pressure are set as targets for the control system during the WLTC. The performance is validated with the different variables but the four most relevant will be shown: torque, turbine outlet temperature, coolant and oil temperatures. In order to facilitate the comprehension, the engine speed and load during the WLTC is shown in Figure 10.

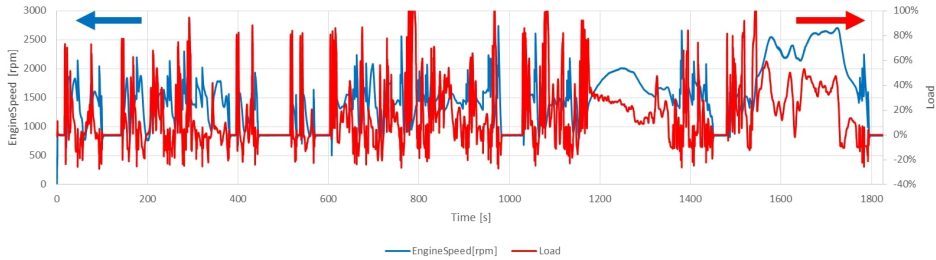

Figure 10. Engine speed and load

Brake torque

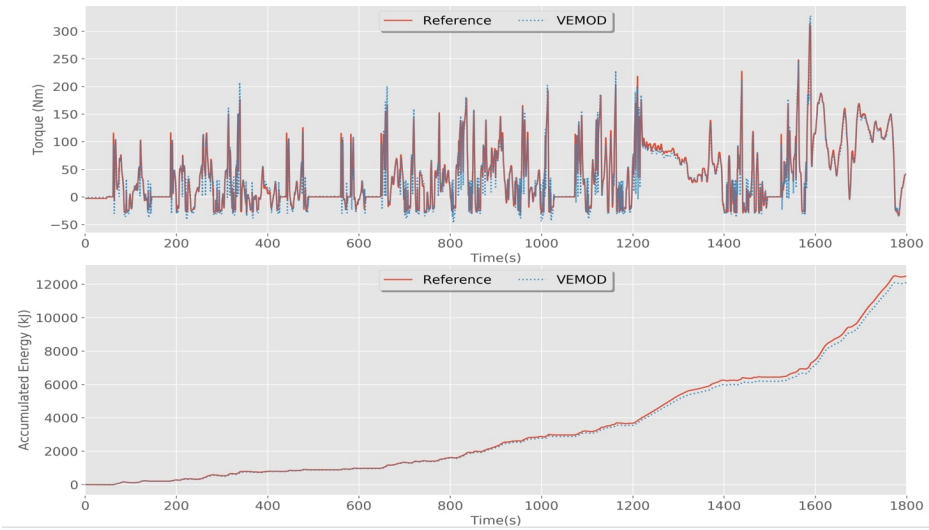

Figure 11. Brake torque and brake power in transient at cold conditions

Figure 11 shows the torque and cumulated brake power during a complete WLTC, starting at 20°C. It can be seen that the variations in the torque are well followed by the

model, in particular during the fast load changes. The model prediction has a mean error of about 8 Nm (mean relative error is about 5%), having 92% of the total points an error below 9 Nm. Even though some discrepancy can be observed at the low load variations, the cumulative effect during the complete cycle is only 2.5%.

Turbine outlet temperature

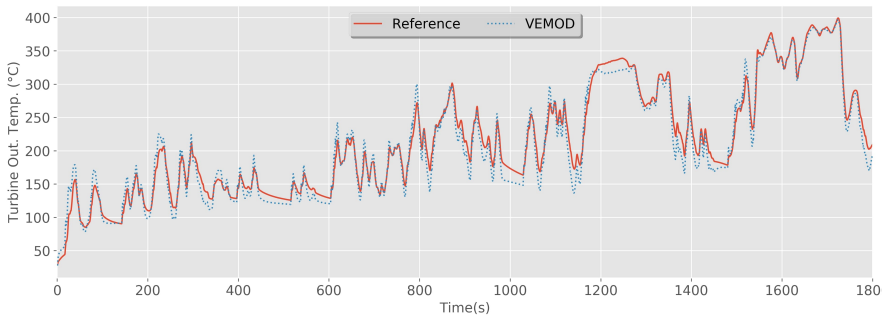

Figure 12. Turbine outlet temperature in transient at cold conditions

Turbine outlet temperature, is a key variable for the aftertreatment operation. It is plotted in Figure 12 and, as can be seen, it shows a good model response to variations, however, in general, it has a higher model peak values. The mean error for the turbine outlet temperature is 8°C (2%). Even though the prediction of the instantaneous temperature evolution can be improved, 90% of the points present an error below 12°C. In any case, the global performance of the outlet temperature ensures that the exhaust enthalpy analysis will be accurate enough for the Global Energy Balance.

Coolant temperature and oil temperature

Figure 13 and Figure 14 shows the coolant and oil temperature in transient conditions. The mean error of the coolant temperature is 3.5°C and the relative error is about 2%. Whereas, the mean error of the oil temperature is 2°C and the relative error is about 1%. Also, 82% of points show relative error below 5°C for both coolant and oil temperatures, which shows a good model prediction. The good performance of the coolant and oil temperatures allow ensuring that the heat rejection, key term in the energy balance, is well predicted by the model. The results in the warmed conditions have been omitted for the sake of brevity. but, they are pretty similar to those shown.

GEB analysis

After the validation of VEMOD, the GEB is carried out. Before starting with the analysis, it is interesting to provide a preliminary discussion. When performing the energy balance

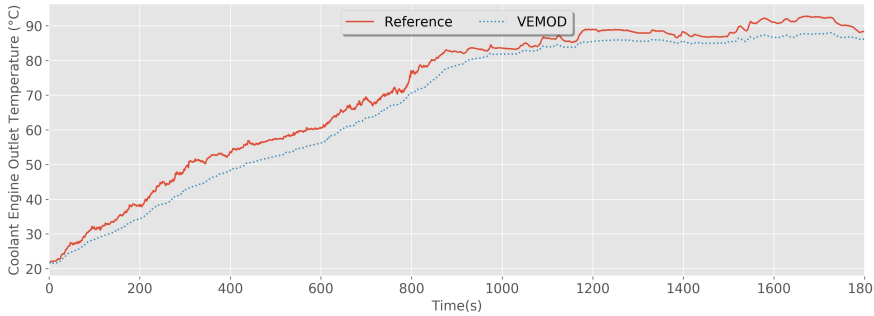

Figure 13. Coolant temperature in transient at cold conditions

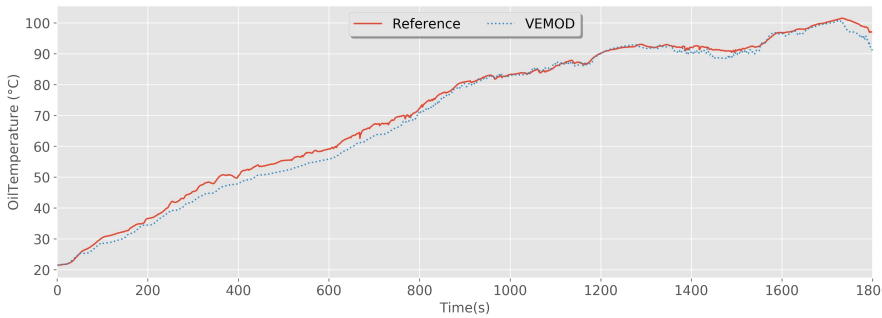

Figure 14. Oil temperature in transient at cold conditions

in stationary conditions, there is no energy accumulation in the engine. Thus, if the energy split is performed using mean variables that characterize the system state (such as fluid temperatures and mass flows) there wouldn't be any unbalance, except that due to the experimental uncertainty [26] or numerical error. This can be applied to whichever system boundaries considered (only engine block, complete engine including pipes, turbo, exchangers, etc.). However in transient operation, two important phenomena affecting the energy balance must be considered.

On the one hand there is an energy accumulation in different masses of the system, in particular in the metallic elements of the block, pipes, turbo etc. being the first one, the most important. Also there is heat accumulation in the coolant and oil. The accumulation in the metallic element is explicitly considered, while the fluid accumulation is implicitly considered because the heat rejection to coolant and oil will be internally used for both fluid heating and heat rejection in the exchangers.

On the other hand there is an important issue due to the "delay" of the mass and energy transfer at different engine position due to the distance of the elements in the gas path. This leads to an apparent unbalance depending on the system boundary limits considered, thus if only cylinder and ports are considered, the system response in the ports is almost instantaneous and the exhaust temperature changes cycle to cycle. However, if the complete gas pipes including high pressure and low pressure lines, turbo, exchanger, etc., are considered, there is an apparent inconsistency between the instantaneous heat release in the cylinder and the addition of the rest of energy terms. In fact this effect can be seen as an energy accumulation effect in the gas along the complete engine. When the enthalpy flow is integrated along a long period, this unbalance tends to become negligible. In order to perform a complete analysis two engine boundary limits are going to be considered for the cold conditions: on the one hand the engine block, on the other hand the complete engine. The "delay" effect will be clearly seen in the second one.

It is important to highlight that during the transient operation the instantaneous terms fluctuate fast (for the sake of rigor, take into account that terms described in 'Global Energy Balance (GEB) description' section are instantaneous power terms), thus being impossible to identify properly the relevant trends. Thus, the energy balance will be plotted in relative cumulated terms and hence each term will be finally computed as:

$$E_i(t) = \frac{\int_0^t \dot{E}_i(t) \cdot dt}{\int_0^t \dot{m}_f(t) \cdot H_v \cdot dt} \cdot 100 \tag{7}$$

where $E_i(t)$ is the relative cumulated term at the instant t, $\dot{E}_i(t)$ is each of the instantaneous power terms described and $m_i(t) \cdot H_v$ is the instantaneous injected fuel energy.

Cold conditions

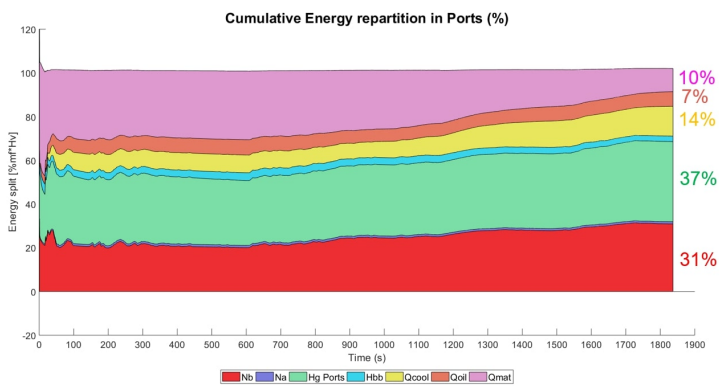

Figure 15. Cumulative energy repartition in engine block in WLTC at cold conditions

Figure 15 shows the energy balance considering the engine block (cylinders and ports) at cold conditions. As it can be seen, the fluctuations of the energy distribution are higher at the beginning and becomes smoother as the time increases. The reason is that the fast load variation at the beginning leads to modify importantly the numerator (and in some extent also the denominator) of Equation 7. But later, fast transient changes have a lower effect on the accumulated energy terms and thus they stabilize gradually. As explained, it can be seen that in this case there is an almost perfect agreement between the input fuel energy and the addition of the exhaust energy, brake power, auxiliary power, heat transfer to coolant, oil and cumulated heat in the material. As shown, the usual energy distribution of 30%-35% brake power, 60%-70% heat rejected and exhaust enthalpy can be seen at the end of the cycle, but there are important variations during the WLTC evolution, as the different energy terms tends to stabilize gradually with time. At the end of the cycle, brake power, N_b constitutes about 31% of total fuel energy output of engine. However, it is clearly lower during initial operation because of the high mechanical losses and heat rejection, but mainly due to the high amount of energy dedicated to heat the engine, as discussed below.

It can be observed that when the operating conditions of the engine cover higher loads, during the second part of the cycle, the weight of the brake energy increases up to the final values. Heat rejected to coolant, oil and material heating contribute about 25% of total energy output. The evolution of the heat rejection to coolant and oil along the cycle is quite stable, however it must be analyzed in combination with the energy used to heat the block ($\dot{Q}_{mat}$). Thus, it can be seen that at the beginning this is the main term, with an initial weight of about 50%. Due to the low temperature of metal, most of the heat rejected to the cylinder walls (also very high at the beginning due to cold conditions and low load) is used to increase the block temperature, thus reducing the heat rejected to coolant and oil. As the metal and fluids get hotter the average power used to heat the block tends to become zero and thus the fraction of accumulated energy also diminishes. Simultaneously there is a trend to slightly increase the heat rejected to coolant ($\dot{Q}_{cool}$) and oil ($\dot{Q}_{oil}$). It can be identified the effect of the thermostat opening around 800 seconds, when a fast reduction in $\dot{Q}_{mat}$ begins and there is an increase of $\dot{Q}_{cool}$. Regarding the heat repartition towards the oil and coolant circuits, $\dot{Q}_{oil}$ is higher at the first half of the cycle due to the higher importance of the friction losses at the beginning, mainly due to the lower oil temperature, as later discussed. Progressively, the cumulated $\dot{Q}_{cool}$ fraction increases in the second half of the cycle, becoming more than two times higher than the $\dot{Q}_{oil}$ at the end of WLTC (14% vs 7%).

The third main term, along with brake energy and heat rejection, is the exhaust enthalpy flow, $H_{g,ports}$ which contributes about 37% of the total cumulated energy at the end of the WLTC. It is quite stable along the complete cycle with a global trend to increase, mainly in the second half of the WLTC where higher loads and speeds are reached [28]. Two small terms complete the balance of the block: The energy to drive the auxiliary systems, which are lower to 1% during all the cycle and the enthalpy losses due to the blow-by leakage. This term diminishes gradually from 3% to 2%, being higher at the beginning due to the higher blow-by leakage flow (in comparison with the trapped mass) at low load and speed.

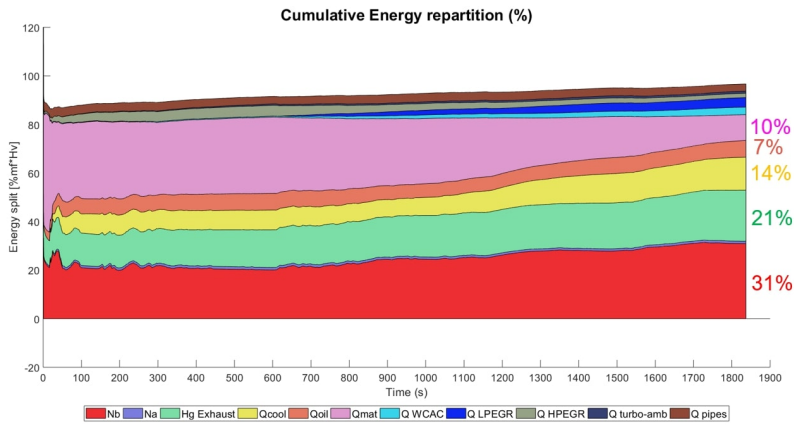

Figure 16. Total cumulative energy repartition in WLTC at cold conditions

Figure 16 shows the energy balance considering the entire engine during WLTC starting at 20°C including gas path (high and low pressure EGR lines, turbo, etc.), between inlet (from ambient) to exhaust. Unlike in Figure 15 , there is an apparent unbalance at the beginning of the cycle, diminishing progressively. As discussed, this can be explained by the delay effect in the calculation of the enthalpy flows due to the physical non-synchronize phenomena in the pipes and the in-cylinder conditions. Thus there is a lag of energy at the beginning, which diminishes as the time increases and tends to be negligible at the end of the WLTC.

When the complete engine is considered, extra energy terms like heat rejected from high pressure and low pressure EGR, WCAC (intercooler) and to ambient are included in GEB. The brake power, N_b and the heat rejection to coolant are the same as in the block (shown in Figure 15) because the EGR exchangers that are cooled by the block coolant has been considered separately. Heat rejection to oil is slightly higher due to the cooling effect of the turbocharger, being 7.5% at the end, only about 0.5% higher than in the previous analysis. Also auxiliaries are the same, while blow-by term is not explicitly considered as the blow-by mass flow is recirculated to the intake. This way, main changes are related to exhaust enthalpy flow and heat rejection in the exchangers.

The net exhaust enthalpy, $H_{g,exhaust}$ (calculated between engine intake and downstream the low pressure EGR pipe), contributes about 21% of total engine energy output at the end of the cycle. The difference with respect to $H_{g,ports}$ (about 16%) is due to the heat rejection in the intercooler, EGR exchangers and finally turbo and pipes to ambient. Cumulated heat rejected to the intercooler is about $3\%\dot{m}_f H_v$, being negligible until 500 seconds of operation because of the small difference between the air temperature at the compressor outlet and the intercooler coolant. 6% of total energy is rejected from the HPEGR and LPEGR lines at the end of the cycle. During the

initial operation, HPEGR loop, which promotes the increase of inlet temperature, is activated and LPEGR loop is used in the later transient operation, when the coolant temperature is hotter. About 3% of heat is rejected to ambient through turbocharger and pipes ($\dot{Q}_{turbo-amb}$ and $\dot{Q}_{pipes}$).

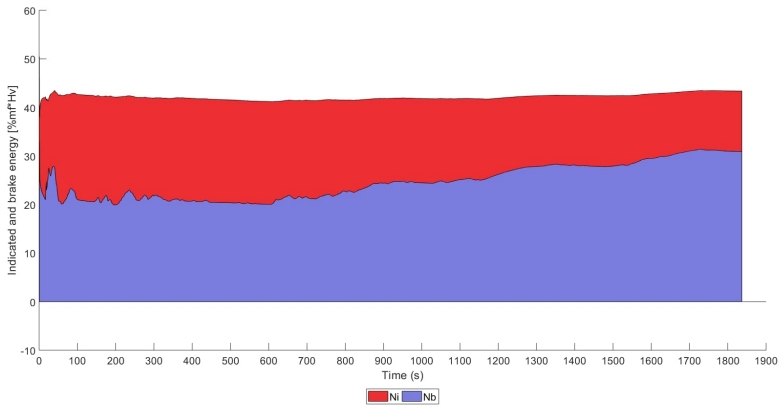

Figure 17. Cumulative indicated and brake energies in WLTC at cold conditions

In order to complete the analysis, Figure 17 shows the percentage of accumulated indicated and brake energies at cold conditions with respect to time. Indicated energy is around 44% of the total engine fuel energy during all the cycle, while brake power is 31% at the end, showing a clear trend to increase as the WLTC progresses. The lower values of brake energy at the beginning of the operation can be explained by the higher mechanical losses, as shown in Figure 18, because of low coolant and oil temperatures during the beginning of the operation, thus affecting the oil viscosity.

Figure 18 top shows that friction is the main component of the mechanical losses, being about 10% of the fuel energy at the end of the cycle, while pumping (N_p) is about 2.5% and auxiliaries (N_a) are 1%. When analyzing the evolution along the cycle, it is also clear that there is a large reduction of the mechanical losses weight, in particular due to the friction, which at the end has a cumulative effect about 4 times lower than at the initial part of the WLTC.

As shown in the bottom of Figure 18 , main component of the friction is the piston friction, N_{fr} piston, that is about two thirds of the total friction (7% of the fuel energy), being the valve train the less important and the bearing friction the intermediate contribution. This friction repartition is consistent with some previous analysis performed in stationary conditions [28].

Warmed conditions

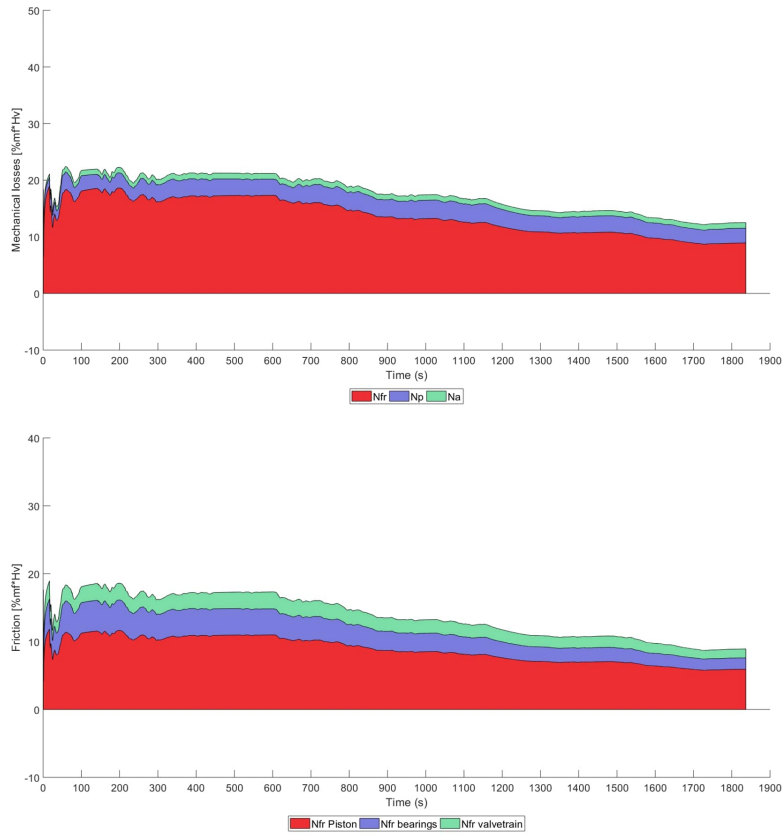

Figure 18. Cumulative mechanical losses (top) and friction split (bottom) in WLTC at cold conditions

As described, one of the purposes of this work is to compare the energy split starting at cold conditions with warmed engine, which energy balance considering the complete engine (including pipes, exchangers, turbo, etc., as in Figure 16) can be seen in Figure 19.

The most evident changes in comparison with results starting at cold conditions are related with heat transfer cumulated at the metal elements and the heat rejection to coolant and to oil. These changes are due to the change in the temperatures of the fluids and metal at the beginning of the cycle in comparison with cold condition. Thus, initially all the metal and fluid are around 21°C in cold start while in warmed conditions coolant is at 80°C, oil is at 85°C (these values were initialized at the model from experimental data) while metal temperatures range from about 90°C at the liner to more than 100°C in some parts of the piston. Hence, at the beginning of the cycle the coolant temperature

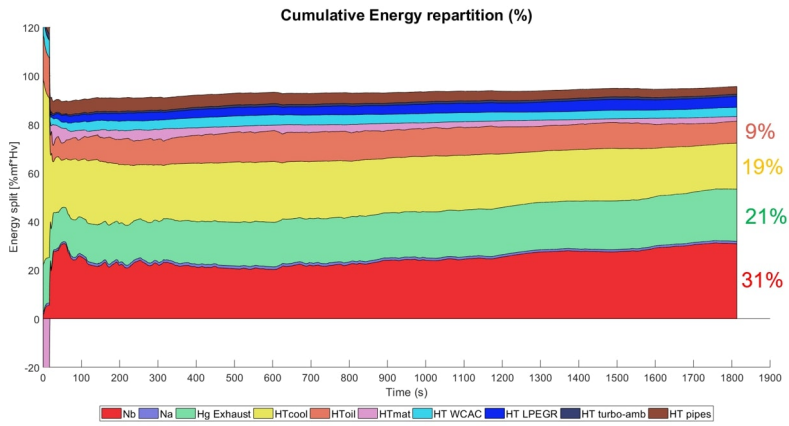

Figure 19. Total cumulative energy repartition in WLTC at warmed conditions

is higher to the thermostat opening temperature and the engine is rejecting heat to the radiator from the starting.

As shown in Figure 19, when the cycle starts there is a peak of heat coming from the metal which is rejected mainly to coolant and oil, due to their temperature difference. Later, after first idle of the WLTC (finishing about 17 seconds), instantaneous power rejection towards and from the metal parts start to oscillate (not shown) according to the operating conditions. As finally the engine reaches slightly different thermal condition in comparison with the initial ones (coolant temperature increases 4°C and oil 10°C), the cumulated heat rejection to metal is not completely negligible, but only less than 2%, much lower as in cold start.

Regarding coolant heat rejection, is much higher than in cold start at the beginning and it reaches a final value of 19%. On the other hand, the heat rejection to oil does not show such an important peak at the beginning because, most of $\dot{Q}_{mat}$ is rejected to the coolant exchanger. As later discussed, the final cumulated values of the heat rejected to coolant and oil are higher than in cold conditions.

The rest of the terms in particular brake efficiency, heat rejection in the EGR coolers and intercooler, do not show an important variation. The only remarkable results are that in warmed condition the engine is running with low pressure EGR from the beginning (while in cold conditions the engine started with high pressure EGR), but the total fraction of heat rejected to the EGR coolers is similar. Also a slightly higher heat rejection from metal elements to ambient (pipes, turbo) can be seen in warmed conditions during the initial part of the cycle, but at the end of the WLTC is similar.

The comparison of energy terms at the end of the WLTC in at warmed and cold conditions is shown in Figure 20. It can be seen that cumulated brake efficiency during cold conditions is slightly lower than warmed conditions, but the difference is only about

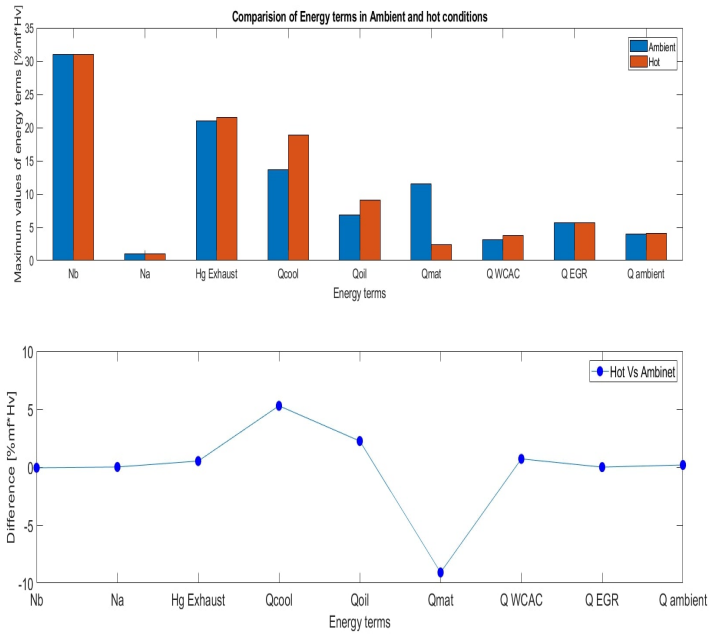

Figure 20. Comparison of energy terms in WLTC in cold and warmed conditions at the end of the cycle

0.1%. This benefit is achieved, thanks to the lower mechanical losses during warmed conditions, due to the high engine temperatures in warmed conditions in particular the oil temperature.

As it can be seen in Figure 21 global trend of the mechanical losses are similar to those shown in Figure 18, for cold conditions. However, some changes can be highlighted, the first is the slightly higher pumping work in warm condition mainly due to the change of EGR strategy at the beginning of the cycle; at the end of the cycle differences are small (3% vs 2.7%). The second one is the lower friction, clearly seen in the half initial part of the WLTC, where the change in the fluid temperatures is relevant (at about 1000 s, from the beginning engine temperatures are very similar in warmed and cold conditions). At 1000 seconds the reduction of the friction energy is about 2% of the fuel energy injected up to this instant in comparison with the cold conditions, as a result of the lower friction shown in Figure 22. However this difference is clearly reduced during the second part of the cycle, where oil temperatures are similar and the amount of fuel is much higher than in the first half (because of the higher load), hence, at the end of the cycle the friction differences are reduced to only 0.1%. In any case, this reduction contributes to the slightly higher brake efficiency discussed.

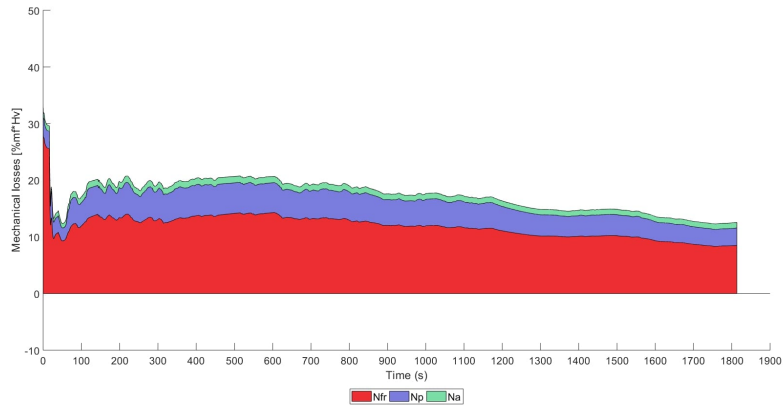

Figure 21. Cumulative mechanical losses in WLTC at warmed conditions

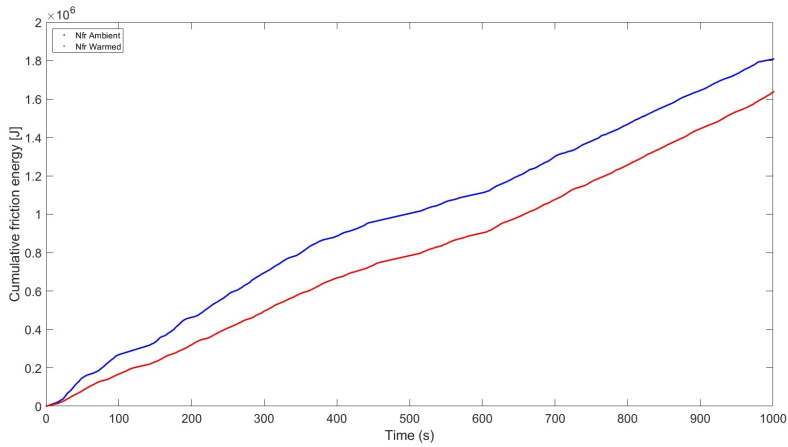

Figure 22. Cumulative friction energy during initial 1000 seconds at cold and warmed cycle

Conclusions

Simulation tool, VEMOD have been calibrated and validated using a 4-cylinder 1.6 L DI Diesel engine, before being used for the energy balance analysis. Good global performance has been found between the modeled and experimental results (in stationary and transient), when key outputs like pressure, heat released, turbine inlet/outlet temperatures, coolant temperature, oil temperatures and torque are considered.

A comprehensive analysis of the Global Energy Balance, using VEMOD has been done. This analysis contributes to understand the mechanism affecting the engine

consumption and allows to assess the effect of different operating conditions on the global energy repartition during a WLTC.

The GEB analysis in cold conditions was performed, by considering two engine boundary limits (the engine block and the complete engine), where a "delay" effect due to the unsynchronized phenomena in the cylinders and far from them in the gas lines. This delay causes an unbalance at the beginning of the cycles that can reach more than 10% of the cumulated fuel energy, however, it diminishes progressively during the cycle. It was seen that N_b, N_a, $\dot{Q}_{cool}$ and $\dot{Q}_{oil}$ are same when considering two boundary limits and the main changes are related to exhaust heat rejection in the exchangers and exhaust enthalpy flow, $H_{g,exhaust}$, whose difference with respect to $H_{g,ports}$ is about 16%. This difference is due to the split of exhaust enthalpy in to several sub terms i.e., heat rejection in the turbo and pipes to ambient, the intercooler and EGR exchangers.

It has been shown that the lower values of brake energy at the beginning of the WLTC is promoted by the higher mechanical losses, which in turn were result of the higher oil viscosity because of lower coolant and oil temperatures. It has been found that the most important term in the mechanical losses is friction with a percentage of about 65% of the total mechanical losses and about 10% of the total fuel energy at the end of the WLTC, being the piston friction the most important with a weight of 60% of the total friction losses. A noticeable finding include the lower friction values in warmed conditions (difference is around 2% of the fuel energy) at 1000 seconds of the cycle. However, this difference diminishes by the end of the cycle with a final difference around 0.1%.

The energy repartition considering the complete engine, at cold conditions was compared with warmed engine conditions. It has been seen that important changes take place in $\dot{Q}_{mat}$, $\dot{Q}_{cool}$ and $\dot{Q}_{oil}$ due to the different initial temperatures in cold and warmed conditions. It was seen that $\dot{Q}_{cool}$, which tends to increase when engine starting temperature increases, and $\dot{Q}_{oil}$ are higher in warmed conditions (21% vs 28%) because the rejection to the exchanger take place from the beginning, while in the case of the cold starting the thermostat is closed during the initial part of the cycle and the heat rejected to coolant and oil is used to increase the fluid temperatures. With the decrease in initial temperature $\dot{Q}_{mat}$ tends to increase being 10% at the end of the WLTC in cold starting and negligible in warm starting. It was found that there is a minor effect of the ambient conditions on N_b (difference is less than 1%), $\dot{Q}_{WCAC}$, $\dot{Q}_{HPEGR}$ and $\dot{Q}_{LPEGR}$. Finally, it was seen that despite of few uncertainties like the "delay" effect, the model shows good performance with final cumulated unbalance of about 3% in both cold start and warmed conditions.

Acknowledgments

This research has been partially funded by the European Union's Horizon 2020 Framework Programme for research, technological development and demonstration under grant agreement 723976 ("DiePeR") and by the Spanish government under the grant agreement TRA2017-89894-R. The authors wish to thank Renault SAS, especially P. Mallet and E. Gaïffas, for supporting this research.

References

1. Rakopoulos. *Diesel Engine Transient Operation - Principles of Operation and Simulation Analysis*. ISBN 9781848823747.
2. Rakopoulos CD, Giakoumis EG, Hountalas DT et al. The Effect of Various Dynamic, Thermodynamic and Design Parameters on the Performance of a Turbocharged Diesel Engine Operating under Transient Load Conditions. *SAE Technical Paper Series* 2010; 1(724). DOI: 10.4271/2004-01-0926.
3. European Parliament and Council of the European Union. Regulation (EC) No 852/2004 of the European Parliament and of the Council. *Official Journal of the European Communities* 2004; 2006(December 2006): 1–54. URL http://eur-lex.europa.eu/LexUriServ/LexUriServ.do?uri=OJ:L:2004:139:0001:0054:en:PDF.
4. Martin J, Arnau F, Piqueras P et al. Development of an Integrated Virtual Engine Model to Simulate New Standard Testing Cycles. *SAE Technical Paper Series* 2018; 1: 1–17. DOI: 10.4271/2018-01-1413.
5. Payri F, Lopez JJ, Pla B et al. Assessing the Limits of Downsizing in Diesel Engines. *SAE Technical Paper Series* 2014; 1. DOI:10.4271/2014-32-0128.
6. Tauzia X, Maiboom A, Karaky H et al. Experimental analysis of the influence of coolant and oil temperature on combustion and emissions in an automotive diesel engine. *International Journal of Engine Research* 2019; 20(2): 247–260. DOI:10.1177/1468087417749391.
7. Payri F, Olmeda P, Martin J et al. A New Tool to Perform Global Energy Balances in DI Diesel Engines. *SAE International Journal of Engines* 2014; 7(1): 43–59. DOI: 10.4271/2014-01-0665.
8. Payri F, Martin J, Garcia A et al. Experimental and Theoretical Analysis of the Energy Balance in a DI Diesel Engine. *SAE Technical Paper Series* 2015; 1(x). DOI:10.4271/2015-01-1651.
9. Tauzia X and Maiboom A. Experimental study of an automotive Diesel engine efficiency when running under stoichiometric conditions. *Applied Energy* 2013; 105: 116–124. DOI:10.1016/j.apenergy.2012.12.034. URL http://dx.doi.org/10.1016/j.apenergy.2012.12.034.
10. Abedin MJ, Masjuki HH, Kalam MA et al. Energy balance of internal combustion engines using alternative fuels. *Renewable and Sustainable Energy Reviews* 2013; 26: 20–33. DOI: 10.1016/j.rser.2013.05.049. URL http://dx.doi.org/10.1016/j.rser.2013.05.049.
11. Ajav EA, Singh B and Bhattacharya TK. Thermal balance of a single cylinder diesel engine operating on alternative fuels. *Energy Conversion and Management* 2000; 41(14): 1533–1541. DOI:10.1016/S0196-8904(99)00175-2.
12. Dimopoulos P, Bach C, Soltic P et al. Hydrogen-natural gas blends fuelling passenger car engines: Combustion, emissions and well-to-wheels assessment. *International Journal of Hydrogen Energy* 2008; 33(23): 7224–7236. DOI:10.1016/j.ijhydene.2008.07.012. URL http://dx.doi.org/10.1016/j.ijhydene.2008.07.012.
13. Taymaz I. An experimental study of energy balance in low heat rejection diesel engine. *Energy* 2006; 31(2-3): 364–371. DOI:10.1016/j.energy.2005.02.004.

14. Smith LA, Preston WH, Dowd G et al. Application of a First Law Heat Balance Method to a Turbocharged Automotive Diesel Engine. *SAE Technical Paper Series* 2010; 1. DOI: 10.4271/2009-01-2744.
15. Olmeda P, Martín J, Novella R et al. Assessing the optimum combustion under constrained conditions. *International Journal of Engine Research* 2018; : 1–13DOI:10.1177/1468087418814086.
16. Durgun O and Şahin Z. Theoretical investigation of heat balance in direct injection (DI) diesel engines for neat diesel fuel and gasoline fumigation. *Energy Conversion and Management* 2009; 50(1): 43–51. DOI:10.1016/j.enconman.2008.09.007.
17. Jia M, Gingrich E, Wang H et al. Effect of combustion regime on in-cylinder heat transfer in internal combustion engines. *International Journal of Engine Research* 2016; 17(3): 331–346. DOI:10.1177/1468087415575647.
18. Jung D, Yong J, Choi H et al. Analysis of engine temperature and energy flow in diesel engine using engine thermal management, 2013. DOI:10.1007/s12206-012-1235-4.
19. Caresana F, Bilancia M and Bartolini CM. Numerical method for assessing the potential of smart engine thermal management: Application to a medium-upper segment passenger car. *Applied Thermal Engineering* 2011; 31(16): 3559–3568. DOI:10.1016/j.applthermaleng.2011.07.017. URL http://dx.doi.org/10.1016/j.applthermaleng.2011.07.017.
20. Payri F, López JJ, Martín J et al. Improvement and application of a methodology to perform the Global Energy Balance in internal combustion engines. Part 1: Global Energy Balance tool development and calibration. *Energy* 2018; 152: 666–681. DOI:10.1016/j.energy.2018.03.118.
21. Romero CA, Torregrosa A, Olmeda P et al. Energy Balance During the Warm-Up of a Diesel Engine. *SAE Technical Paper Series* 2014; 1. DOI:10.4271/2014-01-0676.
22. Arrègle J, López J, García J et al. Development of a zero-dimensional Diesel combustion model. *Applied Thermal Engineering* 2003; 23(11): 1319–1331. DOI:10.1016/s1359-4311(03)00080-2.
23. Arrègle J, López JJ, García JM et al. Development of a zero-dimensional Diesel combustion model. Part 1: Analysis of the quasi-steady diffusion combustion phase. *Applied Thermal Engineering* 2003; 23(11): 1301–1317. DOI:10.1016/S1359-4311(03)00079-6.
24. Arrègle J, López JJ, Martín J et al. Development of a Mixing and Combustion Zero-Dimensional Model for Diesel Engines. *SAE Technical Paper Series* 2010; 1(724). DOI: 10.4271/2006-01-1382.
25. Olmeda P, Martin J, Garcia A et al. Evaluation of EGR Effect on the Global Energy Balance of a High Speed DI Diesel Engine. *SAE Technical Paper Series* 2016; 1. DOI: 10.4271/2016-01-0646.
26. Benajes J, Olmeda P, Martín J et al. A new methodology for uncertainties characterization in combustion diagnosis and thermodynamic modelling. *Applied Thermal Engineering* 2014; 71(1): 389–399. DOI:10.1016/j.applthermaleng.2014.07.010.
27. Payri F, Margot X, Gil A et al. Computational Study of Heat Transfer to the Walls of a DI Diesel Engine. *SAE Technical Paper Series* 2010; 1(724). DOI:10.4271/2005-01-0210.
28. Payri F, Olmeda P, Martín J et al. Experimental analysis of the global energy balance in a di diesel engine. *Applied Thermal Engineering* 2015; 89(x): 545–557. DOI:10.1016/j.

applthermaleng.2015.06.005.

29. Carreño Arango R. A comprehensive methodology to analyse the Global Energy Balance in Reciprocating Internal Combustion Engines. *Doctoral thesis* 2016; (September 2016). DOI: 10.4995/Thesis/10251/73069. URL http://hdl.handle.net/10251/73069.
30. Olmeda P, Dolz V, Arnau FJ et al. Determination of heat flows inside turbochargers by means of a one dimensional lumped model. *Mathematical and Computer Modelling* 2013; 57(7-8): 1847–1852. DOI:10.1016/j.mcm.2011.11.078. URL http://dx.doi.org/10.1016/j.mcm.2011.11.078.
31. Torregrosa A, Olmeda P, Degraeuwe B et al. A concise wall temperature model for di Diesel engines. *Applied Thermal Engineering* 2006; 26(11-12): 1320–1327. DOI:10.1016/j.applthermaleng.2005.10.021.
32. Payri R, Salvador FJ, Gimeno J et al. A new methodology for correcting the signal cumulative phenomenon on injection rate measurements. *Experimental Techniques* 2008; 32(1): 46–49. DOI:10.1111/j.1747-1567.2007.00188.x.
33. Payri F, Arnau FJ, Piqueras P et al. Lumped Approach for Flow-Through and Wall-Flow Monolithic Reactors Modelling for Real-Time Automotive Applications. *SAE Technical Paper Series* 2018; 1: 1–24. DOI:10.4271/2018-01-0954.
34. Tormos B, Martín J, Carreño R et al. A general model to evaluate mechanical losses and auxiliary energy consumption in reciprocating internal combustion engines. *Tribology International* 2018; 123(March): 161–179. DOI:10.1016/j.triboint.2018.03.007. URL https://doi.org/10.1016/j.triboint.2018.03.007.

-

Journal Title
XX(X):1–39

DOI: 10.1177/ToBeAssigned
www.sagepub.com/
SAGE

Analysis of temperature and altitude effects on the global energy balance during WLTC

Francisco Payri, Jaime Martín*, Francisco J. Arnau and Sushma Artham

Abstract

In this work, the Global Energy Balance (GEB) of a 1.6 L compression ignition engine is analysed during WLTC using a combination of experimental measurements and simulations, by means of a Virtual Engine. The energy split considers all the relevant energy terms at two starting temperatures (20°C and 7°C) and two altitudes (0 and 1000 meters). It is shown that reducing ambient temperature from 20°C to -7°C decreases brake efficiency by 1 % and increases fuel consumption by 4 %, mainly because of the higher friction due to the higher oil viscosity, while the effect of increasing altitude 1000 m decreases brake efficiency by 0.8% and increases fuel consumption by 2.5% in the WLTC mainly due to the change in pumping. In addition, GEB shows that ambient temperature is affecting exhaust enthalpy by 4.5%, heat rejection to coolant by 2% and heat accumulated in the block by 2.5%, while altitude does not show any remarkable variations other than pumping and break power.

Keywords

Transient, Global Energy Balance, Virtual Engine, WLTC, Cold-start, Altitude, Ambient

Corresponding author:
Martín Díaz Jaime, CMT-Motores Térmicos, Universitat Politècnica de València, Camino de Vera s/n. 46022 València, Spain, www.cmt.upv.es, Tel: +34963877650, fax: +34963877659
Email: jaimardi@mot.upv.es

Prepared using sagej.cls *[Version: 2017/01/17 v1.20]*

Nomenclature

ACS	Ambient cold start
CI	Compression ignition
DI	Direct injection
ECU	Engine control unit
EGR	Exhaust gas recirculation
GEB	Global energy balance
HPEGR	High pressure exhaust gas recirculation
HSDI	High speed direct injection
ICE	Internal combustion engines
IMEP	Indicated mean effective pressure
LPEGR	Low pressure exhaust gas recirculation
LTCS	Low temperature cold start
NEDC	New european driving cycle
1D	One-dimensional
VEMOD	Virtual engine model
WLTC	World harmonized light vehicles test cycle
WLTP	World harmonized light vehicles test procedure
0D	Zero-dimensional

Introduction

For decades, CI engine has dominated market because of their fuel efficiency and reliability. They have been extensively used in the transport sector whose development is aimed at achieving high efficiency [1,2] and low emission [3,4]. Nowadays, CI engines have to face challenges including improved thermal efficiency and real driving emissions [5,6]. In fact, important efforts have been made in the recent years to improve the combustion, emissions and performance of CI engine, mainly in warmed conditions [7–10].

Engines are mostly used under transient conditions and only a small proportion of daily driving schedules involve steady-state operation [11]. When compared to the steady-state conditions, the transient operation is closer to the real-world engine operation and thus, new driving cycles are based on this operation mode [12,13]. The global concern regarding environmental pollution has led to the increase in the interests on transient operation and real driving emissions, which led to the World harmonized Light vehicles Test Procedure (WLTP) [14]. It came into force in September 2017 in Euro 6d-Temp and has more realistic testing conditions, including the extended ambient temperature ranges covering low temperature operation [15] . WLTC has forced the automotive industry to optimize different technologies [15,16], but research in transient operation is still limited when compared to the steady-state operation. However, different engine phenomena still require improving predictive modelling performance in transient, beyond the results extrapolated from steady-state conditions [17–19].

When considering the engine behavior in transient operation, ambient, coolant and oil temperatures, are important as they affect the heat rejection and in-cylinder conditions, thus affecting combustion, emissions formation and mechanical losses. Moreover, usually engine calibration changes according to the coolant and oil temperatures[20]. Because of the dramatic spatial and temporal thermal variation, the initial stage after the cold starting is one of the most important transient processes of CI engines. Moreover, low ambient temperatures during start process have a notable influence on the combustion process [21–23]. Research on cold-start in CI engines have shown that emissions tend to increase when ambient temperature diminishes[6,24]. Also, low ambient temperature leads to enhance incomplete combustion[6,25,26]. Fuel consumption also increases with the lower combustion efficiency and higher mechanical losses[6]. The reduction of cold start emissions in CI engines has become an increasingly important issue, because the fuel consumption and exhaust gas emissions associated with cold-start conditions are higher than those associated with warmed engine conditions[6,27]. Due to the regulations requirement, cold-start has received the attention of the researchers, in particular engine operation under WLTC and real driving emissions [24,28–33]. Some researchers focused on the cold start performance of CI engines and had investigated the impacts of exhaust gas recirculation on engine performance[28–30,33–36]. Thus, Christos Dardiotis et al.[24] experimentally investigated CO, HC and NOx emissions of Euro 4/5/6 CI passenger cars at low temperature of -7°C based on the cold start driving cycle, whose research results proved emission pollutants increased remarkably at low temperature (-7°C) compared to the ambient test. Apart of temperature conditions, altitude is a second key issue affecting engine operation. Liu et al.[37] investigated the change of intake oxygen content caused by altitude variation and its affect on the performance of CI engines. They found that the brake specific fuel consumption (BSFC) decreases with the increase of atmospheric pressure.

Reduction of consumption and emissions requires evaluating new strategies in the transient operation. In this framework, Global Energy Balance (GEB)[38,39] is a useful approach for the assessment of parameters affecting engine consumption. Various paths followed by the chemical energy can be identified and quantified using GEB. A simple energy balance can be carried out by considering the fuel power, brake energy, heat transfer, mechanical losses and the exhaust gas energy. Some works dealing with experimental and theoretical energy balance can be found in the literature[40–43]. Abedin et al.[41] did a thorough study on GEB using various alternative fuels[42] and determining the key variables effecting GEB and performance of the engine. In few previous works, various injection strategies at different operating conditions were studied with the help of the analysis of energy repartition[40,44,45]. The energy balance can be performed in a more detailed way by considering the heat transfers to the coolant and oil[44]. The neglected terms that account for energy losses with minor impact include unburnt fuel, heat rejection to the ambient and blow-by enthalpy[46].

In order to perform the engine thermal balance in detail, 0D/1D simulation tools have a large potential, as showed at[43,47,48]. Also the combination of experiments and theoretical analysis provides a deep insight in the key issues controlling the energy degradation in the engine as shown in two previous works [43,47–49].

Steady-state conditions are the main focus in most of the described publications and thus, very few works can be found dealing with the analysis of energy balance in transient operation[50], and with the effect of ambient conditions, including the temperature or altitude[51]. Moreover, the few available works do not offer a deep analysis of the energy balance from experimental or modeled point of views. This leaves a gap in the engine research that this work tries to cover.

The first contribution is the methodology used to perform the analysis of the energy balance by combining experimental and simulated information. On the one hand, experimental fluid temperatures are used to validate the model performance, while some experimental settings (such as instantaneous fuel and air mass flows) are imposed as targets, for the engine control, during simulations. On the other hand, detailed simulated energy split is assessed along WLTC by means of a 0D/1D tool called VEMOD. The tool, once validated in cold conditions (validation in ambient conditions was carried out in a previous work[52]), provides information that is hard or even impossible to obtain experimentally such as, among others, the heat rejection to different engine parts or the mechanical loses split.

A cumulative approach has been applied to plot the energy terms along WLTC, thus each of them has been averaged from the start until a determined instant to provide a mean transient evolution. Although not conventional in other works, this approach is necessary to avoid the excessive noise of raw instant evolution.

The second main contribution of the work is the results and discussion on the effect of ambient temperature and engine altitude on the GEB in transient operation in a 1.6 L CI engine. Thus, two starting temperatures, 20°C (Ambient Cold Start -ACS-) and -7°C (Low Temperature Cold Start -LTCS-) and two altitudes (0 and 1000 meters), both at LTCS are considered. The analysis is performed, on the one hand, discussing the instantaneous evolution of the energy terms at different conditions, justifying the observed trends, and highlighting the most interesting differences along WLTC. On the other hand, a final comparison of the total cumulated terms, at the end of WLTC, allows providing a clear summary of the main effects. For the sake of clarity, the analysis includes some in-cylinder and combustion parameters, and finally NOx emissions.

The work is organized in different sections devoted to firstly describe the experimental and modeling tools, followed by the methodology description. Thereafter, a brief description of the Global Energy Balance and the model validation is provided. Then the GEB discussion for different ambient conditions is carried out, finishing the work with the most relevant conclusions in the last section.

Experimental and modeling tools

Experimental tool

The research was carried out in a multi-cylinder, HSDI Diesel engine. The engine is a 1.6L four-stroke Euro 6 compliant engine. The specifications of the engine can be seen in Table 1.

Table 1. Engine specifications

Type	**HSDI Diesel engine**
Displacement	1598 cm³
Bore	80 mm
Stroke	79.5 mm
Compression ratio	15.9:1
Number of valves	4 / cylinder
Number of cylinders	4
Air management	VGT, HP-EGR, LP-EGR
Maximum power @ speed	96 kW @ 4000 rpm
Maximum torque @ speed	320 Nm @ 1750 rpm
Engine oil	0W-30
Engine coolant	50% glycol-50% water

The test cell as shown in Figure 1, is fully equipped to measure main operation mean variables (e.g. air and fuel mass flows, temperature and pressure at intake and exhaust lines, etc.), some liquids (oil and coolant) temperatures, coolant mass flows and in-cylinder pressures in the four cylinders. Table 2 summarizes the relevant instrumentation used for this study.

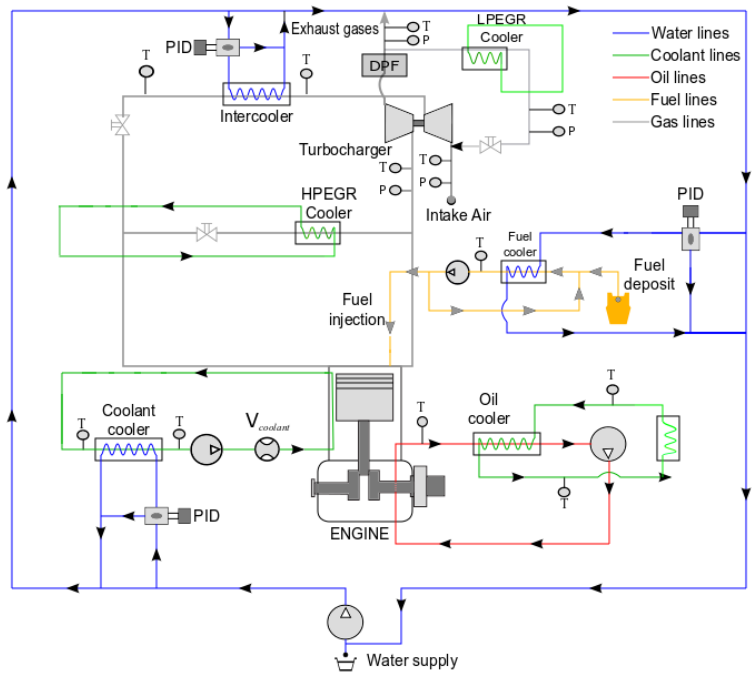

Figure 1. Test cell scheme

Table 2. Test cell instrumentation

Variable	Instrument	Range	Accuracy
Crank angle	Encoder	0-360°	±0.02°
Torque	Dynamometer	0-400 Nm	±0.5 Nm
Gas temperature	k-type thermocouple	70-1520 K	±2 K
Air mass flow	Sensyflow DN80	0-1700 kg/h	±2 %
Coolant flow	Krohne 4010 Optiflux	4.5-90 L/min	±0.5 %
Oil pressure	Piezoresistive transducer	0-10 bar	±25 mbar
In-cylinder pressure	AVL GH13P	0-200 bar	Linearity 0.3%

The steady-state tests for calibration were performed at 26 operating points. They cover a wide range of the engine map and testing points belonging to the WLTC as shown in Table 3.

Table 3. Steady-state tests performed

Engine speed in rpm	Load in %
1000	Motoring
2000	Motoring
3000	Motoring
4000	Motoring
850	idle
1000	21, 44, 66, 88
1250	13, 26, 50, 76, 100
1500	11, 25*, 50, 75*, 100
2500	25, 50, 75, 100
3500	25*, 50, 75, 100

* Both conventional (20°C) and cold ambient conditions (-7°C)

The test bench in which the engine is installed includes a control of ambient temperature and also of the temperature of the water in a large reservoir. This water is used to cool down the intercooler, fuel and coolant. In the case of LTCS, the water temperature is at -7°C and in the case of ACS, it is around 20°C. The control of the coolant temperature, which is a key parameter for thermal performances, is carried out automatically through the engine thermostat, thus mimicking real operation. The coolant temperature is around 85 ± 5°C in hot conditions. In the case of motoring tests, the temperature of the coolant will stabilize at a determined temperature that depends on the engine speed.

To measure and simulate WLTC, the instantaneous load and engine speed was obtained from the vehicle speed profile of a vehicle class 3 (W/kg>>34), which is a multi-purpose vehicle, powered by the 1.6 L Diesel engine. The transient analysis is performed in three WLTC tests, measured with ACS and LTCS conditions (starting at -7°C) at 0 m. Table 4 summarizes the different engine temperatures at these conditions at the beginning of the test. Three repetitions of each steady-state point and WLTC were measured.

Table 4. Initial temperatures in the WLTC tests performed

Test conditions	Room temperature	Initial block temperature	Initial Coolant temperature	Initial Oil temperature
ACS	20°C	20°C	20°C	20°C
LTCS	-7°C	-7°C	-7°C	-7°C

Predictive tool

The Virtual Engine Model (VEMOD)[15] is a home-developed standalone tool aimed at simulating new standard testing cycles. It covers the calculation of different processes as outlined in Figure 2, where the sub-models included are summarized. The entire

sub-models used are shown in Figure 2. The 1D gas dynamics model computes air management and by means of explicit sub-models, it is able to calculate the processes in all the engine components such as heat exchangers, turbocharger, aftertreatment systems etc. The gas dynamics model is combined with a cylinder model that predicts in-cylinder conditions taking into account the injection-combustion process. The whole set of sub-models, marked with a blue box in Figure 2, make up the engine model[15]. The red boxes in Figure 2 represent the various control sub-models. They have been developed in Matlab/Simulink[15]. The control sub-model allows controlling the operating points (during steady-state and transient conditions) of the engine model. The vehicle dynamics model allows calculating the instantaneous vehicle velocity taking into account the engine torque, road characteristics and driver behavior. However, as in this study the focus is put on the engine performances, the vehicle calculation has been omitted by imposing the engine speed and target torque to follow the WLTC.

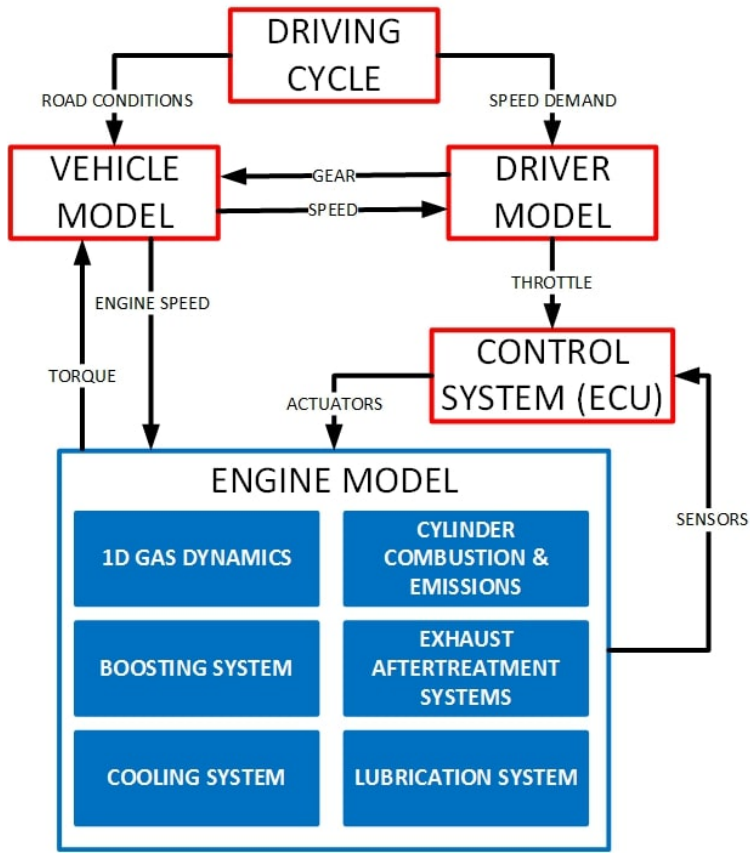

Figure 2. Flow-chart of Virtual Engine Model (VEMOD) subsystems

Steady-state operating points can be simulated by VEMOD without the control system sub-model, by imposing the target value of actuator, in the engine model. Whereas, for transient operation, control system sub-model is needed to follow certain targets by acting on the different actuators related to air management (turbine rack position, EGR valve...) and injection settings (pressure and injection timing and fuel mass injected in each pulse). Virtual ECU allows mapping the injection settings as a function of speed and fuel mass. Different energy terms will be modelled to complete the energy balance of the system using VEMOD.

Combustion diagnosis tool

A combustion diagnosis tool called CALMEC[38,53], developed at CMT-Motores Térmicos was used to calculate the heat release and to calibrate the in-cylinder heat transfer in VEMOD[53–55], based on the experimental measurements in steady-state conditions as described in [54].

Methodology

The scheme of the methodology followed is shown in Figure 3. It was structured as follows:

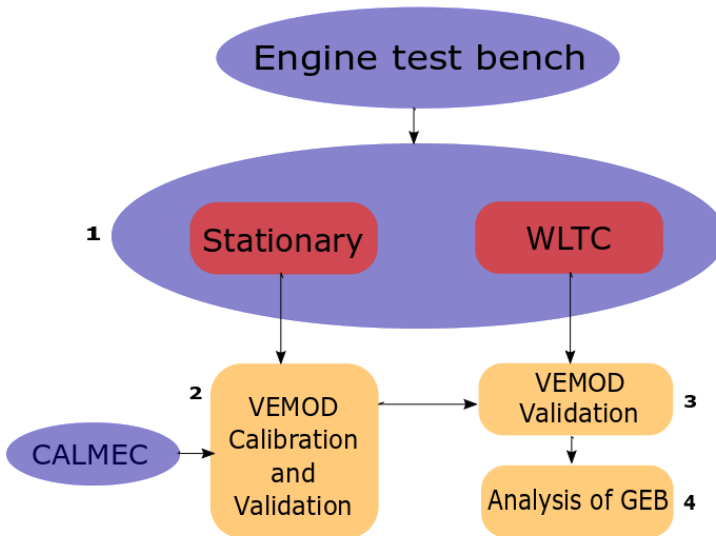

Figure 3. Methodology

1. The steady-state and WLTC transient tests were measured in the installation described in the experimental tool section. The parameters required for the analysis (engine speed, torque, air and fuel mass flows, oil and coolant temperatures,

temperature and pressure at intake and exhaust lines, coolant mass flows and in-cylinder pressures in the four cylinders) were measured as described.

2. Calibration of the combustion sub-models[15], in-cylinder heat transfer[54] and mechanical losses[38] were carried out using the set of steady-state points. As the results were presented in Olmeda et al[52], a brief description of the results is included to avoid reccurence.

3. The VEMOD validation in various transient tests is performed by comparing simulated WLTC cycle with experimental result. The validation was performed using experimental data of the evolution of fluid temperatures and brake torque.

4. An extensive analysis of the energy repartition was carried out to assess the effect of different variables on the Global Energy Balance (GEB) and engine performance. GEB during WLTC was obtained at different altitudes (0 m and 1000 m) and thermal conditions, using some experimental data to set target conditions during simulation, as detailed below.

For the calculation of both steady-state points and WLTC, the experimental values of the torque, air mass flow and boost pressure were set as targets and the injection settings and engine speed were directly imposed along the cycle.

Global Energy Balance (GEB)

The basis of the analysis is the first law of thermodynamics. Different paths followed by energy terms are represented in Figure 4, where all the energy transformations taking place in a turbocharged engine are considered [38,39,52,56,57].

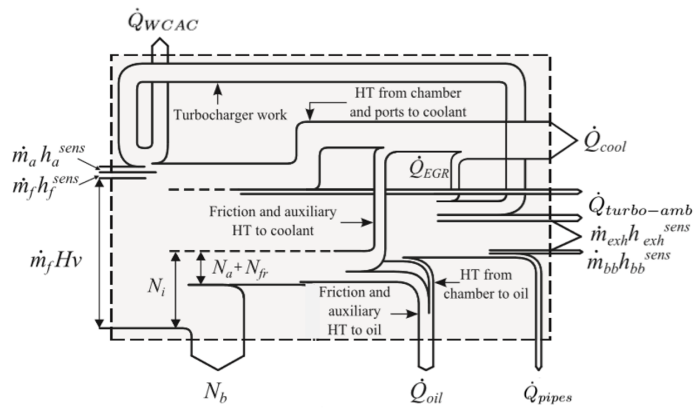

Figure 4. Schematic representation of GEB

The energy flows entering the engine are the sensible enthalpy of air $\dot{m}_a h_a^{sens}$, the sensible enthalpy of fuel $\dot{m}_f h_f^{sens}$ and the chemical energy of the fuel $\dot{m}_f H_v$. The

outlet energy flows are the brake energy N_b, the power to run auxiliary elements[58] N_a, the heat flow to the coolant[59,60] $\dot{Q}_{cool}$, the flow of sensible enthalpies of the exhaust gases $\dot{m}_{exh}h_{exh}$, the heat rejection to oil[59] $\dot{Q}_{oil}$, the heat cumulated in the engine block $\dot{Q}_{mat}$, the heat rejection in the intercooler $\dot{Q}_{WCAC}$, the heat rejection in the EGR heat exchangers, $\dot{Q}_{LPEGR}$ and $\dot{Q}_{HPEGR}$, the heat from the external walls of the engine to the ambient due to the heat rejection in the pipes $\dot{Q}_{pipes}$ and turbo case[59,60] $\dot{Q}_{turbo-amb}$, and finally the enthalpy flow of blow-by losses, H_{bb}[38,39,56].

In order to perform the detailed analysis of energy repartition, sensible enthalpy terms are rearranged to obtain the net flow of sensible enthalpy, H_{exh}, determined by means of a balance between the enthalpy flow of incoming air and fuel and outgoing exhaust gases. Thus, the first law of thermodynamics can be expressed as:

$$\begin{aligned}\dot{m}_f H_v =& N_b + N_a + H_{exh} + \dot{Q}_{cool} + \dot{Q}_{oil} + \dot{Q}_{mat} + \dot{Q}_{WCAC} + \dot{Q}_{HPEGR} \\ &+ \dot{Q}_{LPEGR} + \dot{Q}_{pipes} + H_{bb} + \dot{Q}_{turbo-amb}\end{aligned} \tag{1}$$

More details about the terms and how they are determined in the GEB analysis is explained in Olmeda et al[52].

Model calibration and validation

Calibration in steady-state conditions

In order to proceed with the analysis of energy balance, the calibration of the Virtual Engine, VEMOD, was previously performed. The calibration includes the determination of the fitting constants of different sub-models of VEMOD. It was performed using motoring tests, which were used to perform an initial convective heat transfer tuning and combustion tests, which were used for commissioning the rest of sub-models, in steady-state conditions. Experimental matrix used for the calibration is detailed in Table 3.

Experimental heat release is the main source of information for combustion model calibration; however, it is affected by the heat transfer rejection. Thus, the combustion model calibration was performed after the calibration of the heat transfer model. The combustion model is composed of three main sub-models: ignition delay, premix combustion and diffusion combustion models; along with a 1D model describing the mixing process. The approach for the mixing process, key issue for both the heat release and emissions predictions, is a physical model based on the turbulent gas jet theory[61]. The ignition delay (ID) model is based on a simplification and parameterization of a complete n-heptane chemical kinetics description from[62]. The premixed combustion model is an empirical model based on the propagation velocity of a premixed flame that considers in-cylinder conditions (pressure, temperature and composition). The diffusion combustion phase is assumed to be mixing controlled: the fuel mass in each fuel parcel will be burned when it reaches stoichiometric conditions, and mixing model determines when these conditions are reached. It is necessary to indicate that to achieve an accurate prediction of the diffusion combustion, quasi-steady conditions and transient processes at the start and end of the injection are considered separately. The calibration of the

combustion model includes the determination of the different constants of the three sub-models. The criterion for the determination of the sub-model fitting constants was to minimize the difference between the experimental heat release and the simulated one.

The detailed description of the calibration can be found in the previous work of Olmeda et al[52]. Some brief results can be seen in Figure 5. Top two plots of Figure 5 show the experimental and modeled heat release at engine speed of 2500 rev/min at different loads (25% and 100%). The dotted lines represent the modeled values from VEMOD for one cylinder and the solid lines represent the experimental values of the four cylinders. As shown, the heat release evolutions are quite well predicted and the discrepancy is, in general, similar to differences between cylinders. Bottom two plots of Figure 5 represent the heat release at engine speeds of 1250 and 3500 rev/min and load of 50%. Also, a good global agreement of modeled vs experimental results can be seen. It can be highlighted that the modeled heat release is slightly slower than the experimental ones at high speed and load. The reason for the slightly poorer performance at these conditions is because the focus was put on the low-mid ranges because they are critical for the WLTC simulation, main objective of the work. In the previous work of Olmeda et al[52] the pressure and heat release evolutions at various speeds and loads were shown in detail, they have been omitted here for the sake of brevity.

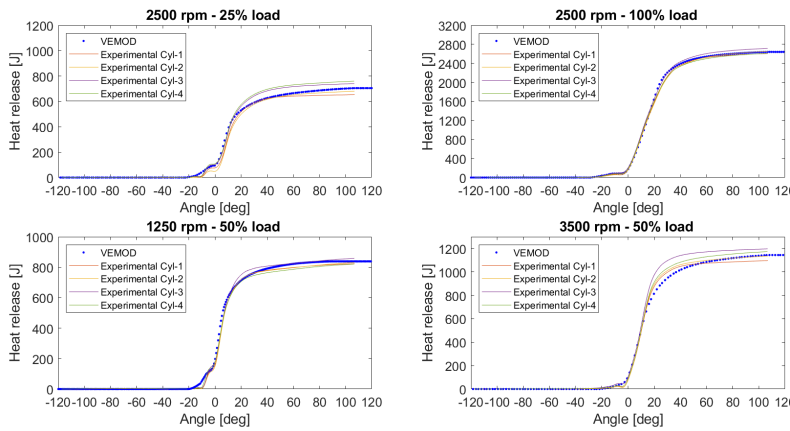

Figure 5. Heat release at different loads (top) and speeds(bottom) in steady-state conditions.

The analysis was extended to other key outputs in the complete engine map such as IMEP, with a mean error about 3%, turbine inlet temperature, with a mean error of 2.5% and coolant temperature, which mean error is 0.5%. In any case, the global performance of the model was shown to be good, with a slightly higher uncertainty at high load conditions that are less critical for WLTC simulation.

Transient validation of at low temperature cold start

In order to ensure the good performance of the model in transient conditions before performing the energy balance, the validation at low temperature cold start (at -7°C) is presented in this section. Validation at ambient cold start (at 20°C) was presented in a previous work[52]. As mentioned in the methodology section, the experimental speed and torque, injection settings, air demand and boost pressure are set as targets for the control system during the WLTC, while brake torque and some key temperatures of gas and liquids circuits are compared with their experimental values to check the model performance.

Tests performed at ambient conditions by Olmeda et al[52] were conducted with engine settings calibrated for Euro 5 regulation. In that calibration, no EGR strategy is applied until almost half of the cycle for low temperature start. However, in this work, calibration has been updated in order to face upcoming Euro 7 regulation. Thus, in the current calibration high pressure EGR is used from the very beginning, to promote the increase of inlet temperature and later, when coolant temperature reaches 80°C, low pressure EGR strategy is applied.

For the sake of brevity, the following four relevant variables are shown for validation in Figure 6 to Figure 8 : torque, turbine outlet temperature, coolant and oil temperatures.

Figure 6 shows the torque and cumulated brake energy during a complete WLTC, starting at -7°C. It can be seen that the evolution of the torque is well followed by the model, in particular during the fast load changes. The torque prediction has a mean error of 10 Nm (mean relative error is about 7%), having 90% of the total points an error below 11 Nm. Even though some discrepancy can be observed at the low load variations, the cumulative effect at the end of the complete cycle is only 4%.

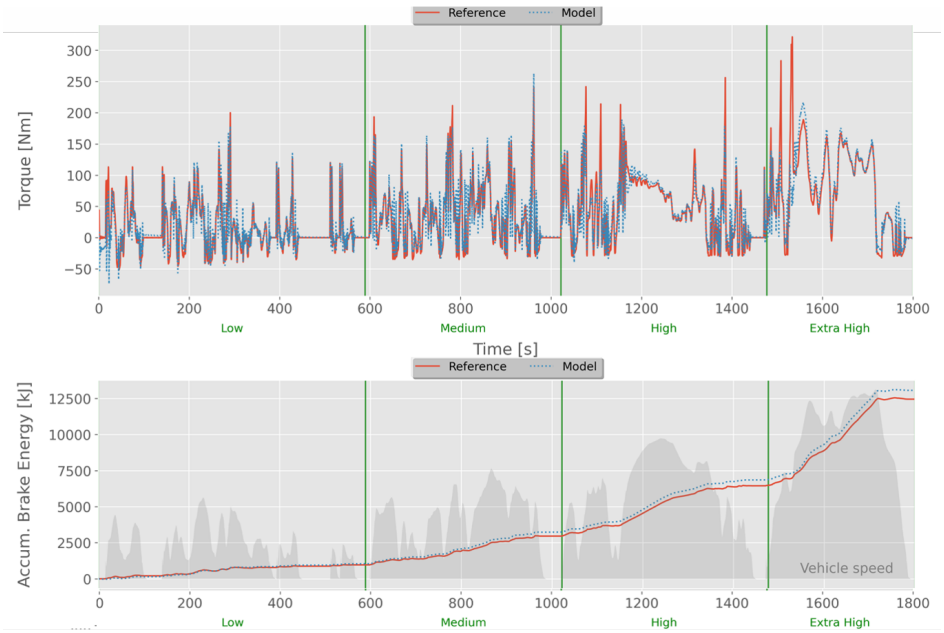

Figure 6. Brake torque and brake energy in transient at LTCS conditions

Figure 7 and Figure 8 shows the coolant and oil temperature in transient conditions, key parameters to track the thermal performance of the engine in low temperature conditions. The mean error of the coolant temperature is 3°C and the relative error is 1%. Whereas, the mean error of the oil temperature is 4°C and the relative error is about 1.5%. Also, 90% of points show relative error below 6°C for both coolant and oil temperatures, which shows a good model prediction. The good performance of the coolant and oil temperatures allow ensuring the accuracy of heat rejection prediction, key issue in the energy balance in low temperature conditions. Results at ambient cold start conditions have been omitted for the sake of brevity, but they are pretty similar to those shown for low temperature cold start and even though with a different calibration, Euro7 target vs Euro 5, also similar to those reported by Olmeda et al.[52] in ambient conditions.

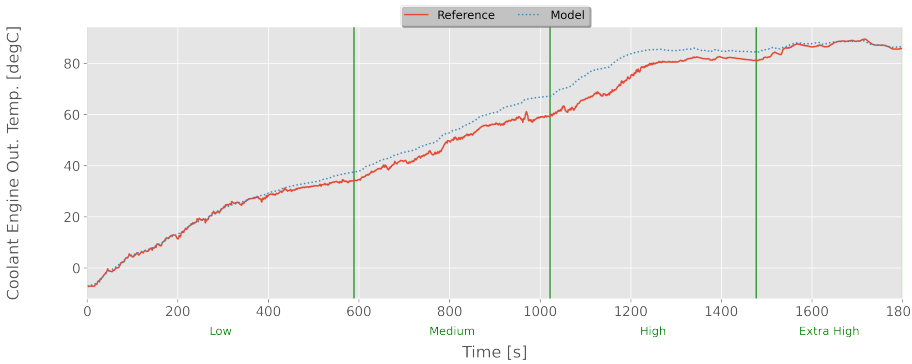

Figure 7. Coolant temperature in transient at LTCS conditions

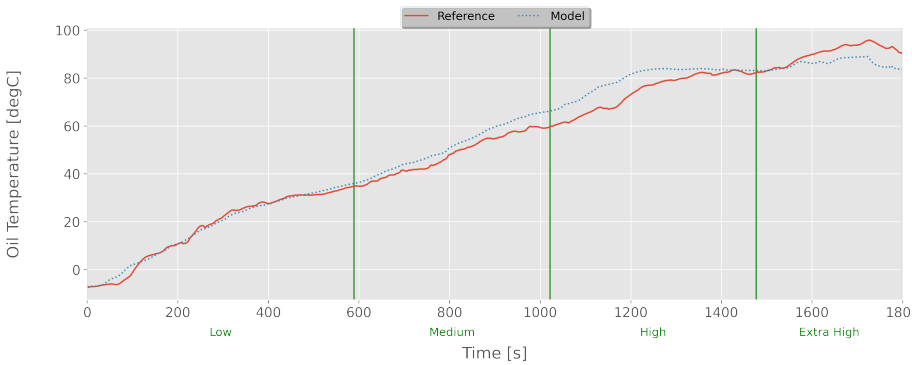

Figure 8. Oil temperature in transient at LTCS conditions

GEB analysis

It is interesting to provide an initial discussion before starting with the GEB analysis. If the energy balance was performed in steady-state conditions, the addition of all the energy flows would provide a residual close to zero, and only an small unbalance would remain due to some experimental uncertainty[54](if analysis is based on measurements) or numerical error. However, as detailed in a previous work[52], a "delay" phenomenon have to be considered in the energy balance during transient conditions. System response is almost instantaneous when the engine cylinder and ports are considered for the energy balance. If the complete engine including heat exchangers and all the gas lines are considered, there is an apparent inconsistency between the instantaneous heat release in the cylinders due to the combustion process (main term at the left in Equation (1) and main input for the GEB) and the addition of the rest of energy terms. This inconsistency tends to be negligible when the enthalpy is integrated during a long time, as discussed below.

In the GEB analysis, the cumulative energy terms are plotted by integrating the power of each term and dividing it by the the cumulated fuel energy until a determined instant.

Low temperature cold start conditions

Figure 9 shows the energy balance considering the complete engine during WLTC starting at -7°C. The analysis includes all the elements from engine inlet (ambient conditions) to the exhaust. As stated, there is an apparent unbalance from the beginning of the cycle. Thus, there is no perfect agreement between the input fuel energy and the addition of the exhaust energy, brake energy, auxiliary power, heat transfer to coolant, oil, cumulated heat in the material, heat rejected at high pressure and low pressure EGR coolers, WCAC (intercooler) and to the ambient. As justified, this can be explained because of the non-synchronized phenomena taking place in the pipes and the in-cylinder leading to a delay in the calculation of the enthalpy flows, that causes a global lag of energy at the beginning. This effect diminishes as the time increases and is small at the end of the WLTC, after 1800 seconds, where the total cumulated energy reaches 85% of the injected energy. However, when the cycle is extended and run for a longer time, energy balance tend to stabilize gradually to reach the agreement of about 100% between input and output energies of engine. This can be seen in Figure 10, where simulation has continued after the WLTC, repeating the cycle until 5700 s. This effect is similar at ambient cold start conditions, where the total cumulated energy reaches about 86% of the injected energy, after 1800 seconds and stabilizes gradually when the cycle is extended.

In Figure 9, at the end of cycle, brake energy, N_b constitutes about 29% of total fuel energy (mean brake efficiency of 29%). However, it is clearly lower during initial operation and increases during the second part of the cycle, where engine operates at higher loads. This can be justified because of the large mechanical losses and the high amount of energy rejected to the walls and used to heat the metal and liquids at the beginning of the cycle, because of the low initial temperatures. The heat rejected to coolant ($\dot{Q}_{cool}$), oil ($\dot{Q}_{oil}$) and material ($\dot{Q}_{mat}$) contribute about 30% of the total energy output at the end of the cycle. However, initially, $\dot{Q}_{mat}$ is the most important term,

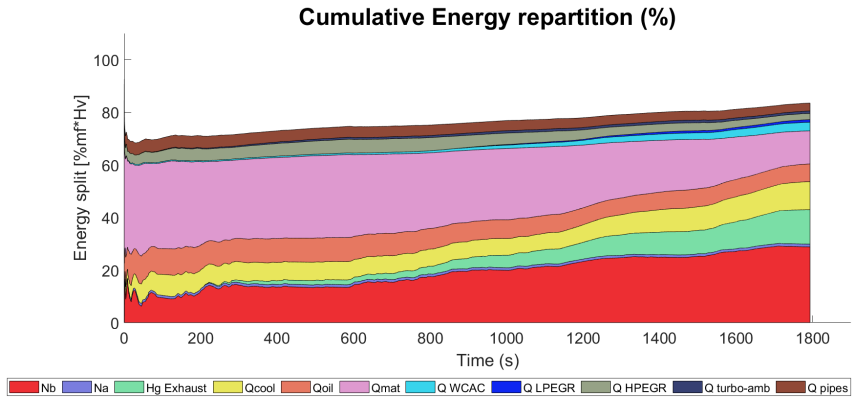

Figure 9. Total cumulative energy repartition in WLTC at LTCS conditions

reaching about 50% of total energy because of the block temperature during the initial operation is cold. As the metal and fluids temperatures increase, the power used to heat the block tends to reduce. A slight increase in the heat rejected to coolant ($\dot{Q}_{cool}$) was obtained from around 1200 seconds on, because of the thermostat opening. $\dot{Q}_{cool}$ is quite stable and slightly lower to 7% until this point. However, at 1250 seconds the value starts to be higher to 7% and a continuous increase takes place until 1800 seconds, when $\dot{Q}_{cool}$ is about 11%. $\dot{Q}_{oil}$ is slightly higher at the first half of the cycle due to the higher friction losses at the beginning, due to the lower oil temperature. $\dot{Q}_{oil}$ is about 7% at the end of the cycle.

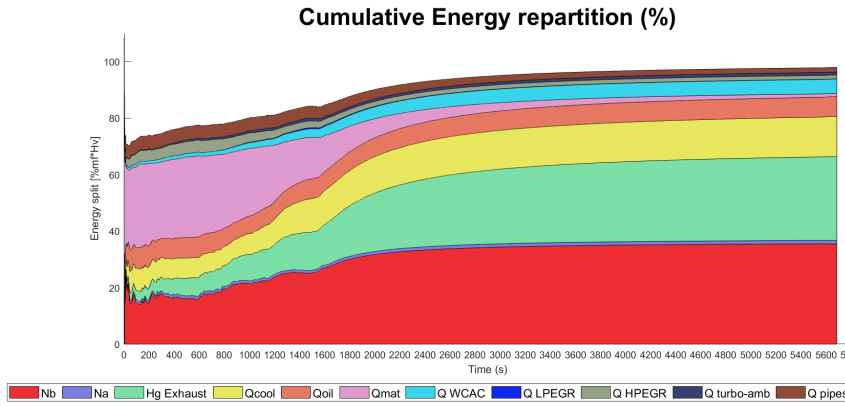

Figure 10. Extended cycle of Total cumulative energy repartition in WLTC

The net exhaust enthalpy, $H_{g,exhaust}$ (calculated between engine intake and downstream the low pressure EGR pipe), contributes about 13% of total engine energy output at the end of the cycle. A trend to increase $H_{g,exhaust}$ can be seen in the second half of the WLTC mainly due to the higher load and speed during the high and extra-high parts of the cycle but also due to the progressive reduction of the relative effect of heat accumulation in the block[56]. Cumulated heat rejected to the intercooler is about 4% of the fuel energy, being negligible until 500 seconds after cycle beginning due to the small difference of the air temperature between the compressor outlet and the intercooler coolant because of the low boost pressure in this part of the cycle. HPEGR and LPEGR loops are activated depending on the coolant temperature, thus LPEGR is activated when coolant reaches 70°C. At the end of the cycle only about 4% of the total energy is rejected in the EGR coolers. About 4% of heat is rejected to ambient through turbocharger and pipes ($\dot{Q}_{turbo-amb}$ and $\dot{Q}_{pipes}$).

Going deeper in the analysis of the efficiencies, Figure 11 shows the percentage of accumulated indicated and brake energies at LTCS conditions along the WLTC. Indicated energy ranges from 40% at the beginning to 44% at the end of the cycle, while brake energy ranges from about 10% at the WLTC start to 29% at the end, showing a clear trend to increase with time. Having in mind that indicated efficiency is not affecting dramatically brake efficiency, its evolution must be understood by analysing mechanical losses that are shown in Figure 12.

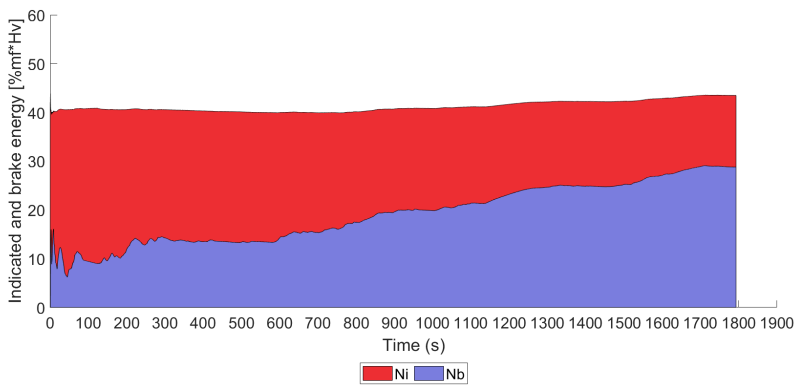

Figure 11. Cumulative indicated and brake energies in WLTC at LTCS conditions

Top of Figure 12 shows that there is a large reduction of the mechanical losses weight, in particular due to the friction, reaching about 30% of the fuel energy at the start of the WLTC and diminishing to 11% at the end of the cycle, while pumping (N_p) is only about 3% and auxiliaries (N_a) are 1% both of them with a negligible variation along the cycle. Having a look to these results, the lower values of brake energy at the beginning of the operation can be explained by the higher mechanical losses, because of low coolant and thus oil temperatures during the beginning of the operation, thus affecting the oil viscosity.

As shown in the bottom of Figure 12, piston friction, N_{fr} piston, is the main component of the friction. It is about two thirds of the total friction (7% of the fuel energy). Bearing friction has the intermediate contribution and the valve train is the less important one among all the three. This friction repartition is consistent with some previous analysis performed in steady-state conditions [56].

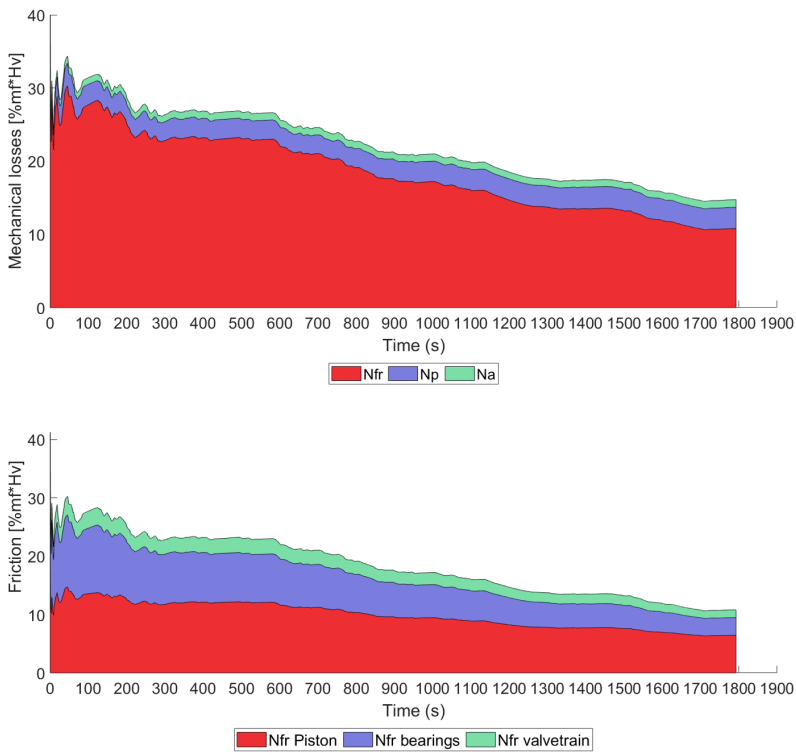

Figure 12. Cumulative mechanical losses (top) and friction split (bottom) in WLTC at LTCS conditions

Ambient cold start conditions

Main purpose of this work is to compare the energy split starting at LTCS conditions with ACS conditions, which energy balance considering the complete engine can be seen in Figure 13. At a first glance, Figure 9 and 13 are similar, but a deeper analysis will show differences in detail, specially for brake efficiency and exhaust enthalpy that are quite different, in particular during the first half of the cycle. N_b at the beginning of WLTC is clearly higher with ACS (about 25%) than with LTCS (about 15%). As shown in Figure 14 and 15, even though the indicated efficiency during first half of the WLTC is slightly lower to LTCS (39% vs 40%), the differences in N_b has to be majorly attributed to mechanical losses that are comparitively lower in ACS as shown in Figure 15. When comparing Figure 15 and top figure in Figure 12 it can be concluded that the difference is mainly due to the friction term, up to about 10% of the fuel energy higher at LTCS at the beginning of the WLTC; even though this discrepancy is later reduced.

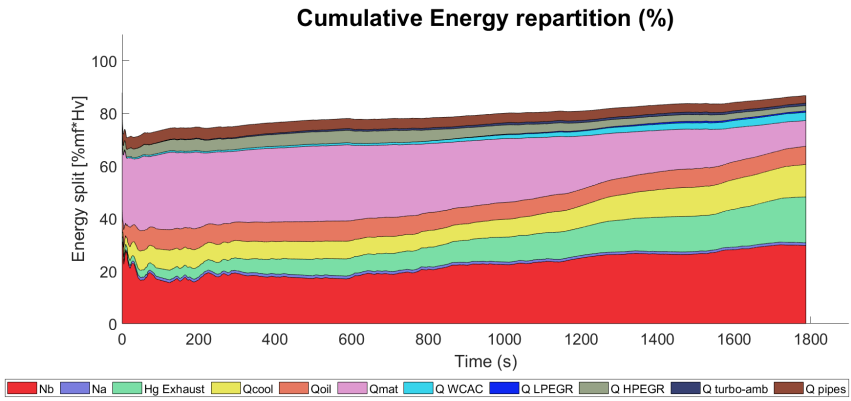

Figure 13. Total cumulative energy repartition in WLTC at ACS conditions

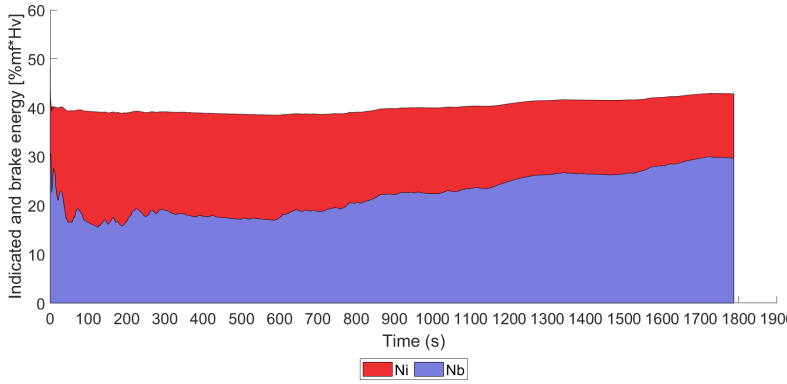

Figure 14. Cumulative indicated and brake energies in WLTC at ACS conditions

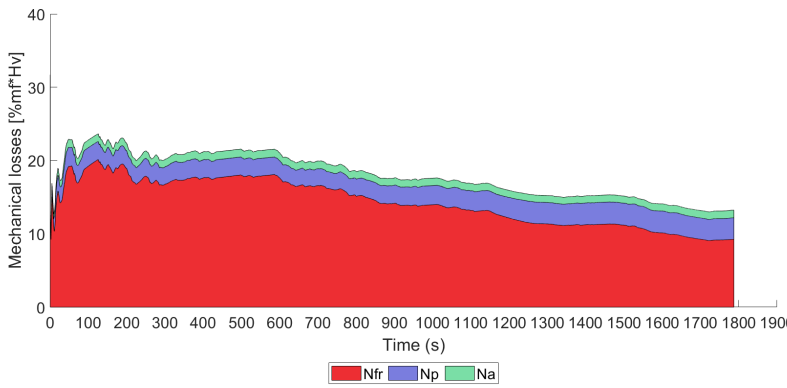

Figure 15. Cumulative mechanical losses in WLTC at ACS conditions

The comparison of energy terms at the end of the WLTC in LTCS and ACS at an altitude of 0 m, is summarized in Figure 16. The first change when comparing with results starting at LTCS conditions can be seen in the brake energy, which is about 30% in ACS conditions, 1% higher than in LTCS. This can be mainly explained because of the higher mechanical losses in LTCS, that is partially compensated by indicated efficiency, which is also higher, as seen in the Figure 17, where friction is about 9% in ACS (2% lower than in LTCS) and N_i is about 43%. It is interesting to highlight that Ni during ACS is 1% lower than during LTCS. This result is apparently strange because at a first approach lower ambient temperature is expected to reduce indicated efficiency because of, among other effects, the higher heat transfer. Figure 18 shows some key in-cylinder parameters such as temperature and oxygen concentration at intake valve closing (the key observers to follow the air path changes due to the ambient conditions) and also combustion duration, key parameter effecting the indicated efficiency. As shown, the temperature and oxygen (O2) concentration are higher in ACS than in LTCS. The effect of the temperature is directly related with the ambient temperature, while higher O2 is due to higher EGR with LTCS because the air setting is kept and intake density is higher (the effect is partially compensated in altitude, as later discussed). Higher temperature and O2 concentrations should enhance combustion and lead to shorter durations in ACS. However, this trend is not observed during the initial low part of the WLTC, where combustion duration is slightly higher for ACS. This can be explained because the injection pressure, which is higher for LTCS due to the higher fuel mass injected (Figure 19 top) to compensate mechanical losses. According to the calibration, this has a positive effect specifically in the initial low part of the cycle, where the effect of oxygen is not critical because of low load. Later, as the load increases, thermal and friction differences diminish, relative variation in the injection settings becomes smaller and then ACS shows a shorter average combustion duration, as expected. Hence, after 600 seconds, the combustion of ACS becomes faster than LTCS at 0 m. This combustion performance is affecting the indicated efficiency. However, the effect of the higher fuel injected seems to be the key. As seen in Figure 19 (top), fuel injected is clearly higher for LTCS and thus also the total indicated energy (Figure 19 middle). The ratio between them is the average indicated efficiency (Figure 19 bottom) that is clearly lower for ACS. As stated, the reason justifying this trend is the higher load (in indicated parameters terms) because of the more fuel injected (which is burned faster than in ACS). As the cycle advances, the combustion performance described can also be seen in the indicated efficiency: ACS and LTCS difference tends to diminish.

The noticeable changes can be seen in the heat rejection to coolant and oil along with the heat cumulated in engine structure. There is higher heat accumulation in the material at LTCS conditions because of the low initial temperature of fluids and metal. As the temperature of the material increases, the accumulated energy of the metal decreases, slightly increasing the heat rejected to the coolant. Also, the thermostat opens earlier for ACS, leading to the higher heat transfer. Hence, there is high heat rejection to the coolant at ACS than in LTCS (13% vs 11%). On the other hand, the heat rejection to oil does not show such an important variation (7% in ACS vs 6.7% in LTCS). The final cumulated values of the heat rejected to coolant and oil are slightly higher in ACS

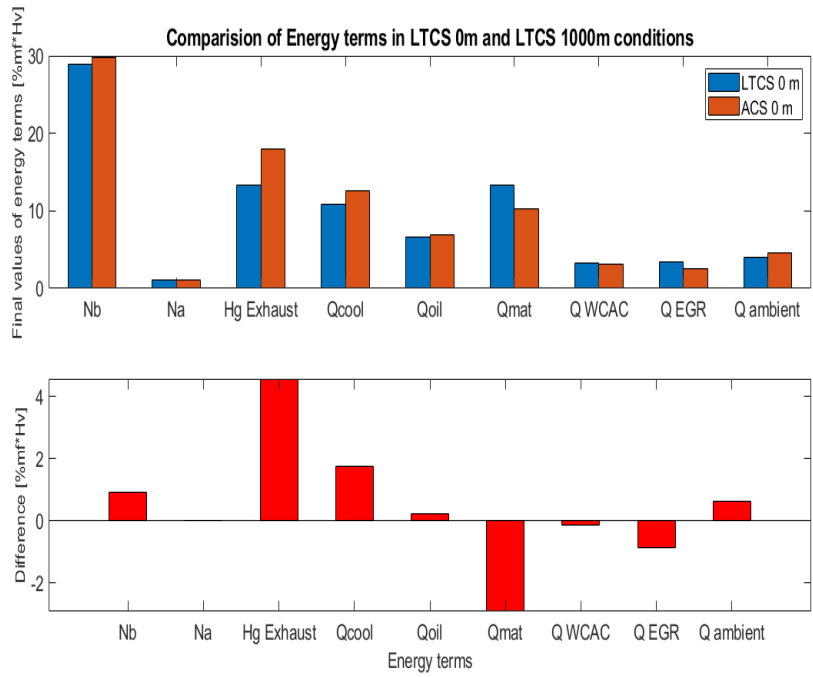

Figure 16. Comparison of energy terms in WLTC in LCTS 0 m and ACS 0 m conditions at the end of the cycle

conditions. Whereas, the heat rejected to material ($\dot{Q}_{mat}$) is higher in LCTS (12.5% vs 10%).

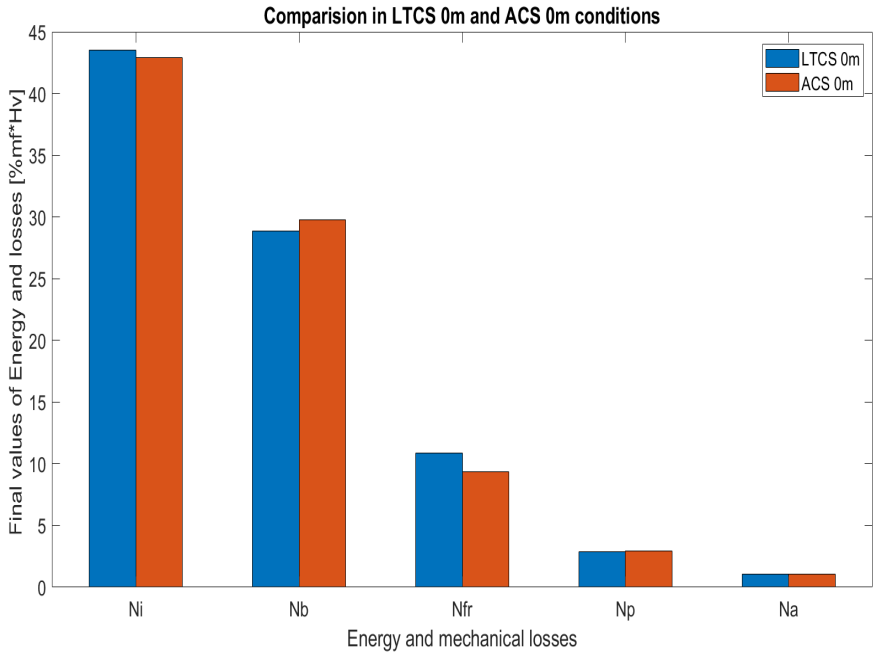

Figure 17. Comparison of energy and losses in WLTC in LCTS 0 m and ACS 0 m conditions

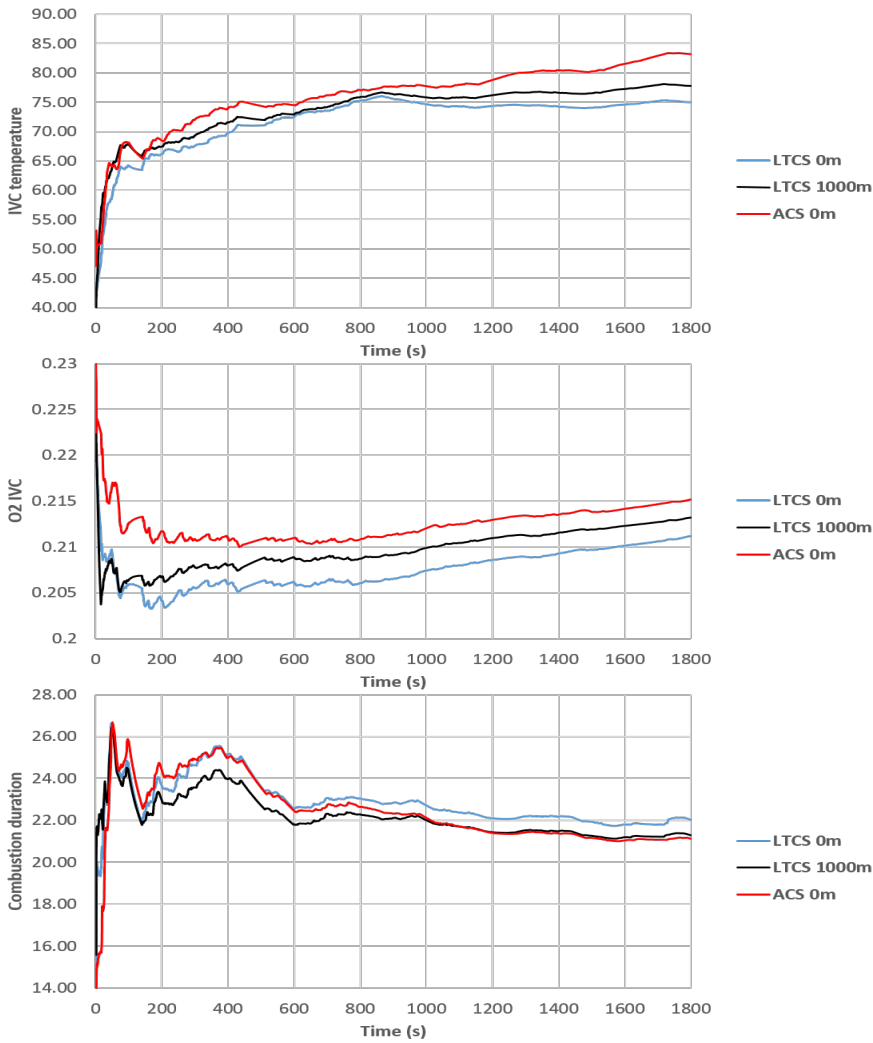

Figure 18. Temperatue at IVC, O2 at IVC and combustion duration in WLTC at LCTS 0 m, LTCS 1000 m and ACS 0 m conditions

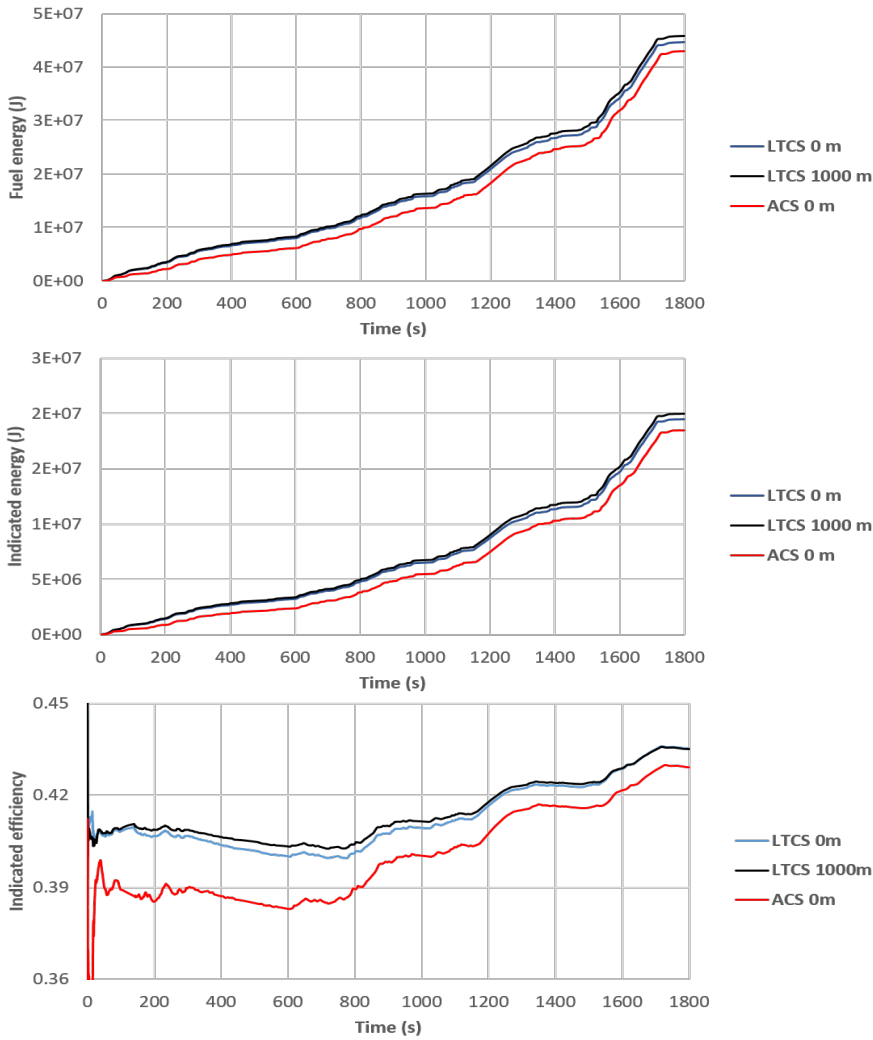

Figure 19. Fuel, indicated energy and indicated efficiency in WLTC at LCTS 0 m, LTCS 1000 m and ACS 0 m conditions

The energy term with higher variation is net exhaust enthalpy, $H_{g,exhaust}$, which is higher in ACS conditions (18% vs 13.5%). This can be considered as a result of the reduction of cumulated heat in the block and lower cumulated EGR in ACS (2.5% vs 3.5%). In the Figure 13, it can be seen that the rejected heat in the LPEGR heat exchanger, $\dot{Q}_{LPEGR}$, is low (less than 1%) when compared to $\dot{Q}_{HPEGR}$. This can be explained by the low temperature at the LPEGR cooler. As shown in Figure 20, despite of only having a net mass flow through the LPEGR cooler during the LPEGR operation, natural convection, pulsing effect and much higher temperature of the gas at the HPEGR cooler, lead to higher heat rejection in it. The rest of the terms, heat rejection in the intercooler, to ambient (pipes, turbo) do not show any important variation.

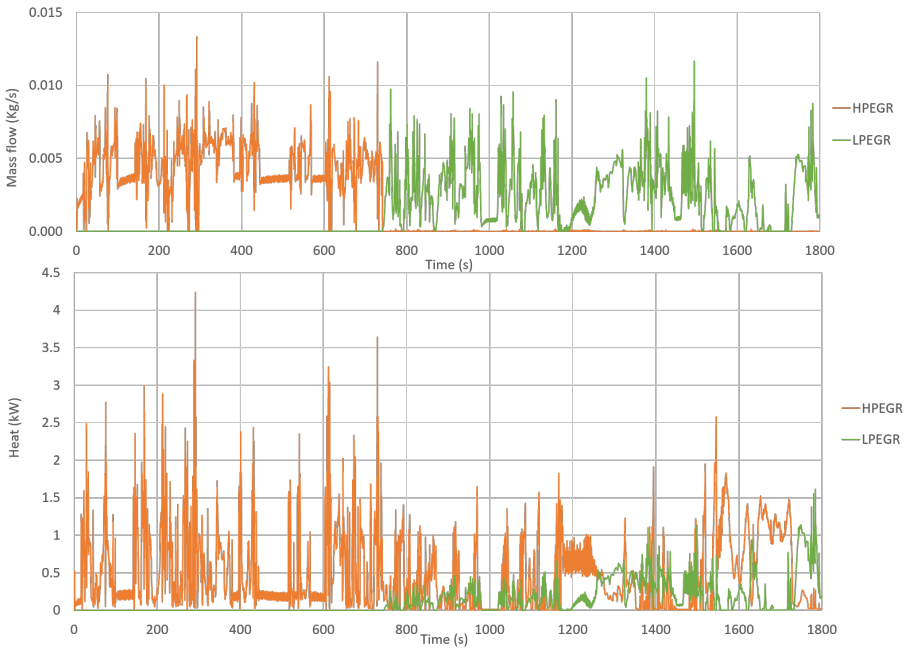

Figure 20. Mass flow and heat at HPEGR and LPEGR in WLTC at ACS conditions

Analysis of altitude effect

After analysing the effect of the starting temperature, this section is devoted to complete the analysis by assessing the effect of altitude in the engine operation. WLTC simulations were launched for LTCS conditions at the altitude of 0 m and 1000 m above the sea level. The LTCS at 0 m is considered the baseline case for the analysis.

Instantaneous energy balances similar to those shown in Figure 9 and 13 were obtained for simulations at altitude of 1000 m. As instantaneous evolution is similar to that presented for LTCS at 0 m, the analysis is going to be focused only on the final results

at the end of the WLTC, to highlight main cumulated differences. In general, it can be observed that differences are small and only one term is changing more than 0.5%. Comparison of energy terms at the end of the WLTC in LTCS at 0 m and 1000 m is shown in Figure 21. It can be seen that cumulated brake efficiency at LTCS 1000 m conditions is slightly lower than LTCS 0 m conditions, but the difference is only about 0.8%. As shown in Figure 22, mean indicated efficiency is similar in both conditions. This can be justified because accordingly to the calibration, VEMOD control follows the same boost pressure target at the two altitudes and thus trapped mass at the inlet valve closing is similar at 0 m and 1000 m. The additional fuel required to reach the demanded torque, even though affecting the combustion process, doesn't affect importantly the indicated performance at the end of the WLTC. As seen in Figure 18, O2 concentration at intake valve closing is slightly higher at 1000 m in comparison to 0 m. This can be explained because the boost pressure is the same, but not the temperature. Due to the higher compression ratio in the compressor, the outlet temperature is higher and hence the intake temperature, thus diminishing EGR (for the same air demand). More O2 and slightly higher temperatures enhance the combustion. As in this case, total fuel is not very different from 0 m, injection settings are similar and thus combustion duration is slightly shorter for 1000 m. This has an effect on indicated efficiency shown in Figure 19 (bottom), where there is a slight higher value at LTCS 1000 m with respect to LTCS 0 m. Hence, the lower mechanical losses during LTCS at 0 m, can be considered as the main reason for the lower brake efficiency. If mechanical losses split is analysed in detail, it can be seen in Figure 22 that both auxiliaries and friction are almost constant because coolant, oil and fuel pumps don't change their operation and oil temperature, main variable for friction, is very similar, as confirmed by the constant heat to oil shown in Figure 21. Thus, the main reason for the brake efficiency diminution is pumping, that increase from 2.9% to 4% of the total fuel energy.

Among the rest of energy terms plotted in Figure 21, there are other two that show a significant increase: heat rejected in the intercooler and coolant heat exchanger. Both of them increase about 0.5%. Heat rejected to the intercooler increases due to the higher compressor outlet temperature because of the higher compression ratio (boost pressure is maintained while compressor inlet pressure is lower due to the ambient conditions). The higher heat rejection to coolant is justified because of the slightly higher intake temperature which is also consequence of higher temperature at the compressor outlet. The rest of variables does not show a remarkable variation.

Having in mind the results discussed in the previous section and here, it can be concluded that the engine response is mainly affected by the ambient temperature while the effect of the altitude is lower.

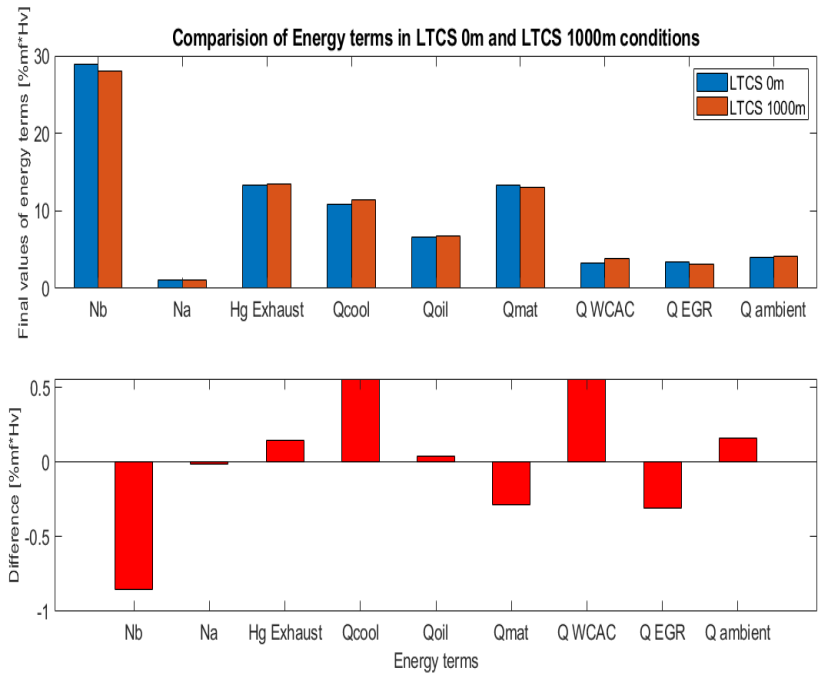

Figure 21. Comparison of energy terms in WLTC in LTCS 0m and LTCS 1000m conditions at the end of the cycle

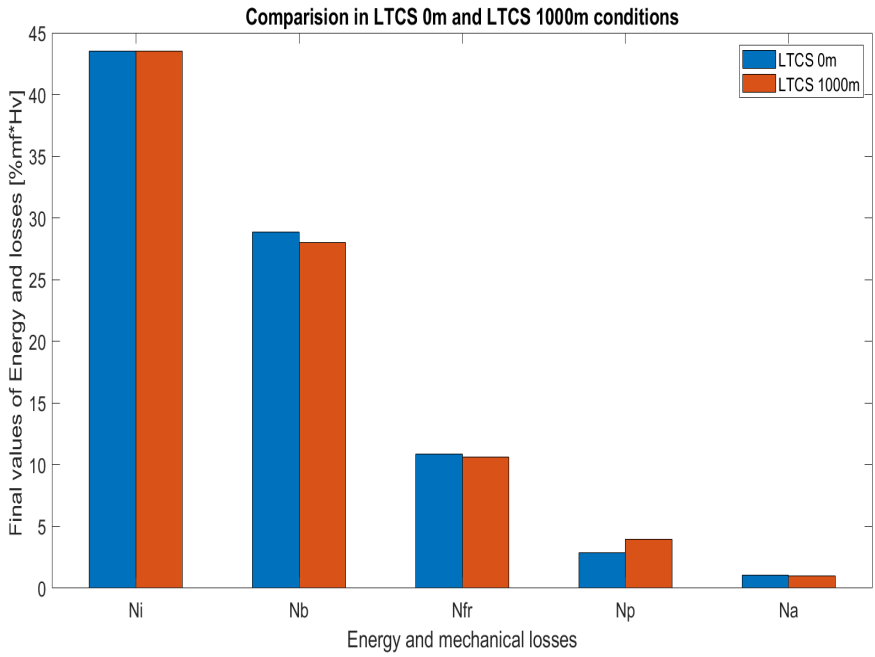

Figure 22. Comparison of energy and losses in WLTC in LTCS 0m and LTCS 1000m conditions at the end of the cycle

Analysis of NOx emissions

Figure 23 shows the NOx at different operating conditions. It can be seen that NOx is higher in LTCS 0 m conditions (with respect to ACS) until around 1300 seconds, and then the trend changes to lower NOx until the end of the cycle. This can be explained with the NOx dependency on temperature and EGR. When the temperature is lower, as air target is kept in the settings, the EGR rate will be higher due to the higher intake density; this should reduce NOx. The higher NOx in LTCS during the initial part of the cycle can be explained because of the higher injected fuel to compensate higher mechanical losses and thus maintaining the torque. However, as the fluid temperature increases along the cycle, the effect of the ambient conditions diminishes (it can be seen in Figure 19 that, in the last part of the cycle, fuel consumption difference between LTCS at 0 m and ACS does not increase) and thus the benefits of LTCS can be seen in NOx in the last part of the WLTC. When comparing LTCS 0 m and LTCS 1000 m, a continuous NOx increase for higher altitude can be seen. The effect can be explained because of the lower EGR rate for 1000 m, as described in the previous section.

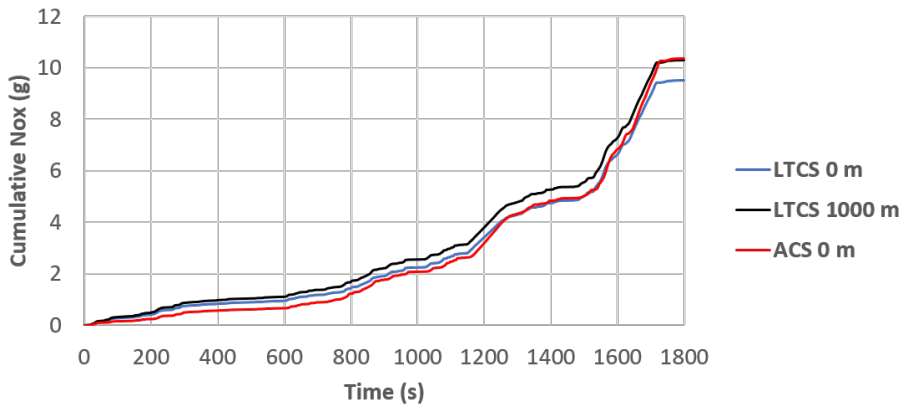

Figure 23. NOx in WLTC at ACS and LTCS conditions

Conclusions

The calibration and validation of the simulation tool, VEMOD have been using a 4-cylinder 1.6 L DI Diesel engine. Key parameters such as pressure, heat released, coolant temperature, oil temperatures and torque have been considered. In both steady-state and transient conditions, a good global performance has been found between the modeled and experimental results.

An extensive analysis of the Global Energy Balance (GEB) has been carried out to assess the effect of various operating conditions on the energy repartition during a transient operation. The GEB was performed considering the complete engine with two starting temperatures : ambient cold start (ACS) and low temperature cold start (LTCS) and two altitudes (0 and 1000 meters).

In all the above mentioned conditions, a "delay" effect due to the unsynchronized phenomena in the gas lines and cylinders has been shown and discussed. This effect diminishes with time, improving the apparent unbalance. It has been shown that the energy balance is reaching around 85% when it was run until 1800 seconds. However, when the simulation is extended, the energy balance reaches about 100%.

It has been shown that at LTCS conditions, the indicated energy is quite stable along the WLTC, while reaching about 44% at the end of the cycle, while brake energy is 29%, showing a clear trend to increase along the WLTC. The lower values of brake energy at the beginning of the operation, can be explained by the higher mechanical losses, being friction the main component, which reaches about 30% of the fuel energy at the start of the WLTC and diminishes to 11% at the end. The higher friction has been justified because of the low oil temperatures during the initial part of WLTC. Also, it has been found that the piston friction is the most important component, accounting for 60% of the total friction losses. Pumping (N_p) and auxiliaries (N_a) are only about 3% and 1% of the fuel energy respectively.

The energy split starting at LTCS conditions has been compared with ACS conditions at 0 m altitude. It has been shown that important changes take place in N_i, N_b, $\dot{Q}_{oil}$, $\dot{Q}_{cool}$ and $\dot{Q}_{mat}$ due to the different initial temperatures in LTCS and ACS conditions. It has been shown that air path changes are affecting IVC conditions both in temperature and composition terms. This is changing the combustion duration, but the main effect is the change of fuel injected, that is leading to operate in LTCS at slightly higher load (from the point of view of in-cylinder conditions). Thus indicated efficiency is lower in ACS. N_b is slightly higher in ACS conditions, when compared to LTCS (30% vs 29%) mainly because of the friction variation. In spite of the small variation in N_b, the fuel consumption increases by 4% in LTCS. It has been seen that $\dot{Q}_{cool}$ is higher in ACS conditions (13% vs 11%) and $\dot{Q}_{oil}$ is higher as well in ACS conditions (7% vs 6.7%). The heat rejected to material ($\dot{Q}_{mat}$) is lower in ACS (12.5% vs 10%). It has been found that the energy term with higher variation is the net exhaust enthalpy, $H_{g,exhaust}$, which is higher in ACS conditions (18% vs 13.5%). The rest of the terms, $\dot{Q}_{WCAC}$, $\dot{Q}_{pipes}$ and $\dot{Q}_{turbo-amb}$ do not show any important variation.

The assessment of altitude was done in LTCS at 0 m and 1000 m. It has been found that apart from the change in pumping and brake energy, the rest of variables does not show a remarkable variation.

The analysis of NOx emissions was done in ACS at 0 m, LTCS at 0 m and 1000 m. It has been found that cumulative NOx is higher in LTCS 0 m when compared to ACS 0 m at the beginning of the cycle, due to the higher fuel required. However, in the last part of the WLTC, NOx has become lower for LTCS 0 m due to the higher EGR achieved. It has been shown that there is a continuous NOx increase for higher altitude when comparing LTCS at 0 m and 1000 m because of the lower EGR rate due to the slightly higher intake temperature, that is also promoting NOx formation.

As a brief summary, it can be concluded that reducing ambient temperature from 20°C to -7°C decreases brake efficiency by 1% mainly due to the higher friction. The effect of increasing altitude 1000 m decreases brake efficiency by 0.8% in the WLTC because of the change in the pumping, while the fuel consumption increases by 2.5%. Altitude does not seem to have any important effect on the rest of the energy terms. However, different inital temperatures are majorly effecting the exhaust enthalpy, heat rejected to coolant and heat accumulated in the block as discussed.

Acknowledgments

This research has been partially funded by the European Union's Horizon 2020 Framework Programme for research, technological development and demonstration under grant agreement 723976 ("DiePeR") and by the Spanish government under the grant agreement TRA2017-89894-R ("MECOEM") and Sushma Artham was supported by FPI grant with reference PRE2018-084411. The authors wish to thank Renault SAS, especially P. Mallet and E. Gaïffas, for supporting this research.

References

1. E J, Liu T, Yang W et al. A skeletal mechanism modeling on soot emission characteristics for biodiesel surrogates with varying fatty acid methyl esters proportion. *Applied Energy* 2016; 181: 322–331. DOI:10.1016/j.apenergy.2016.08.090. URL http://dx.doi.org/10.1016/j.apenergy.2016.08.090.
2. Wu G, Lu Z, Xu X et al. Numerical investigation of aeroacoustics damping performance of a Helmholtz resonator: Effects of geometry, grazing and bias flow. *Aerospace Science and Technology* 2019; 86: 191–203. DOI:10.1016/j.ast.2019.01.007.
3. Li Y, Chen Y, Wu G et al. Experimental evaluation of water-containing isopropanol-n-butanol-ethanol and gasoline blend as a fuel candidate in spark-ignition engine. *Applied Energy* 2018; 219(March): 42–52. DOI:10.1016/j.apenergy.2018.03.051. URL https://doi.org/10.1016/j.apenergy.2018.03.051.
4. Giakoumis EG. A statistical investigation of biodiesel effects on regulated exhaust emissions during transient cycles. *Applied Energy* 2012; 98: 273–291. DOI:10.1016/j.apenergy.2012.03.037. URL http://dx.doi.org/10.1016/j.apenergy.2012.03.037.

5. Triantafyllopoulos G, Katsaounis D, Karamitros D et al. Experimental assessment of the potential to decrease diesel NOx emissions beyond minimum requirements for Euro 6 Real Drive Emissions (RDE) compliance. *Science of the Total Environment* 2018; 618(x): 1400–1407. DOI:10.1016/j.scitotenv.2017.09.274. URL https://doi.org/10.1016/j.scitotenv.2017.09.274.
6. Park H, Bae C and Ha C. A comprehensive analysis of multiple injection strategies for improving diesel combustion process under cold-start conditions. *Fuel* 2019; 255(June): 115762. DOI:10.1016/j.fuel.2019.115762. URL https://doi.org/10.1016/j.fuel.2019.115762.
7. E J, Han D, Deng Y et al. Performance enhancement of a baffle-cut heat exchanger of exhaust gas recirculation. *Applied Thermal Engineering* 2018; 134(January): 86–94. DOI:10.1016/j.applthermaleng.2018.01.109. URL https://doi.org/10.1016/j.applthermaleng.2018.01.109.
8. Jiaqiang E, Zhao X, Xie L et al. Performance enhancement of microwave assisted regeneration in a wall-flow diesel particulate filter based on field synergy theory. *Energy* 2019; 169: 719–729. DOI:10.1016/j.energy.2018.12.086.
9. Jiaqiang E, Liu G, Zhang Z et al. Effect analysis on cold starting performance enhancement of a diesel engine fueled with biodiesel fuel based on an improved thermodynamic model. *Applied Energy* 2019; 243(March): 321–335. DOI:10.1016/j.apenergy.2019.03.204. URL https://doi.org/10.1016/j.apenergy.2019.03.204.
10. Ramadhas AS and Xu H. Improving Cold Start and Transient Performance of Automotive Diesel Engine at Low Ambient Temperatures. *SAE Technical Papers* 2016; 2016-April(April). DOI:10.4271/2016-01-0826.
11. Rakopoulos CD, Dimaratos AM, Giakoumis EG et al. Investigating the emissions during acceleration of a turbocharged diesel engine operating with bio-diesel or n-butanol diesel fuel blends. *Energy* 2010; 35(12): 5173–5184. DOI:10.1016/j.energy.2010.07.049. URL http://dx.doi.org/10.1016/j.energy.2010.07.049.
12. D Rakopoulos, Evangelos G Giakoumis. *Diesel Engine Transient Operation - Principles of Operation and Simulation Analysis*. ISBN 9781848823747.
13. Rakopoulos CD, Giakoumis EG, Hountalas DT et al. The Effect of Various Dynamic, Thermodynamic and Design Parameters on the Performance of a Turbocharged Diesel Engine Operating under Transient Load Conditions. *SAE Technical Paper Series* 2010; 1(724). DOI: 10.4271/2004-01-0926.
14. European Parliament and Council of the European Union. Regulation (EC) No 852/2004 of the European Parliament and of the Council. *Official Journal of the European Communities* 2004; 2006(December 2006): 1–54. URL http://eur-lex.europa.eu/LexUriServ/LexUriServ.do?uri=OJ:L:2004:139:0001:0054:en:PDF.
15. Martin J, Arnau F, Piqueras P et al. Development of an Integrated Virtual Engine Model to Simulate New Standard Testing Cycles. *SAE Technical Paper Series* 2018; 1: 1–17. DOI: 10.4271/2018-01-1413.
16. Payri F, Lopez JJ, Pla B et al. Assessing the Limits of Downsizing in Diesel Engines. *SAE Technical Paper Series* 2014; 1. DOI:10.4271/2014-32-0128.
17. Giakoumis EG, Rakopoulos CD, Dimaratos AM et al. Exhaust emissions of diesel engines operating under transient conditions with biodiesel fuel blends. *Progress in Energy and*

Combustion Science 2012; 38(5): 691–715. DOI:10.1016/j.pecs.2012.05.002. URL http://dx.doi.org/10.1016/j.pecs.2012.05.002.

18. Cui Y, Deng K and Wu J. A direct injection diesel combustion model for use in transient condition analysis. *Proceedings of the Institution of Mechanical Engineers, Part D: Journal of Automobile Engineering* 2001; 215(9): 995–1004. DOI:10.1243/0954407011528563.
19. Pamminger Michael CMHRVWT Wang Buyu. The impact of water injection and exhaust gas recirculation on combustion and emissions in a heavy-duty compression ignition engine operated on diesel and gasoline. *INTERNATIONAL JOURNAL OF ENGINE RESEARCH* 2020; 21. DOI:10.1177/1468087418815290.
20. Tauzia X, Maiboom A, Karaky H et al. Experimental analysis of the influence of coolant and oil temperature on combustion and emissions in an automotive diesel engine. *International Journal of Engine Research* 2019; 20(2): 247–260. DOI:10.1177/1468087417749391.
21. Cárdenas MD, Gómez A and Armas O. Pollutant emissions from starting a common rail diesel engine fueled with different biodiesel fuels. *Journal of Energy Engineering* 2016; 142(2). DOI:10.1061/(ASCE)EY.1943-7897.0000328.
22. Giakoumis EG, Dimaratos AM, Rakopoulos CD et al. Combustion Instability during Starting of Turbocharged Diesel Engine Including Biofuel Effects. *Journal of Energy Engineering* 2017; 143(2). DOI:10.1061/(ASCE)EY.1943-7897.0000402.
23. García-Contreras R, Armas O, Mata C et al. Impact of Gas To Liquid and diesel fuels on the engine cold start. *Fuel* 2017; 203: 298–307. DOI:10.1016/j.fuel.2017.04.116.
24. Dardiotis C, Martini G, Marotta A et al. Low-temperature cold-start gaseous emissions of late technology passenger cars. *Applied Energy* 2013; 111: 468–478. DOI:10.1016/j.apenergy.2013.04.093. URL http://dx.doi.org/10.1016/j.apenergy.2013.04.093.
25. Tinprabath P, Hespel C, Chanchaona S et al. Influence of biodiesel and diesel fuel blends on the injection rate under cold conditions. *Fuel* 2015; 144: 80–89. DOI:10.1016/j.fuel.2014.12.010. URL http://dx.doi.org/10.1016/j.fuel.2014.12.010.
26. Park H, Shin J and Bae C. Spray and Combustion of Diesel Fuel under Simulated Cold-Start Conditions at Various Ambient Temperatures. In *SAE Technical Paper*. SAE International. DOI:10.4271/2017-24-0069. URL https://doi.org/10.4271/2017-24-0069.
27. Roberts A, Brooks R and Shipway P. Internal combustion engine cold-start efficiency: A review of the problem, causes and potential solutions. *Energy Conversion and Management* 2014; 82: 327–350. DOI:10.1016/j.enconman.2014.03.002. URL http://dx.doi.org/10.1016/j.enconman.2014.03.002.
28. Horng RF and Chou HM. Effect of input energy on the emission of a motorcycle engine with an electrically heated catalyst in cold-start conditions. *Applied Thermal Engineering* 2004; 24(14-15): 2017–2028. DOI:10.1016/j.applthermaleng.2004.02.005.
29. Clairotte M, Adam TW, Zardini AA et al. Effects of low temperature on the cold start gaseous emissions from light duty vehicles fuelled by ethanol-blended gasoline. *Applied Energy* 2013; 102(2013): 44–54. DOI:10.1016/j.apenergy.2012.08.010. URL http://dx.doi.org/10.1016/j.apenergy.2012.08.010.
30. Chen RH, Chiang LB, Chen CN et al. Cold-start emissions of an SI engine using ethanol-gasoline blended fuel. *Applied Thermal Engineering* 2011; 31(8-9): 1463–1467. DOI:10.1016/j.applthermaleng.2011.01.021. URL http://dx.doi.org/10.1016/j.applthermaleng.2011.01.021.

31. Gumus M. Reducing cold-start emission from internal combustion engines by means of thermal energy storage system. *Applied Thermal Engineering* 2009; 29(4): 652–660. DOI:10.1016/j.applthermaleng.2008.03.044. URL http://dx.doi.org/10.1016/j.applthermaleng.2008.03.044.
32. Deng Y, Liu H, Zhao X et al. Effects of cold start control strategy on cold start performance of the diesel engine based on a comprehensive preheat diesel engine model. *Applied Energy* 2018; 210(October 2017): 279–287. DOI:10.1016/j.apenergy.2017.10.093. URL http://dx.doi.org/10.1016/j.apenergy.2017.10.093.
33. Luján JM, Dolz V, Monsalve-Serrano J et al. High-pressure exhaust gas recirculation line condensation model of an internal combustion diesel engine operating at cold conditions. *International Journal of Engine Research* 2019; DOI:10.1177/1468087419868026.
34. Luján JM, Climent H, Ruiz S et al. Influence of ambient temperature on diesel engine raw pollutants and fuel consumption in different driving cycles. *International Journal of Engine Research* 2019; 20(8-9): 877–888. DOI:10.1177/1468087418792353.
35. Galindo J, Dolz V, Monsalve-Serrano J et al. Advantages of using a cooler bypass in the low-pressure exhaust gas recirculation line of a compression ignition diesel engine operating at cold conditions. *International Journal of Engine Research* 2020; : 1–12DOI: 10.1177/1468087420914725.
36. Kawaguchi A, Wakisaka Y, Nishikawa N et al. Thermo-swing insulation to reduce heat loss from the combustion chamber wall of a diesel engine. *International Journal of Engine Research* 2019; 20(7): 805–816. DOI:10.1177/1468087419852013.
37. Liu S, Shen L, Bi Y et al. Effects of altitude and fuel oxygen content on the performance of a high pressure common rail diesel engine. *Fuel* 2014; 118: 243–249. DOI:10.1016/j.fuel.2013.10.007. URL http://dx.doi.org/10.1016/j.fuel.2013.10.007.
38. Payri F, Olmeda P, Martin J et al. A New Tool to Perform Global Energy Balances in DI Diesel Engines. *SAE International Journal of Engines* 2014; 7(1): 43–59. DOI: 10.4271/2014-01-0665.
39. Payri F, Martin J, Garcia A et al. Experimental and Theoretical Analysis of the Energy Balance in a DI Diesel Engine. *SAE Technical Paper Series* 2015; 1(x). DOI:10.4271/2015-01-1651.
40. Tauzia X and Maiboom A. Experimental study of an automotive Diesel engine efficiency when running under stoichiometric conditions. *Applied Energy* 2013; 105: 116–124. DOI:10.1016/j.apenergy.2012.12.034. URL http://dx.doi.org/10.1016/j.apenergy.2012.12.034.
41. Abedin MJ, Masjuki HH, Kalam MA et al. Energy balance of internal combustion engines using alternative fuels. *Renewable and Sustainable Energy Reviews* 2013; 26: 20–33. DOI: 10.1016/j.rser.2013.05.049. URL http://dx.doi.org/10.1016/j.rser.2013.05.049.
42. Ajav EA, Singh B and Bhattacharya TK. Thermal balance of a single cylinder diesel engine operating on alternative fuels. *Energy Conversion and Management* 2000; 41(14): 1533–1541. DOI:10.1016/S0196-8904(99)00175-2.
43. Durgun O and Şahin Z. Theoretical investigation of heat balance in direct injection (DI) diesel engines for neat diesel fuel and gasoline fumigation. *Energy Conversion and Management* 2009; 50(1): 43–51. DOI:10.1016/j.enconman.2008.09.007.

44. Smith LA, Preston WH, Dowd G et al. Application of a First Law Heat Balance Method to a Turbocharged Automotive Diesel Engine. *SAE Technical Paper Series* 2010; 1. DOI: 10.4271/2009-01-2744.
45. Olmeda P, Martín J, Novella R et al. Assessing the optimum combustion under constrained conditions. *International Journal of Engine Research* 2018; : 1–13DOI:10.1177/1468087418814086.
46. Taymaz I. An experimental study of energy balance in low heat rejection diesel engine. *Energy* 2006; 31(2-3): 364–371. DOI:10.1016/j.energy.2005.02.004.
47. Jung D, Yong J, Choi H et al. Analysis of engine temperature and energy flow in diesel engine using engine thermal management, 2013. DOI:10.1007/s12206-012-1235-4.
48. Caresana F, Bilancia M and Bartolini CM. Numerical method for assessing the potential of smart engine thermal management: Application to a medium-upper segment passenger car. *Applied Thermal Engineering* 2011; 31(16): 3559–3568. DOI:10.1016/j.applthermaleng.2011.07.017. URL http://dx.doi.org/10.1016/j.applthermaleng.2011.07.017.
49. Payri F, López JJ, Martín J et al. Improvement and application of a methodology to perform the Global Energy Balance in internal combustion engines. Part 1: Global Energy Balance tool development and calibration. *Energy* 2018; 152: 666–681. DOI:10.1016/j.energy.2018.03.118.
50. Romero CA, Torregrosa A, Olmeda P et al. Energy Balance During the Warm-Up of a Diesel Engine. *SAE Technical Paper Series* 2014; 1. DOI:10.4271/2014-01-0676.
51. Kan Z, Hu Z, Lou D et al. Effects of altitude on combustion and ignition characteristics of speed-up period during cold start in a diesel engine. *Energy* 2018; 150: 164–175. DOI:10.1016/j.energy.2017.12.103.
52. Olmeda P, Martín J, Arnau FJ et al. Analysis of the energy balance during World harmonized Light vehicles Test Cycle in warmed and cold conditions using a Virtual Engine. *International Journal of Engine Research* 2019; DOI:10.1177/1468087419878593.
53. Olmeda P, Martin J, Garcia A et al. Evaluation of EGR Effect on the Global Energy Balance of a High Speed DI Diesel Engine. *SAE Technical Paper Series* 2016; 1. DOI: 10.4271/2016-01-0646.
54. Benajes J, Olmeda P, Martín J et al. A new methodology for uncertainties characterization in combustion diagnosis and thermodynamic modelling. *Applied Thermal Engineering* 2014; 71(1): 389–399. DOI:10.1016/j.applthermaleng.2014.07.010.
55. Payri F, Margot X, Gil A et al. Computational Study of Heat Transfer to the Walls of a DI Diesel Engine. *SAE Technical Paper Series* 2010; 1(724). DOI:10.4271/2005-01-0210.
56. Payri F, Olmeda P, Martín J et al. Experimental analysis of the global energy balance in a di diesel engine. *Applied Thermal Engineering* 2015; 89(x): 545–557. DOI:10.1016/j.applthermaleng.2015.06.005.
57. Payri F, López JJ, Martín J et al. Improvement and application of a methodology to perform the Global Energy Balance in internal combustion engines. Part 1: Global Energy Balance tool development and calibration. *Energy* 2018; 152: 666–681. DOI:10.1016/j.energy.2018.03.118.
58. Carreño Arango R. *A comprehensive methodology to analyse the Global Energy Balance in Reciprocating Internal Combustion Engines*. September 2016.

59. Olmeda P, Dolz V, Arnau FJ et al. Determination of heat flows inside turbochargers by means of a one dimensional lumped model. *Mathematical and Computer Modelling* 2013; 57(7-8): 1847–1852. DOI:10.1016/j.mcm.2011.11.078. URL http://dx.doi.org/10.1016/j.mcm.2011.11.078.
60. Torregrosa A, Olmeda P, Degraeuwe B et al. A concise wall temperature model for di Diesel engines. *Applied Thermal Engineering* 2006; 26(11-12): 1320–1327. DOI:10.1016/j.applthermaleng.2005.10.021.
61. Jose M Desantes JJLAC Jean Arregle. Scaling laws for free turbulent gas jets and Diesel like sprays, Atomization and Sprays 16. *Atomization and Sprays* 2006; 16: 443–474. DOI: 10.1615/AtomizSpr.v16.i4.60.
62. Vasileios Hamosfakidis RR. Optimization of a hydrocarbon fuel ignition model for two single component surrogates of diesel fuel. *Combustion and Flame* 2003; 132. DOI: 10.1016/S0010-2180(02)00489-3.

-